FINAL PROJECT REPORT #00049070

GRANT: DTRT13-G-UTC45
Project Period: 09/01/2014 – 12/31/15

RAPID PAVEMENT CONSTRUCTION: RESEARCH ON THIXOTROPY AND WORKABILITY LOSS OF VIBRATION-FREE CONCRETE IN VIEW ACCELERATING PAVEMENT CONSTRUCTION BY SLIPFORMING

Participating Consortium Member:
Missouri University of Science and Technology

Authors:
Dimitri Feys, Ph.D., Assistant Professor
Azadehalsadat Asghari, Ph.D. candidate

RE-CAST:
REsearch on Concrete Applications for Sustainable Transportation
Tier 1 University Transportation Center

DISCLAIMER

The contents of this report reflect the views of the authors, who are responsible for the facts and the accuracy of the information presented herein. This document is disseminated under the sponsorship of the U.S. Department of Transportation's University Transportation Centers Program, in the interest of information exchange. The U.S. Government assumes no liability for the contents or use thereof.

TECHNICAL REPORT DOCUMENTATION PAGE

1. Report No. RECAST UTC #00049070	**2. Government Accession No.**	**3. Recipient's Catalog No.**
4. Title and Subtitle Rapid Pavement Construction: Research on Thixotropy and Workability Loss of Vibration-free Concrete in View Accelerating Pavement Construction by Slipforming		**5. Report Date** January 2016 **6. Performing Organization Code:**
7. Author(s) Dimitri Feys and Azadehalsadat Asghari		**8. Performing Organization Report No.** Project #00049070
9. Performing Organization Name and Address RE-CAST – Missouri S&T 500 W. 16th St., 223 ERL Rolla, MO 65409-0710		**10. Work Unit No.** **11. Contract or Grant No.** USDOT: DTRT13-G-UTC45
12. Sponsoring Agency Name and Address Office of the Assistant Secretary for Research and Technology U.S. Department of Transportation 1200 New Jersey Avenue, SE Washington, DC 20590		**13. Type of Report and Period Covered:** Final Report Period: 09/01/2014 – 12/31/15 **14. Sponsoring Agency Code:**
15. Supplementary Notes The investigation was conducted in cooperation with the U. S. Department of Transportation.		

16. Abstract

This report describes a parametric study to better understand the changes in rheological properties of cement pastes with time and shearing energy. It includes the investigation of structural build-up at rest, the evolution of dynamic rheological properties with time and the breakdown generated by applying different levels of shearing. The main purpose of this research work is to generate a knowledge platform to facilitate research on tuning the rheological properties of self-consolidating concrete (SCC), making it suitable for slipforming.

However, in this research work, another interesting research question was addressed simultaneously: how much does the applied rate of shear affect the breakdown of internal structure? A question which was stated by Wallevik when describing internal connections between cement particles: some connections are reversible, some are permanent, dependent on the amount of work applied to the system [3]. Similarly, Feys at al. had demonstrated some significant changes in viscosity in SCC induced by pumping [4]. These changes were hypothesized to be caused by additional shearing compared to the initial shearing conditions inside the concrete mixer. Inspired by the large-scale pumping testing procedure from Feys et al. [4] [5], a similar procedure was developed for cement pastes to investigate how the maximum applied shear rate affects the rheological properties. The procedure and results are summarized in this report, however, some inexplicable effects are still remaining after analysis.

As a consequence, this report contains the description of the evolution of static and dynamic rheological properties of cement paste with time and the results of the shear-dependency, preceded by the utilized procedures and a short literature review on the basics of rheology of suspensions, cement pastes and their changes with time.

17. Key Words Rheology, cement past, SCC, slipform	**18. Distribution Statement** No restrictions. This document is available to the public.	
19. Security Classification (of this report) Unclassified	**20. Security Classification (of this page)** Unclassified	**21. No of Pages** 71

Form DOT F 1700.7 (8-72) Reproduction of form and completed page is authorized.

Table of Contents

List of Figures

List of Tables

1 Introduction

This report describes a parametric study to better understand the changes in rheological properties of cement pastes with time and shearing energy. It includes the investigation of structural build-up at rest, the evolution of dynamic rheological properties with time and the breakdown generated by applying different levels of shearing. The main purpose of this research work is to generate a knowledge platform to facilitate research on tuning the rheological properties of self-consolidating concrete (SCC), making it suitable for slipforming [1] [2].

However, in this research work, another interesting research question was addressed simultaneously: how much does the applied rate of shear affect the breakdown of internal structure? A question which was stated by Wallevik when describing internal connections between cement particles: some connections are reversible, some are permanent, dependent on the amount of work applied to the system [3]. Similarly, Feys at al. had demonstrated some significant changes in viscosity in SCC induced by pumping [4]. These changes were hypothesized to be caused by additional shearing compared to the initial shearing conditions inside the concrete mixer. Inspired by the large-scale pumping testing procedure from Feys et al. [4] [5], a similar procedure was developed for cement pastes to investigate how the maximum applied shear rate affects the rheological properties. The procedure and results are summarized in this report, however, some inexplicable effects are still remaining after analysis.

As a consequence, this report contains the description of the evolution of static and dynamic rheological properties of cement paste with time and the results of the shear-dependency, preceded by the utilized procedures and a short literature review on the basics of rheology of suspensions, cement pastes and their changes with time.

2 Literature Review

This section contains a short overview on the basics of suspension rheology, cement paste rheology and cement hydration, as knowledge in these fields is required for further understanding of the contents of this report.

2.1 Principles of rheology

Rheology is defined as the science of deformation of matter and encompasses the study of many different material types, including but not limited to solids and liquids [6]. For solid materials, the rheologist attempts to find the relationship between stress and strain. Steel is a linearly elastic material (as long as the yield stress is not exceeded), and the relationship between stress and strain is a constant: Young's modulus. Rubber is a non-linear elastic material for which the proportionality between stress and strain is dependent on the stress or strain [6].

For liquids, the proportionality between stress and strain rate is investigated. If the strain rate, shear rate or velocity gradient is a linear function of the stress, the material is called Newtonian [6]. Water and oil are primary examples of Newtonian liquids. If the relationship between stress and strain is no longer linear, does not pass through the origin, or is time-dependent, the material is non-Newtonian [6].

However, in some cases, the material can exhibit combined behavior. For example, the aforementioned steel, or clay, behave elastically as long as a critical stress, i.e. the yield stress, is not exceeded [6] [7]. If the yield stress is surpassed, the material flows. Secondly, some materials can behave either as an elastic or as a viscous fluid dependent on the duration of the applied load. These materials are called visco-elastic [6] and two prime

examples in civil engineering are hardened concrete and asphalt. For prolonged durations of loading, the material will creep: it flows.

The remaining part of the literature review will focus on different aspects of suspension rheology in order to explain certain behavior of cement pastes, and will focus on hydration of cement and its consequences on early-age rheological behavior.

2.2 Suspension rheology

2.2.1 Forces in colloidal suspensions

Colloid generally refers to the dispersed phase of a two-component system that are barely noticed by an optical microscope. In addition, thermal forces influence their motion. Hunter mentioned the ancient Egyptians and Chinese used lampblack and natural polymer mixtures as inks which is a first case of manmade colloidal dispersions [6]. Macosko suggested a size range from ∼1 nm (10^{-9} m) to ∼1 μm (10^{-6} m) for colloidal particles [7]. While the smaller size limit is required to consider the suspending medium as a continuum on the time and length scale of colloidal motion, the upper size limit is critical to observe thermal forces in defining the colloidal particles motion.

2.2.1.1 Brownian Motion

Mewis et al. stated that the fundamental unit of energy in a colloidal suspension is thermal energy [7]. The thermal energy has been defined as k_BT, where k_B is Boltzmann's constant (1.381×10^{-23} JK^{-1}) and T is the absolute temperature (K). The colloidal particle forces considered as Brownian force, is defined in terms of the thermal energy as

$$F^B = k_BT/a \qquad \textit{(Eq. 1)}$$

For a particle with radius a = 1 μm, the colloidal particle force is on the order of 4×10^{-15} N.

Perrin evaluated the motion of colloidal particles (also named Brownian particles) [9]. The colloidal particles move permanently in a random pattern because of Brownian force. As particle size decreases, Brownian motion plays a more important role compared to other forces.

2.2.1.2 Interparticle forces

Hiemenz investigated the effect of fluctuating polarization on the colloidal particles [10] [11]. The electron cloud polarization of one atom by the fluctuating electron cloud of another atom leads to dispersion forces: that is the interaction between atoms and molecules. An attractive force between the atoms has been induced by this fluctuation polarization, most of the time. A similar effect has been observed in colloidal particles whereby the atoms of one colloid particle create polarization in the atoms of another colloidal particle. The fluctuating polarization influence is described as the London-van der Waals force between the particles. A plot of the London-van der Waals force is shown in Figure 1 (dashed line) [7]. Hiemenz also described the electrostatic potential in colloidal particles [10] [11]. A double layer of positively charged counter ions covering a negatively charged surface has been illustrated in Figure 2 [7]. The thick line in Figure 1 presents the electrostatic potential.

The two colloidal particles interact in close distance where their respective electrostatic fields overlap (Figure 3). Each colloidal particle is considered electro-neutral with its associated counter-ions. In solution, the osmotic repulsion increases because of the excess number of ions in the surrounding double layer. This osmotic pressure neutralizes this overconcentration of counter-ions and the colloidal particles will be repelled from each other.

Derjaguin et al. [12] and, independently, Verwey et al. [13] discovered the linear addition of the dispersion attraction potential to the electrostatic repulsion potential to describe the complicated behavior of colloidal

dispersions. Figure 1 depicts the combined potential, the DLVO potential $\phi^{DLVO} = \phi^{d} + \phi^{el}$, for a typical system. The combined curve displays, with enhancing separation distance, an initial minimum, an electrostatic barrier, and a secondary minimum. Particles that are originally separated experience a long-range attraction. The particles will flocculate if the secondary minimum is adequately deep. This secondary flocculation is reversible, by means of shear.

Maranzano et al. investigated the steric repulsions induced by grafted or adsorbed polymers [14]. It is shown that grafted polymers can provide thermodynamic stability to dispersions. Conceptually, an end-grafted polymer brush and end-grafted polymer brush system are depicted in Figure 4. With sufficient graft density and molecular weight, particles can be prevented from aggregating by the steric repulsion. The absolute value of the potential induced by the polymers is not a uniform reduction function of the inter-particle distance. In contrast to the van der Waals forces and the electrostatic repulsion potentials, steric hindrance presents a more abrupt change from its characteristic value near the particle surface, to zero at a particle distance equal to the effective length of the polymers and is a purely geometrical phenomenon.

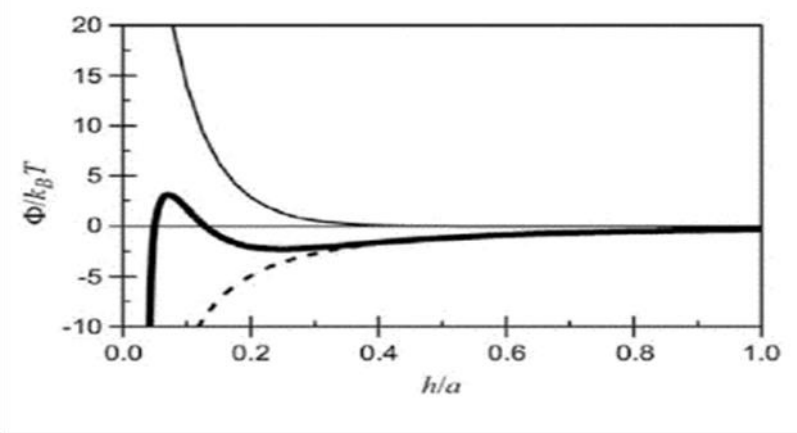

Figure 1. Interaction (DLVO) force for spherical colloid particles. The total force present as solid line, constituting of the London-van der Waals force (dashed line) plus the electrostatic force, (thin line). Figure from [7].

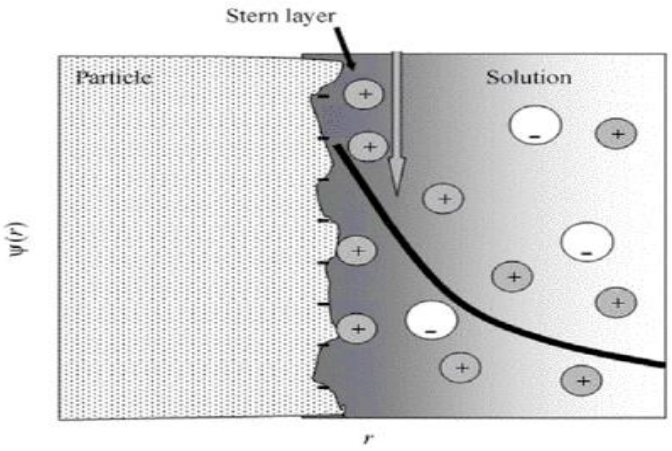

Figure 2. A double layer schematic in solution at the surface of a colloidal particle [7].

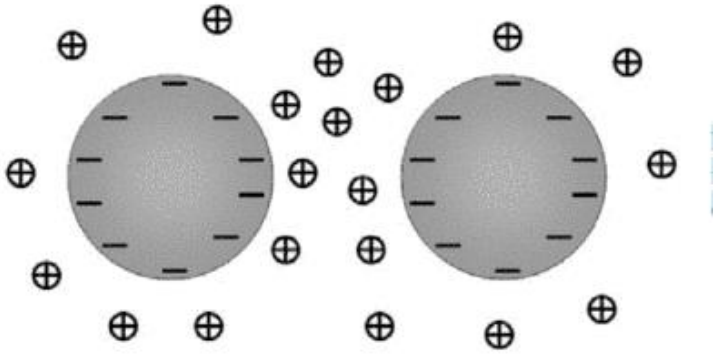

Figure 3. The corresponding ion distribution presented in two similar colloidal particles [7].

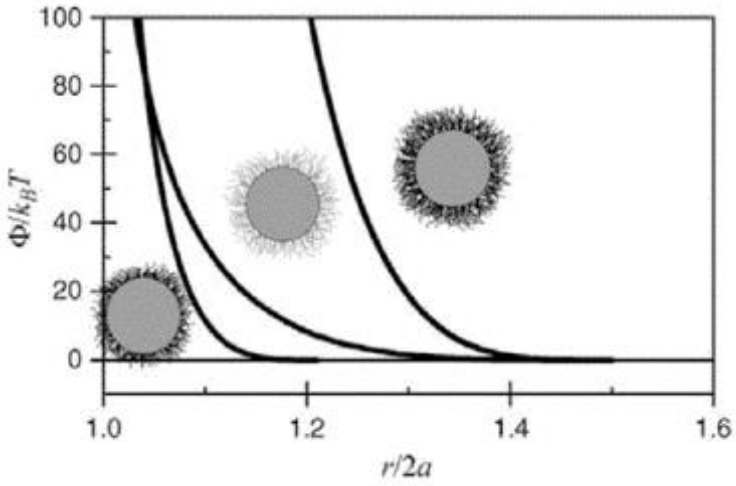

Figure 4. Potential of interaction because of steric repulsion between grafted polymer brushes of different length and different graft density [14].

2.2.2 Hydrodynamic forces

Non-colloidal particles have been characterized in dimensions of a few micrometers or more. In suspensions of non-colloidal particles, the contributions to the suspension stress from Brownian motion and from interparticle forces such as electrostatic interactions can be neglected. However, for colloidal and non-colloidal particles, the hydrodynamic effects are significant in many occurrences.

The existence of particles distorts the flow field which enhances the energy dissipation during flow, and therefore increases the viscosity. In suspension rheology, evaluating a dilute suspension of spherical particles is the easiest problem. Einstein calculated the energy dissipation in a sphere of radius R around the particle, as R→∞ by equation 2 [15] [16]. Only the flow field close to the surface of the particles requires to be known to calculate the additional energy dissipation created by the presence of particles.

$$\eta = \eta_m(1 + 2.5\,\phi) \qquad \textit{(Eq. 2)}$$

The suspension viscosity is in proportion to the viscosity of the suspending medium. As the system is dilute and particles do not interact with each other, the contributions of the individual particles are additive and the

viscosity is linear in particle concentration. Only the particle volume fraction enters the equation while the size of the particles is not relevant because absolute length scales do not enter the equation. The factor 2.5, calculated by Einstein is only valid for special conditions: no slip at the particle surface, spherical particles, and absence of particle interactions [15] [16].

Mewis and Wagner consider suspensions with volume fractions of more than 0.15 as concentrated [7]. Enhancing the volume fraction results to a more rapid increase in viscosity and, finally, the formation of a paste or solid. Concentrated systems of particles are a complicated problem due to evaluation of many-body hydrodynamic interactions. In order to resolve the many-body hydrodynamic interactions, different researchers perform particle simulations using various levels of approximation, from Stokesian by Brady and Bossis [17] and Sierou and Brady [18], lattice Boltzmann by Ladd [19] and Chen and Doolen [20] or dissipative particle dynamics by Martys [21], through to extremely intensive methods employing boundary integral representations by Kim and Karrila [22].

Brady and Morris [23] presented particle simulations to evaluate the trajectories of a relatively small number of particles by solving the equations of motion concluding hydrodynamic interactions. Ball and Melrose [24] demonstrated by increasing the particle volume fraction, the particles dramatically cluster together. Dratler and Schowalter [25] simulated a short-range repulsive force to exist between the particles to avoid clustering. In fact, a type of shear ordering at high packing fractions has been observed in simulations for non-Brownian suspensions of spheres. Sierou and Brady [26] reported a flow-induced string formation at volume fractions above 0.50.

Chong et al. presented the viscosity in concentrated suspensions as a function of the maximum volume fraction [27]. Viscosities increase rapidly when increasing the volume fraction. Maximum volume fraction ϕ_{max} is a good scaling factor for the viscosity-concentration curves of suspensions as has been shown in Figure 5. The actual value of ϕ_{max} depends on shape, size distribution, and packing protocol. The maximum volume fraction ranges from 0.524 by Shapiro and Probstein [28] to 0.71 by De Kruif et al. [29] for colloidal particles. Scott and Kilgour [30] and Torquato et al. [31] computed the random close packing (RCP) for identical spheres. RCP is a good measurement to estimate realistically the highest volume fraction that still flows. By compacting particles and by computations a value of approximately 0.64 is presented for random close packing of identical spheres.

The most-commonly used model to predict the viscosity of a concentrated suspension is the Krieger-Dougherty model (eq. 3) [32], in which φ is the volume fraction, φ_{max} is the maximum packing density, η_r is the relative viscosity, which is the ratio between the viscosity of the suspension and the viscosity of the medium, and $[\eta]$ is the intrinsic viscosity. The latter parameter is the value Einstein's equation would take if the volume fraction approaches zero, taking into consideration the shape of the particles.

$$\eta_r = \frac{\eta_s}{\eta_m} = (1 - \frac{\varphi}{\varphi_{max}})^{-[\eta]\varphi_{max}} \qquad \textit{(Eq. 3)}$$

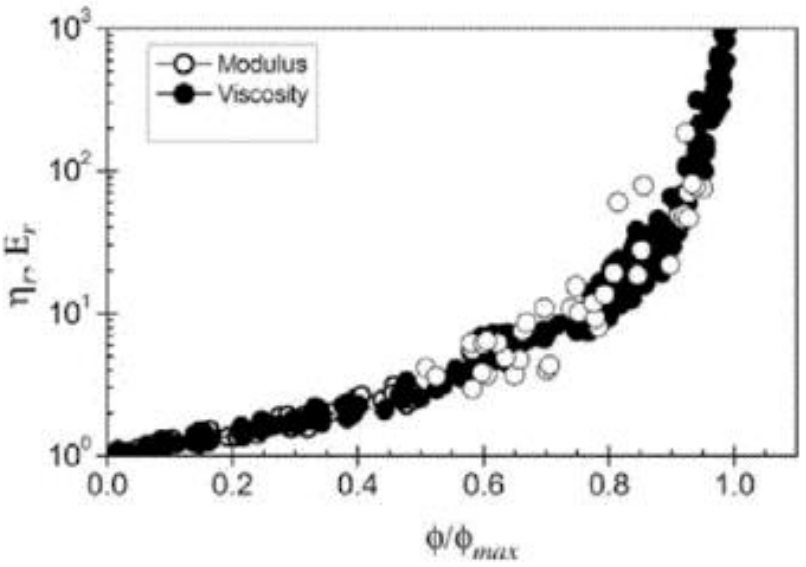

Figure 5. Reduction of the concentration dependence of the relative viscosity η_r and the relative elasticity modulus E_r, using the maximum packing. Figure from [33].

2.2.3 How do these forces affect rheological behavior?

One of the main consequences of the Krieger-Dougherty model is that the addition of particles does not alter the main rheological behavior of a fluid: a Newtonian fluid remains Newtonian. For lower volume fractions, this is generally true, but for higher volume fractions, the aforementioned forces show more interaction and cause differences in rheological behavior due to the presence of the particles.

2.2.3.1 Shear-thinning

Brownian motion in colloidal suspensions causes the particles to be in a randomly dispersed state [7]. Shearing can cause particles to order, align, or deform (in case of soft particles) in the flow direction and this effect is observed immediately [7]. Any of these effects causes a decrease in macroscopic viscosity with increasing shear, which is the definition of shear-thinning. Rheologists typically introduce a zero-shear and infinite-shear viscosity to distinguish between the two extremes [7].

2.2.3.2 Shear-thickening

Multiple causes for shear-thickening have been identified, including grain inertia [34], dilation and hydrocluster formation [35]. Grain inertia is the momentum transfer between sufficiently large particles. Dilation occurs when particles need to move perpendicular to flow direction in order to pass each other. Hydroclusters are temporary assemblies of particles in colloidal suspensions, acting as a solid body in the flow.

2.2.3.3 Yield stress

Figure 1 shows a simplistic view of the total interaction forces between two colloidal particles. It displays a secondary minimum, an energy-well [7]. If a particle gets sufficiently close to another, it can be attracted to it by means of that energy-well. If Brownian motion is sufficiently large to overcome this potential difference, the particles will freely enter and leave this secondary minimum and no major consequence on the flow behavior can be observed. However, if this energy-well is sufficiently deep and Brownian motion cannot exit the particle from this energy-well, it is trapped until an external force is high enough to carry it out of the well [7]. This external force is a typically a shearing force. As such, a minimum shearing energy is required to remove the particle from the secondary minimum to start flow, which is the definition of a yield stress.

2.2.3.4 Thixotropy

Thixotropy is defined as the gradual decrease in viscosity with time when a shear stress or shear rate is applied and the subsequent recovery when that stress or shear rate is removed [36] [7]. Ketchup is a prime example of a thixotropic material. It is caused by the same mechanism as the yield stress, but it has a time-dependency to the effect, as the energy maxima and minima are a complicated distribution in space and are dependent on time.

The consequence of thixotropy is that the rheological properties depend on the applied shear rate [36] [7] [37]. Considering a generalized thixotropy model for colloidal suspensions, a scalar variable λ is introduced to reflect the internal structure of the suspension, as represented in eqs. 4 and 5 [7].

$$\tau(\dot{\gamma},\lambda) = \lambda \cdot \tau_0 + \lambda \cdot K_{st} \cdot \dot{\gamma}^n + K_\infty \cdot \dot{\gamma}^n \qquad \textit{(Eq. 4)}$$

$$\frac{d\lambda}{dt} = -k_1 \cdot \dot{\gamma} \cdot \lambda + k_2 \cdot \dot{\gamma}^m \cdot (1-\lambda) + k_3 \cdot (1-\lambda) \qquad \textit{(Eq. 5)}$$

When the suspension is completely dispersed, λ = 0, when it is completely flocculated, λ = 1. The general model shows the dependency of the yield stress on λ, as theoretically, if there is no flocculation, there is no yield stress (first term in RHS of eq. 4). The shear rate term is split in two parts, reflecting a "viscosity" at infinite shear rate (λ = 0) (last term in RHS of eq. 4), and an increase in the viscosity term as a function of λ (middle term in RHS of eq. 4). λ itself is described to increase with time at rest (flocculation induced by Brownian motion) (last term in RHS of eq. 5), and to decrease with time with increasing shear rate (first term in RHS eq. 5). An intermediate term, typically only significant at low shear rates, enhances the build-up of the material (middle term in RHS of eq. 5). As a consequence, for each shear rate above the critical shear rate, which corresponds to the lowest shear rate for which dλ/dt can be zero [38], there is an equilibrium value of λ, and thus a set of constant rheological properties with time. However, changing the shear rate will change the equilibrium value of λ, and will create a new unique set of observed rheological properties. As such, to determine the rheological properties of a thixotropic suspension, one can await the equilibrium λ at each imposed shear rate and construct the equilibrium rheological curve (dashed line in Figure 6) [39]. However, this can be a time-consuming process, as dλ/dt needs to be equal to zero at each imposed shear rate. It has been generally accepted to bring the material first in its reference state, which corresponds to the highest applied shear rate, and thus the lowest λ value [37] [40] [41]. Once the reference state is reached, the measurement is executed quickly to minimize any effect of a non-zero dλ/dt. As a consequence, the higher the imposed shear rate, the lower λ, the lower the measured rheological properties at each shear rate compared to those determined at a higher constant λ (solid lines in Figure 6).

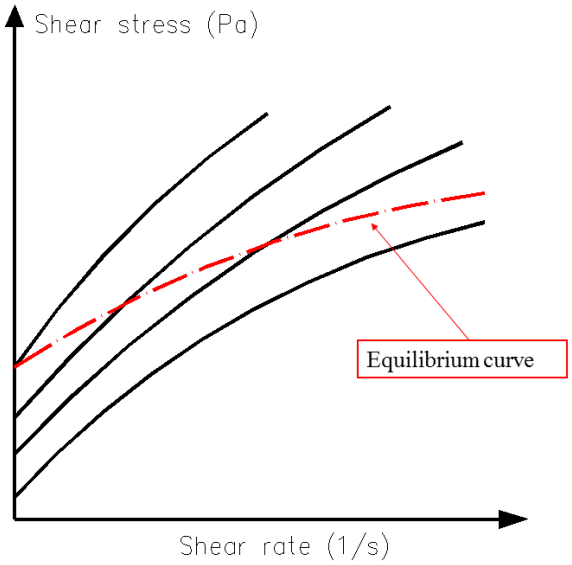

Figure 6. Dependency of rheological properties on the applied shear rate for thixotropic materials. The dashed line represents the equilibrium curve, for which $d\lambda/dt = 0$ at each measurement point. Each solid line correspond to a unique set of rheological properties at each reference state. The lowest curve corresponds to the highest applied shear rate. Figure after [39].

2.3 Rheology of cement-based materials

2.3.1 Steady-state rheological behavior

Cement-based materials are generally accepted to be yield stress fluids. However, the origin of the yield stress can be bi-fold dependent on the initial mix design. One potential source for yield stress is friction and dilation caused by the aggregates [42]. In this case, cement paste rheology plays a minor role, as the behavior of the mortar or concrete is dominated by the aggregate interactions. As the material behaves more or less as a soil, standard rheology techniques (like flow curve) are not suitable for this concrete type. In the other case, when concrete can be regarded as a suspension, the origin of the yield stress is in the cement paste, it is caused by interaction forces, as described in section 2.2.3.3. The presence of aggregates amplifies the yield stress of the material, following a model similar to Krieger-Dougherty [43] [44].

Concerning the flow curve, a large majority of cement-based materials exhibit linear, Bingham behavior, and the rheological behavior can be described by a two-parameter equation: Bingham's law (eq. 6) [45].

$$\tau = \tau_0 + \mu_p \dot{\gamma} \qquad \textit{(Eq. 6)}$$

In eq. 6, τ is the shear stress, τ_0 stands for the yield stress, μ_p is the plastic viscosity, and $\dot{\gamma}$ equals the shear rate. After taking into consideration several measurement artefacts which could cause errors in rheological measurements [40], several authors have discovered non-linear rheological behavior in cement paste, mortar or concrete [46]. This can be shear-thinning or shear-thickening, or a combination of both. Several different rheological models are suitable to describe the behavior, but the authors prefer the modified Bingham model [47] [48]: an extension of the Bingham model with a second order term (Eq. 7):

$$\tau = \tau_0 + \mu\dot{\gamma} + c\dot{\gamma}^2 \qquad \textit{(Eq. 7)}$$

It is beyond the scope of this research and this report to evaluate why certain mixtures show non-linearity, and which parameters influence this behavior. However, the non-linearity has been encountered and needed to be addressed to retrieve reliable rheological parameters. At some point, this has been proven not to be straightforward.

2.3.2 Time-dependent rheological behavior

The main complexity in understanding, predicting and applying the rheological behavior of cement-based materials is situated in the time (and shear) dependency of the properties. Following the distinction put forward by Wallevik, there are reversible and non-reversible connections between the particles. The former create the thixotropic part of the behavior, the latter cause the workability loss [3] [49]. However, as will be shown further in this report, the distinction between reversible and non-reversible is dependent on the applied shear. Figure 7 shows the evolution of the static (reversible) and dynamic (non-reversible) yield stress as a function of time [50]. It is generally known that the reversible increase in yield stress, at least within the first hours, is much larger than the irreversible increase.

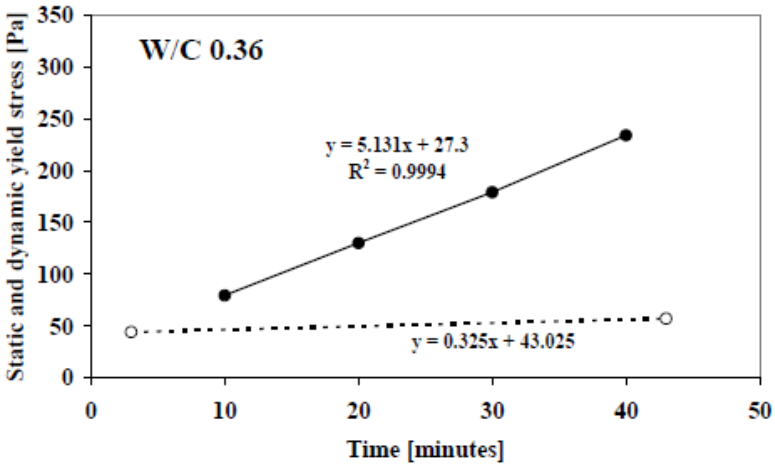

Figure 7. Linear increment in static yield stress over a time at rest. The solid line represents the static yield stress and the dashed line is the dynamic yield stress which only increases due to the workability loss [50].

Concerning the nature of these connections, there is substantial discussion in literature. The initial assumption by several authors was that the reversible connections are caused by flocculation: the effect causing thixotropy in colloidal suspensions, as described in section 2.2.3.4 [50] [51] [52] [3]. Although some authors argued that some of the flocculation bonds could be permanent (dependent on the applied shear) [3]. The non-reversible connections were said to be caused by hydration.

However, starting with Wallevik [49], inspired by Tattersall [53], the reversibility of hydration connections was considered. At first, Wallevik considered hydration connections which could only be broken once: at the first application of shear [49]. However, Roussel et al. have demonstrated that some early hydration connections can also be broken (and rebuilt) during shear [54]. In fact, a quick rise in yield stress at rest can be attributed to flocculation. After a couple of minutes of rest though, all possible flocculation has occurred and any further increase in yield stress is due to the formation of hydration products bridging cement (and other?) particles [54].

2.3.3 Mix design factors influencing thixotropic build-up

2.3.3.1 Water-to-binder ratio

Topcu and Uygunoglu [55] investigated effect of different binders with varying w/b ratio and superplasticizer (SP) content on yield stress of self-consolidating mortar. They reported that yield stress decreases and flowability increases with an increase in w/b ratio and SP content. Billberg [50] has also reported that with

an increase in w/b ratio from 0.34 to 0.42 the structural build-up, i.e. consequences of thixotropy, decreases by almost 80%. He mentioned that w/b ratio is related to the particle concentration and decreasing w/b lowers the interparticle distance, resulting in quicker structural build-up. Furthermore, Rahman et al. [56] stated that thixotropy increases with an increase in binder content when sand and coarse aggregate content is low. Also, w/b ratio influences the average distance between the particle and their interaction level, leading to increase in thixotropy with decrease in w/b ratio. Roby [57] indicated that an increase in w/b ratio increases the lubrication of cement paste and decreases the cohesiveness of the mixture. Assad and Khayat [51] [58] further stated that mixtures with higher w/b ratio and lower coarse aggregate proportion show a reduction in internal friction and increase the mobility of the mixture, yielding higher initial lateral pressure and slower thixotropy development. Thus, it is obvious that on increasing w/b ratio, thixotropy of concrete mixture decreases.

2.3.3.2 Cement properties

According to Nunes et al. [59], the workability is influenced by different cement deliveries and cement-superplasticizer interaction should be studied for different cement deliveries in SCC mixtures. The authors further mentioned that changes in rheological properties are mainly caused by differences in cement fineness and the sulphate amount of cement. Juvas et al. [60] reported the workability of mortars with superplasticizer is substantially more sensitive than for mortars without superplasticizer. Quanji [61] stated that cement pastes with high alkali content yield faster structural rebuilding rate potentially due to the increase in bond strength of particles by the pore solution chemistry. Also, it enhances prismatic crystal formation ability which enhances interlocking of microstructure and increases the structural rebuilding rate.

2.3.3.3 Effect of supplementary cementitious materials and mineral fillers

A small addition of nanoclay, which is a thixotropy enhancing material, has the ability to improve thixotropy [62]. Wang et al. [2] studied the thixotropy of cement paste with an increase in attapulgite clay (0.5%, 1%, 2%, 3%), a nanoclay, using a hysteresis loop method. Results showed that increasing the amount of attapulgite clay increases thixotropic development with time. The addition of attapulgite clay also increased thixotropy of cement paste combined with fly ash or in presence of HRWR (high-range water reducing agent) or AEA (air-entraining agent). Many researchers attributed the influence of nanoclay on improvement of thixotropy due to its surface charge [63], ability to absorb water [63], irregular microstructure [62], smaller size [64] [63] and specific surface area [64]. However, Kawashima et al. [65] reported that nanoclay has immediate effect on thixotropy due to flocculation mechanism, but this effect diminishes over a time.

Rahman et al. [56] studied the thixotropic behavior of SCC containing mineral additives and SCMs such as limestone powder (LSP), silica fume (SF), and fly ash (FA) by means of the static yield stress method proposed by Roussel [37]. They found a significant increase in thixotropy (A_{thix}) with an increase in the amount of fly ash amount from 5% to 10% whereas silica fume showed the opposite trend. LSP had less impact on thixotropy. All binary mixtures in the study [56] showed higher thixotropy index than the reference SCC mix because of higher fineness and structuration rate. Assaad and Khayat [66] investigated the thixotropic and rheological properties of SCC using silica fume (SF), fly ash (FA) and blast furnace slag (BFS). They reported that binary (PC + SF), ternary (PC + SF + FA) and quaternary systems (PC+SF+BFS+FA) showed lower plastic viscosity and higher thixotropy values compared to plain SCC mix during the initial 30 min. Later, after re-mixing a decrease in thixotropy was noticed in the quaternary mixture until 150 min.

2.3.3.4 Effect of dispersing admixtures (HRWRA)

There are some research studies available regarding the influence of superplasticizer on the development of thixotropy. Ore et al. [67] have shown the limited influence of incorporating a water-reducing agent on thixotropy. However, Ferron et al. [64] reported that the use of superplasticizer for adoption of a lower w/c in pastes is the most effective method to enhance the rate of structural build-up. Billberg [50] found that electrostatic hindrance mechanism of melamine SP showed more structural buildup than steric hindrance

mechanism of PCE (poly carboxylate ether)-SP. Adding a HRWRA to enhance workability was reported to increase formwork pressure and thus decrease thixotropy [57] [58], while for a given slump, reducing w/c ratio by using HRWRA developed similar formwork pressure as that of concrete made without HRWRA [57] [58]. Wang et al. [2] indicated that the addition of HRWR and AEA in cement paste made with FA and attapulgite clay decreases thixotropy and viscosity. Roussel et al. [68] have indicated that for a polycarboxylate-based superplasticizer, by increasing the amount of superplasticizer in the mixture, the structuration rate (A_{thix}) decreased.

2.3.3.5 Effect of viscosity-modifying admixtures (VMA)

Viscosity-modifying admixtures are mostly used along with a high-range water reducing agents to control cohesiveness and increase the stability [69]. The thixotropic behavior of cement pastes is related to the interactions between solid particles and the water medium containing chemical admixtures such as HRWRA and VMA [56] [59] [60]. Thixotropic properties were measured by considering the influence of HRWRA and VMA combinations on concrete-equivalent-mortar with equivalent fluidity and by using a parallel plate rheometer [70]. Results [70] showed that powder or liquid polysaccharide-based VMAs develop greater initial static shear stress needed to breakdown the structure after resting time compare to cellulose-based VMA. On the other hand, a higher degree of flocculation has been reported in mixtures containing combinations of VMA with naphthalene-based HRWRA compared to combinations of VMA with polycarboxylate-based HRWRA [70]. In addition, Assaad and Khayat [51] indicated that in SCC made with w/b of 0.36 and ternary cement (6% silica fume, 22% Class F fly ash, and 72% Type 10 (GU) Portland cement), combining cellulose based VMA with PCE-HRWRA led to higher thixotropy compared to mixtures containing polysaccharide-based VMA and poly-naphthalene sulfonate (PNS) HRWRA.

Assaad and Khayat [71] concluded that combination of cellulose-based VMA along with polycarboxylate-based HRWRA increased the degree of thixotropy of SCC compared to mixtures containing powder or liquid polysaccharide-based VMA and naphthalene-based HRWRA. However, the SCC mixtures containing cellulose-based VEA with polycarboxylate-based HRWRA showed a lower rate of increase in thixotropy with time due to its fluidity retention property [71].

2.3.4 Mix design factors influencing workability loss

Cement hydration, mixture composition, and the interaction between the binder particles and chemical admixtures are dominant factors which influence the workability loss over time [72]. In addition, differences in the quantity and composition of superplasticizer influence the cement hydration process and thus affect the workability loss once more [73] [74] [75, 76]. Correlations between mixture compositions, the initial rheological properties of the cementitious system and the development of rheological properties over time have been investigated by several researchers [77, 78, 79, 80]. It is reported that the change of rheological properties as a function of time in cement-based materials is strongly influenced by superplasticizer type and dosage, w/cm, and cement type [79, 81]. Golaszewski and Szwabowski [79] concluded that the type and dosage of superplasticizers affect the rheological behavior of cement mortars. PCE superplasticizer makes mortars with lower workability loss compare to SNF superplasticizers. Zhang et al. [76] investigated the effect of polycarboxylate superplasticizer to cement ratio (Sp/C), water to cement ratio (w/c) and time on the rheological behavior of fresh cement pastes. For Sp/C from 0 to 2.0% and w/c ratio of 0.25 to 0.50, it has been indicated that with an increase in SP dosage, the initial flowability and flowability retention over time increase because of plasticizing and retardation induced by the superplasticizer. At low Sp/C, similar trends have been observed for yield stress and plastic viscosity, while in the case of high Sp/C, the yield stress and viscosity deceased over the elapsed time [76].

Petit et al. have investigated the of influence temperature on the evolution of rheological properties with time [82] [83]. When expressing the elapsed time as a function of the final setting time, nearly linear increases were found for the yield stress and viscosity. However, especially for PCE-based SP, the evolution of the

rheological properties with time could follow a more complex pattern when temperature was below a certain threshold, dependent on the mix design [82] [83].

2.4 Hydration of cement-based materials

From the previous paragraphs, it has become clear that the hydration plays an important role in the time evolution of reversible and non-reversible rheological properties. This section discusses a brief review of the hydration of cement in the early hours after water contact.

2.4.1 Hydration of cement

2.4.1.1 Tricalcium silicate (C_3S)

Kurdowski mentioned the importance of the tricalcium silicate hydration [84]. More than 60% of Portland cement clinker constitutes of tricalcium silicate. Furthermore, the tricalcium silicate hydration model considered as a fine model of cement reaction with water. During reaction of tricalcium silicate with water, calcium silicate hydrate (C–S–H) and calcium hydroxide (CH) is formed. This reaction is presented by the following equation:

$$2C_3S + 6H \rightarrow C_3S_2H_3 + 3CH \qquad \textit{(Eq. 8)}$$

Gartner et al. demonstrated a microcalorimetric curve of C_3S in isothermal conditions, the calcium ions concentration and the hydrated phases (Figure 8) [85]. The following stages determined on the calorimetric curve, specifically: the pre–induction (I), induction (II), Increase of hydration rate (III), reduction of hydration rate (IV) and small hydration rate (V) respectively.

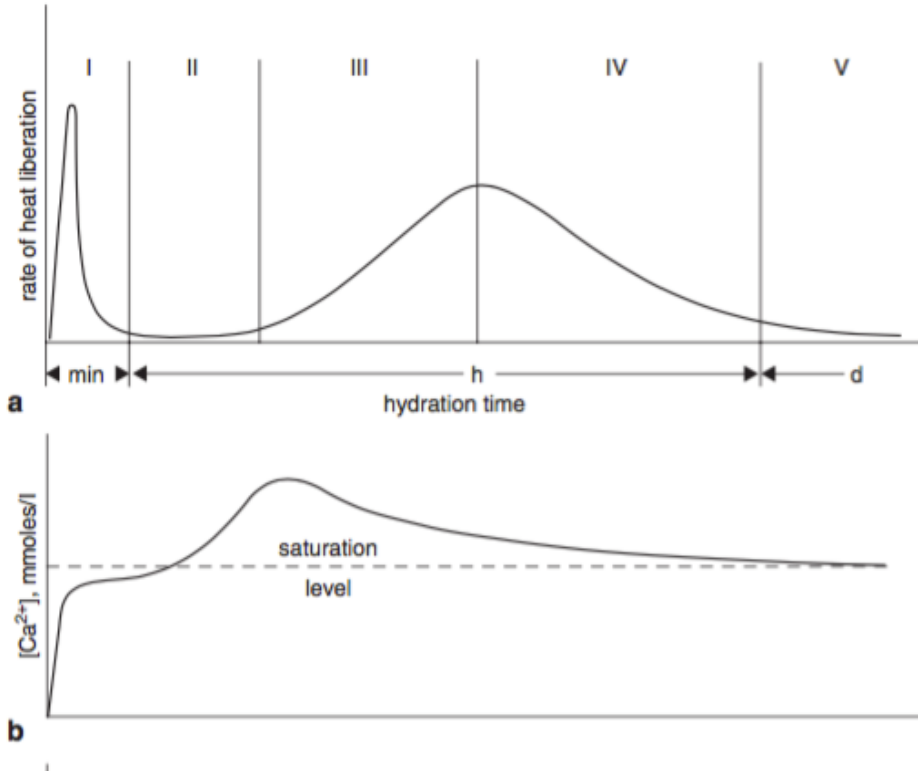

Figure 8. (a) Microcalorimetric curve of C_3S (b), variation of Ca^{2+} ions concentration in the water [85].

De Jong et al. proposed the hypothesis regarding the induction period [86]. In the induction period, a low permeable C–S–H layer that has a gel structure precipitated on the surface of C_3S. In addition, Fuji et al. and

Ménétrier et al. observed the C–S–H layer on the C_3S surface [87, 88]. At first, the nuclei reveal in spherical forms (primary C_3SH hydrate) that thereafter altered to the C–S–H II made the barrier layer. Finally the secondary C-S-H changed to the low C/S ratio hydrate (C/S = 0.8–1.5). In the lower C/S ratio, hydrate is more penetrable and concluded to end of induction period.

Kurdowski reported hydration of a few percent of C_3S at the end of induction period [84]. The enhanced reaction rate that begins after the induction period is strongly related to the sample fineness and the defects degree in C_3S structure. Ménétrier et al. reported the varying forms of C-S-H phase [88]. With concurrent change of C–S–H II to C–S–H I (fibers), the hydration of tricalcium silicate begins at high speed. CH reveals both on the C_3S surface and in the pores.

2.4.1.2 Hydration of tricalcium aluminate (C_3A)

Kurdowski reported that the highest rate of reaction with water among the clinker phases belongs to tricalcium aluminate [84]. As a consequence, tricalcium aluminate effects the initial rheological properties of cement paste. Gartner et al. showed the microcalorimetric curve and the mechanism of this process schematically in Figure 9 [85]. An induction stage is poorly distinguishable in the calorimetric curve after a rapid reaction with water. Ramachandran attributed this event to the hexagonal hydrates layer formation [89]. When the hexagonal hydrates layer break down during changing to the cubic C_3A H6, C_3A hydration no longer was interrupted by the hexagonal hydrates layers. This process related to the high heat of C_3A reaction with water and as consequently the paste temperature increase immediately.

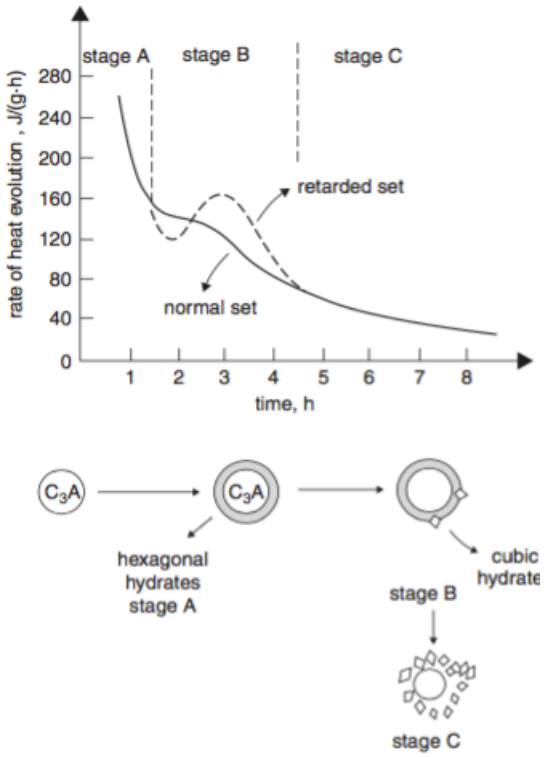

Figure 9. C_3A hydration in water without gypsum [85].

To avoid the immediate set of cement through the C_3A reaction, gypsum is typically added to transform the reaction and create ettringite. This reaction causes near-immediate precipitation of hydration products, which influences the efficiency of any added dispersing admixtures. After a couple of minutes though, the effect of the C_3A reaction should be diminished and should not contribute substantially to the changes in rheological properties with time.

2.4.2 Hydration influenced by supplementary cementitious materials

2.4.2.1 Fly ash

Takemoto et al. reported that the hydration of fly ash with C_3S is complicated [90]. Delays of the C_3S hydration at stages I and II are observed with presence of fly ash, while acceleration of the C_3S hydration at stage III and later is noted. The hydration of C_3S in presence of 30 % fly ash was investigated at a w/c ratio of 0.5. The XRD method was applied to determine hydration degree of C_3S [91]. The hydration degree of C_3S without fly ash after 24 hours was 35 %, while the blends with fly ash shown a hydration degree of 45%. It can be concluded that including fly ash increase the C_3S hydration at stage III. Skalny et al. [92] and Plowman et al. [93] reported that the hydration of C_3A has been delayed by fly ash. The retardation degree can mostly be related to the amount of sulphate in fly ash and potential of calcium adsorption.

2.4.2.2 Silica fume

Stein et al. reported the acceleration of the C_3S hydration in a cement-silica mixture with 20% by weight of silica fume [94]. Fine amorphous silica with a Brunauer–Emmett–Teller (BET) surface area of close to 200 m^2/g decreases the dormant length and enhances the magnitude of the second peak in the calorimetric curve because of the reduction of Ca^{2+} and OH^- concentration in the water. Beedle et al. identified the decrease of induction stage in cement-silica fume mixtures with silica fume a range of 50–380 m^2/g specific surface area [95]. When the silica fume with smaller surface area near 19 m^2/g was applied, the induction period did not decrease. Figure 10 presents that at first; the second peak magnitude enhanced by enhancing the silica fume fineness, while is reduced at very high surface areas.

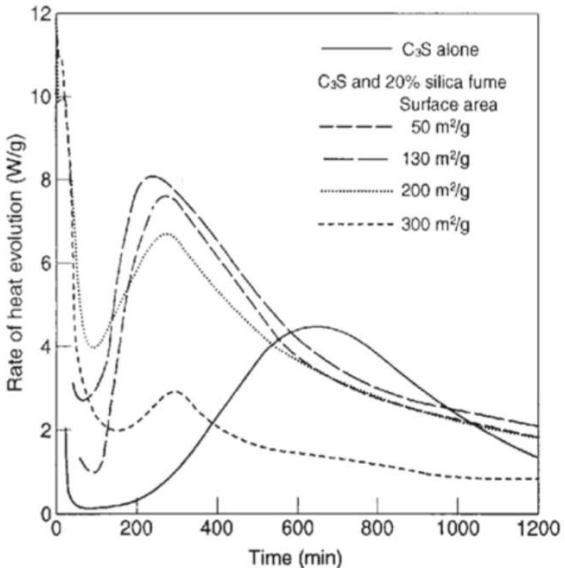

Figure 10. Calorimetric curves for the C_3S in presence of silica fume, comparing different surface area of the silica fume [95].

3 Materials and Methods

3.1 Materials

The following sections discuss the different constituent materials used in this cement paste study.

3.1.1 Cement

A commercially available type I/II ordinary Portland cement has been used throughout this research work. The density is 3160 kg/m^3 and the median particle size is around 15 μm.

3.1.2 Supplementary cementitious materials

The following supplementary cementitious materials (SCMs) were also used:

- Fly ash, at 25% replacement by mass, density 2700 kg/m^3, median particle size 10 μm.
- Silica fume, at 2.5% replacement by mass, density 2300 kg/m^3, median particle size 400 nm.

3.1.3 Chemical admixtures

Two commercially available dispersing admixtures (SP) were employed: both polycarboxylates from two different suppliers. PCE-1 has a density of 1.032 kg/l and a solid content of 26%. PCE-2 has a density of 1.07 kg/l and a solid content of 38%. Unless otherwise mentioned, the PCE dosage was adjusted to ensure a constant mini-slump flow of the paste of 330 mm. In select cases, the dosage was reduced to achieve mini-slump flow values of 300, 270, or 220 mm. Some mixtures did not contain any dispersing admixtures. Most mixtures were produced with PCE-1.

For two mixtures, a viscosity-modifying agent, compatible with each SP was used. VMA-1 had a density of 1.002 kg/l, while the second VMA had a density of 1.207 kg/l.

3.2 Mix design and mixing procedure

3.2.1 Mix designs

The reference mixture was composed of the cement, FA and silica fume, but to study the effect of each SCM, mixtures without either or both were also produced. In case a replacement of fly ash or silica fume was removed, the same volume of cement was added to keep the volume fraction of solids constant. The SP dosage was adjusted to keep the mini-slump flow constant. For the reference mixture (containing SiF and FA), the w/cm = 0.38. The reference mixtures were repeated four times to establish a confidence interval, and two additional repeats were performed at high (37°C) and low (7°C) temperature. The detailed mix designs can be found in Table 1.

Apart from this reference series, other mixtures were produced with altering water and SP contents. The primary goal of these series was to investigate the effect of these parameters on the thixotropy, workability loss and shear-induced breakdown. However, as not every mixture is suitable to be measured successfully in a rheometer, some adjustments were necessary, especially when mixtures without SP were considered. The following series were also investigated:

- Effect of water. Based on the pure OPC mixtures, the water contents were varied corresponding to changes of -5, +5 and +10 l/m^3 of the corresponding concrete, which corresponds to an increase or decrease with 14 or 28 g or water per liter of paste, respectively. The SP quantity was adjusted to keep the mini-slump flow constant.
- Effect of SP on pure OPC mixtures with + 5 water. The SP quantity was reduced to achieve mini-slump flow values of 300, 270, 220 mm, respectively. A mixture without SP was also investigated.

- Effect of SP on pure OPC mixtures with + 10 water. Similarly as the previous series, the SP quantity was adjusted to ensure mini-slump flow values of 300 and 270 mm. The mixture without dispersant had a mini-slump flow of 220 mm.
- Effect of SP on mixtures with FA. Similarly as above, the SP was adjusted to achieve a mini-slump flow of 330 and 270 mm, in addition to a mixture without SP. The water content was increase with 14 g/l ("+5") compared to the reference to ensure a useful measurement on less workable mixtures.
- Effect of SP on mixtures with SiF. This is the same as for the mixtures with FA, but with another increase in water content for workability: 28 g/l (or "+10").

For those second sets of mix designs, comparison can be performed within each series, but evaluating differences with other series is more complicated, although the results of the effect of mini-slump flow can be generalized qualitatively.

Table 1. Mix design of reference series of mixtures. Units in g/l. For the admixtures, the number indicates which producer was used.

	OPC	**FA**	**SIF**	**W**	**SP**	**VMA**	**MINI SF**
REF	989	342	34.5	520	1: 4.96		330 mm
OPC + FA	1035	341		519	1: 5.06		335 mm
OPC + SIF	1445		34.7	523	1: 6.56		315 mm
OPC	1498			520	1: 5.96		340 mm
REF + VMA 1	989	342	34.5	520	1: 4.48	1:0.84	310 mm
REF 2	898	342	34.5	520	2: 5.28		315 mm
REF 2 + VMA 2	985	341	34.4	518	2: 7.92	2: 0.84	330 mm

3.2.2 Mixing procedure

All mixtures were prepared in a small Hobart mixer in 1.5 liter batches. Table 2 shows the different steps in the procedure, in which mixing and scraping are altered to ensure the homogeneity of the sample. The contact time between cement and water is taken as the reference time. The starting time of the rheological measurements is relative to this reference time. The dispersing admixture (SP) is added in delayed fashion. The desired quantity is determined through preliminary tests, evaluating the mini slump flow for different dosages. If a VMA was used, it was added during the mixing step after the addition of the SP.

Table 2. Mixing procedure.

TIME	**DURATION**	**ACTION**	**ADDITION**
-0.5 min	30 s	Mixing	Dry materials
0 min	60 s	Mixing	Water
1 min	60 s	Scraping	
2 min	30 s	Mixing	
2.5 min	120 s	Mixing	SP
4.5 min	30 s	Scraping	
5 min	60 s	Mixing	

3.3 Rheological measurements on cement pastes

3.3.1 Measurement procedure

The rheological properties of the mixtures were evaluated with the Anton Paar MCR 302, in a sandblasted concentric cylinders configuration. The inner radius measures 13.33 mm, the outer radius was 14.56 mm and the height of the vertical portion of the inner cylinder is 40.00 mm. All measurements were conducted at 23°C, except when mentioned otherwise.

The measurement procedure consisted of multiple steps over a period of 90 min in an attempt to determine as many properties as possible on one sample during this period. Four sets of measurements were determined:

- At 15 min: Flow curve at 100 s^{-1}
- At 30 min: Static yield stress and flow curves at different shear rates
- At 60 min: Static yield stress and flow curves at different shear rates
- At 90 min: Static yield stress and flow curve at 100 s^{-1}.

The following sections discuss in detail the procedures for each property.

3.3.1.1 Static yield stress

The static yield stress was determined by imposing a shear rate of 0.001 or 0.005 s^{-1}, according to the rheometer software, and evaluating the maximum stress which was recorded. However, this method has not resulted in a peak stress systematically, which is typically expected within a couple of seconds. Figure 11 shows an example of an adequate measurement of static yield stress. Figure 12 shows a result from which no static yield stress can be derived. In some cases, like in Figure 12, the recorded stress continues to increase over time, indicating continuing structural build-up. Although more useful results are recorded with the larger imposed shear rate, it is no guarantee to obtain valid results. As such, the static yield stress measurement will not be used to evaluate the thixotropic properties.

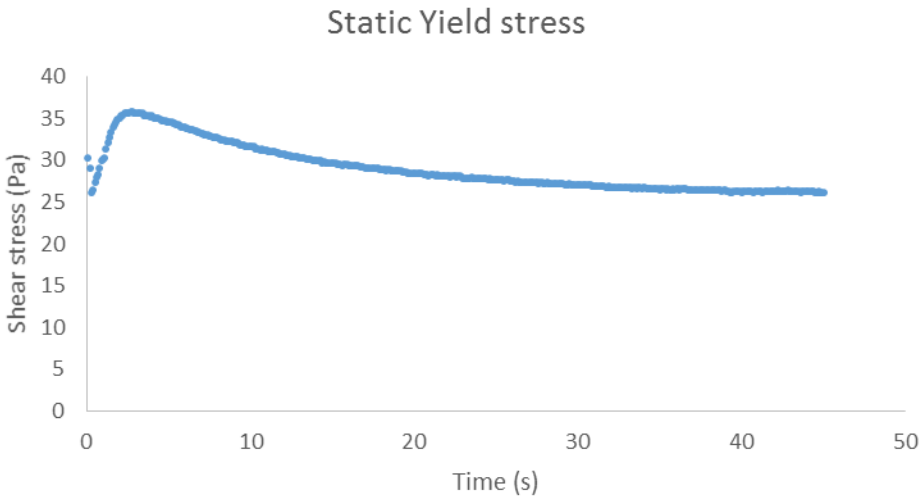

Figure 11. Example of a static yield stress measurement showing a clear peak shear stress.

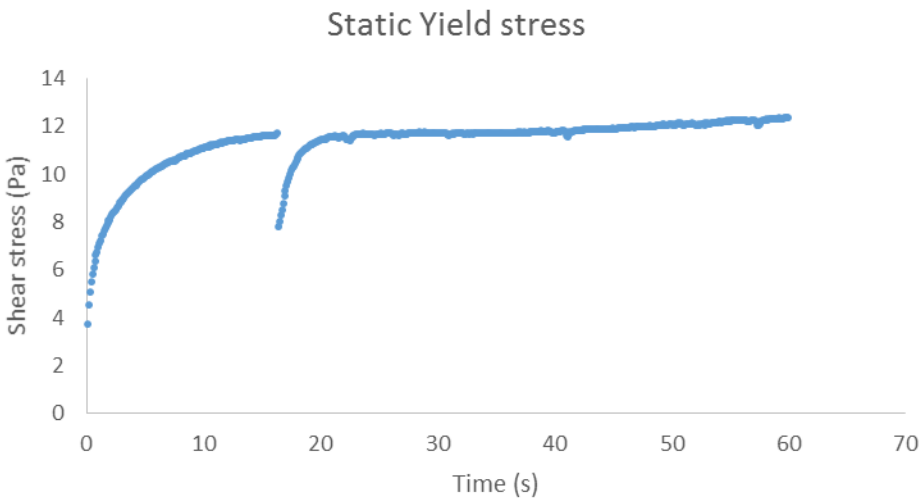

Figure 12. Example of a static yield stress measurement with no clear peak value.

3.3.1.2 Flow curve at 100 s^{-1}

The flow curves at 100 s^{-1} are determined by decreasing the shear rate from 100 to 5 s^{-1} in either 30 or 15 s. The flow curve is preceded by a pre-shear period at 100 s^{-1} for 90 s to break down any formed structure (at 90 min) or to impose the reference state at 15 min. It is assumed that the shearing in the rheometer is more intense than the mixing energy of the mixer. A typical breakdown curve is also observed at 15 min, partially validating this statement.

3.3.1.3 Flow curves at different shear rates

The flow curves at different shear rates are determined in the same way as the flow curve at 100 s^{-1}, but each time with a different maximum imposed shear rate. It is an 8-minute procedure, in which a pre-shear is maintained for 90 s, followed by a flow curve. This is repeated four times, each time with a new maximum shear rate. The imposed shear rates are 12.5, 25, 50 and 100 s^{-1}, in this order (Figure 13). As such, the breakdown and flow curve can be determined at each shear rate, reflecting the influence of each applied shear rate on the total structure of the paste.

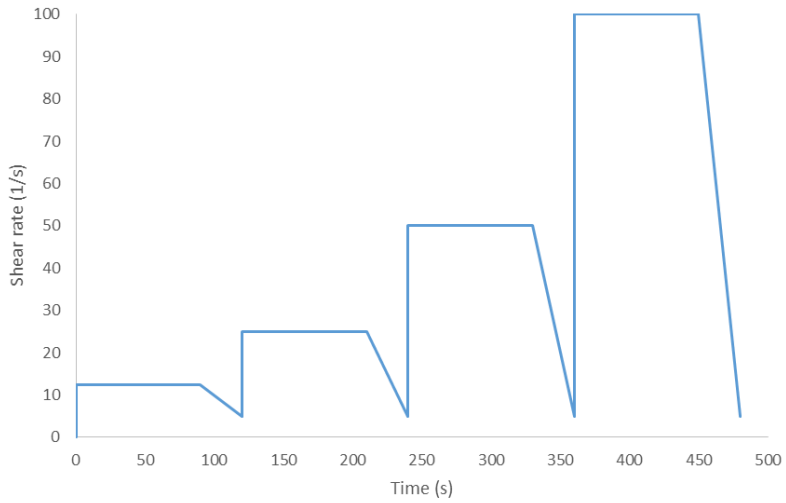

Figure 13. Applied shear rate profile to investigate the effect of different shear rates.

3.3.2 Determination of rheological properties

3.3.2.1 Static yield stress measurements

Static yield stress measurements can be plotted as a function of time, and the slope, A_{thix} could be an indication of thixotropic build-up. However, inherently connected to the procedure, one should not systematically plot the A_{thix} values, but should rather look into the increase of static yield stress with elapsed resting time (12 min for the measurement at 30 min, 21 min for the measurements at 60 and 90 min). Technically speaking, even the difference between the static yield stress and the previous dynamic yield stress should be used. On the other hand, as mentioned above, the static yield stress measurements did not always yield a useful result, and a systematic comparison of values is not possible. Therefore, the research team has abandoned the static yield stress method and has started a new measure to have an indication on the reversibility of the internal structure.

3.3.2.2 Flow curves at 100 s^{-1}

The flow curves at 100 s^{-1} were determined by plotting the shear stress as a function of the shear rate from the rheometer, and fitting the appropriate model. Although this goes against the best practices, this methodology has been retained due to the complexities observed for the flow curves at different shear rates. Verifications of the rheological properties, by using the relationship between torque and rotational velocity and the extended Reiner-Riwlin for the modified Bingham model, have been performed [48]. These indicated that for the performed measurements, the rheometer values for shear stress and shear rate are sufficiently close to the analytical solution from Reiner-Riwlin. The chosen model was the modified Bingham model, as numerous mixtures exhibit shear-thinning or shear-thickening behavior. The reported values are yield stress, μ and c, from which the differential viscosity is determined at the median of the interval as $\mu + 105c$.

Flow curves at 100 s^{-1} are determined at 15, 37, 67 and 90 min, and the parameters can be used as a measure for the workability loss, as the reference state is imposed at each measurement. Although some extrapolation issues have been encountered with the determination of the yield stress, for this purpose, the values are sufficiently reliable to draw conclusions. This can be done as the model determination and extrapolation is over the same range of shear rates for each measurement. As such, the increase in yield stress and differential viscosity are used as a measure for workability loss.

3.3.2.3 Flow curves at different shear rates

For the flow curves at different shear rates, initially, the same procedure was followed. The modified Bingham model was applied, the yield stress was extrapolated and the differential viscosity was determined at the median shear rate of the interval. However, the obtained parameters were not reflective of the flow curves (Figure 14). The differential viscosities were largely influenced by the shear thinning behavior, exaggerating the observed changes in viscosity. The extrapolated yield stress values delivered a similar issue. Due to the difference in shear rate range over which the modified Bingham model is applied, and the different extrapolation, the yield stress values were not reflective of the true behavior. Yield stress evolutions opposite to the flow curves were noted. Taking the example of Figure 14, imposing a modified Bingham model and extrapolating this to zero shear rate resulted in the lowest yield stress for the flow curve at 12.5 s^{-1} and the highest yield stress for the curve at 100 s^{-1}, totally opposite to the order observed in Figure 14.

One of the causes was the inadequate fit of the data by the modified Bingham model at the lower shear rate range for the flow curves at high shear rates, as the data over the entire domain was considered. Adjustments to determine the differential viscosity at 10 s^{-1} and the shear stress at 5 s^{-1} based on the modified Bingham model were also untrue to the reality, for the same reason. And determining a parameter based on a single point on the flow curve is never a good idea.

After many attempts, a very unconventional solution was found: a 6^{th} order polynomial was applied to the flow curve, to ensure an adequate fit. Based on this 6^{th} order polynomial, two parameters were determined:

- The average differential viscosity between 8 and 12.5 s^{-1}, determined by evaluating the derivative of this 6th order polynomial to the shear rate at each measurement point in this interval, and calculating the average.
- The shear stress at 5 s^{-1}, determined by evaluating the 6th order polynomial at 5 s^{-1}. Although a substantial error is induced by taking into account some of the viscosity, it is deemed to be the most reliable assessment of a parameter related to the yield stress.

Based on the average differential viscosity, the shear stress at 5 s^{-1}, and the modified Bingham differential viscosity at 10 s^{-1}, a comparison has been made. A first proposal was to plot the different viscosities and "yield stress" values as a function of the applied shear rate and determine the infinite shear viscosity and yield stress. However, due to a lack of data points (4), choice of profile (exponential or linear?), the results were not suitable for interpretation.

A second proposal was to take the ratio of yield stress and viscosity at a certain shear rate to the value at 12.5 or 100 s^{-1}. However, physically, the effects are additive (see Eq. 4), so the final choice was to calculate the difference between the rheological parameter at a certain shear rate and compare it to its counterpart at 100 s^{-1}. In this way, $\Delta\mu_{ave}$, $\Delta\mu_{diff}$ and $\Delta\tau_5$ were calculated as the difference in average differential viscosity between 8 and 12.5 s^{-1} from the 6th order polynomial, the difference in differential viscosity at 10 s^{-1} based on modified Bingham and the difference in shear stress at 5 s^{-1} based on the 6th order equation, respectively, between a property at a certain shear rate and its value at 100 s^{-1}. Consequently, all $\Delta\mu_{ave}$, $\Delta\mu_{diff}$ and $\Delta\tau_5$ values at 100 s^{-1} are zero, and one would expect only positive values at lower shear rates.

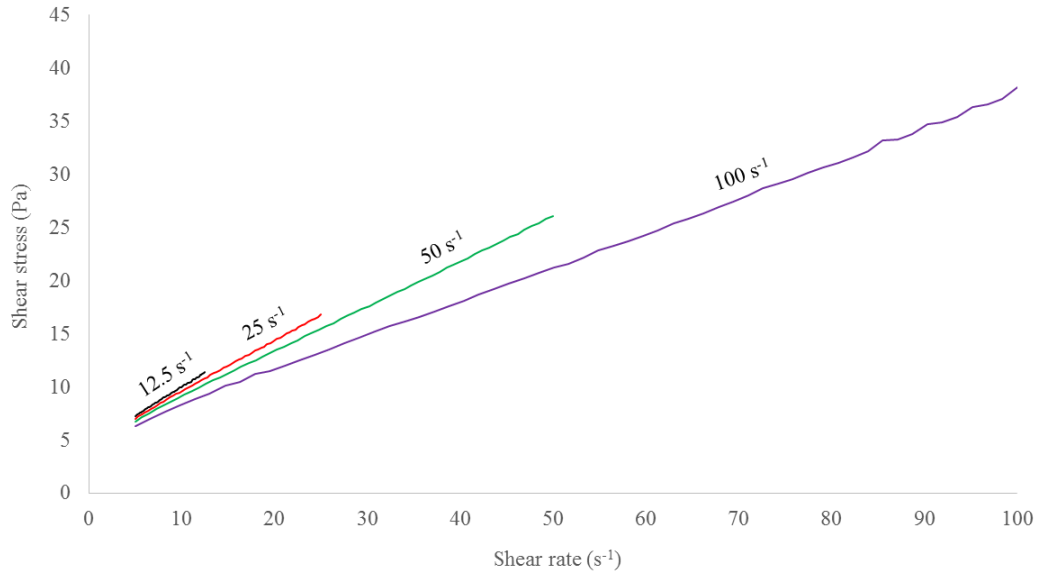

Figure 14. Typical result for flow curves at different shear rates.

3.3.2.4 Pre-shear curves

The pre-shear curves contain also a valuable source of information: it can quantify how much structure is broken (or rebuilt) during the preshear period. Therefore, a decreasing exponential curve of the format:

$$\tau(t) = Ae^{-Bt} + C \qquad \textit{(Eq. 9)}$$

With A, B and C fitting constants. Of interest is the difference between the first and the last point of the pre-shear curve. However, a point-to-point analysis would be too sensitive. However, one can evaluate the shear

stress at 1 s of the pre-shear period by means of eq. 9 and subtract C, the equilibrium value at the end of the pre-shear period. To compare results at different shear rates, one can calculate the change in apparent viscosity by dividing the above determined difference in shear stress by the applied shear rate. As such, one gets $\Delta\eta$, the difference in apparent viscosity between the beginning and end of each pre-shear period.

As will be shown in the results and discussion, the majority of the breakdown occurs at 12.5 s^{-1}, one can use the difference in shear stress between the beginning and the end of the first pre-shear period as a measure for the reversibility of the connections. In this report, this will be used as an alternate for the determination of thixotropy.

4 Results and Discussion

4.1 Evolution of rheological properties with time

4.1.1 Workability loss

4.1.1.1 Repeatability

The first analysis includes the evolution of yield stress and viscosity with time. Table 3 and Table 4 show the results of modified Bingham yield stress and differential viscosity determined at 52.5 s^{-1} for the reference mixtures. It shows a good repeatability for both yield stress and viscosity, indicating that a difference larger than 10 mPa/min for the yield stress and 1.5 mPas/min for the viscosity are significant.

Table 3. Change in yield stress with time (in mPa/min), for the reference mixtures.

	YS SLOPE	YS @ 15 MIN	YS @ 30 MIN	YS @ 60 MIN	YS @ 90 MIN
REF 1	76.1 mPa/min	2.07 Pa	3.66 Pa	5.91 Pa	7.87 Pa
REF 2	70.1 mPa/min	2.00 Pa	3.29 Pa	5.40 Pa	7.30 Pa
REF 3	61.7 mPa/min	2.37 Pa	3.67 Pa	5.54 Pa	7.06 Pa
REF 4	70.5 mPa/min	1.79 Pa	3.06 Pa	5.27 Pa	7.09 Pa
AVERAGE	69.6 mPa/min	2.06 Pa	3.42 Pa	5.53 Pa	7.33 Pa
STDEV	5.95 mPa/min				

Table 4. Change in differential viscosity at 52.5 s^{-1} with time (in mPa/min), for the reference mixtures.

	V SLOPE	V @ 15 MIN	V @ 30 MIN	V @ 60 MIN	V @ 90 MIN
REF 1	3.87 mPas/min	0.200 Pas	0.281 Pas	0.400 Pas	0.493 Pas
REF 2	3.21 mPas/min	0.187 Pas	0.251 Pas	0.353 Pas	0.429 Pas
REF 3	2.29 mPas/min	0.209 Pas	0.275 Pas	0.321 Pas	0.393 Pas
REF 4	2.77 mPas/min	0.182 Pas	0.246 Pas	0.325 Pas	0.395 Pas
AVERAGE	3.04 mPas/min	0.194 Pas	0.263 Pas	0.350 Pas	0.427 Pas
STDEV	0.67 mPas/min				

4.1.1.2 Influence of temperature

Temperature is known to alter the viscosity and yield stress of cement pastes, but also to accelerate or slow down the hydration process. It is expected to see a faster increase in yield stress and viscosity at higher temperatures. Table 5 shows this very clearly, as with increasing temperature and increasing hydration rate, the yield stress increases much faster, and vice-versa. Similarly, Table 6 shows a faster increase in viscosity with increasing temperatures, but the tests at low temperature do not vary significantly compared to the reference values.

Table 5. Change in yield stress with time (in mPa/min), for the reference mixtures at different temperatures.

	YS SLOPE	YS @ 15 MIN	YS @ 30 MIN	YS @ 60 MIN	YS @ 90 MIN
REFS	69.6 mPa/min	2.06 Pa	3.42 Pa	5.53 Pa	7.33 Pa
REF HIGH T	244 mPa/min	3.69 Pa	7.61 Pa	14.45 Pa	22.13 Pa
REF LOW T	22.8 mPa/min	2.42 Pa	2.88 Pa	3.56 Pa	4.15 Pa

Table 6. Change in differential viscosity at 52.5 s^{-1} with time (in mPa/min), for the reference mixtures at different temperatures.

	V SLOPE	V @ 15 MIN	V @ 30 MIN	V @ 60 MIN	V @ 90 MIN
REFS	3.04 mPas/min	0.194 Pas	0.263 Pas	0.350 Pas	0.427 Pas
REF HIGH T	6.18 mPas/min	0.157 Pas	0.232 Pas	0.389 Pas	0.625 Pas
REF LOW T	3.36 mPas/min	0.154 Pas	0.363 Pas	0.415 Pas	0.448 Pas

4.1.1.3 Influence of admixture combinations

Employing different admixtures will deliver different results, depending on the molecular structure of the polymers. Especially the yield stress should be dependent on a change in dispersing admixture. Table 7 shows a much larger yield stress increase when switching from SP 1 to SP 2, although a substantially larger initial yield stress is also noted, despite the minor difference in mini-slump flow. The changing of the dispersing admixture has also resulted in a faster increase in viscosity, as shown in Table 8.

The use of a VMA will also induce changes dependent on the mechanism of action. VMA 1 caused a faster increase in yield stress and viscosity, while VMA 2 has the opposite effect. However, the change in SP dosage when incorporating VMA 1 with SP 1 was minimal, while a substantial increase in SP 2 dosage was required when using VMA 2. It could be that the change in SP dosage is overcoming the effect of VMA 2.

Table 7. Change in yield stress with time (in mPa/min), for mixtures with different admixture combinations.

	YS SLOPE	YS @ 15 MIN	YS @ 30 MIN	YS @ 60 MIN	YS @ 90 MIN
REFS	69.6 mPa/min	2.06 Pa	3.42 Pa	5.53 Pa	7.33 Pa
REF + VMA 1	101 mPa/min	4.29 Pa	6.49 Pa	9.48 Pa	12.00 Pa
SP 2	154 mPa/min	7.33 Pa	12.23 Pa	17.12 Pa	19.32 Pa
SP 2 + VMA 2	82.7 mPa/min	3.27 Pa	5.12 Pa	7.67 Pa	9.56 Pa

Table 8. Change in differential viscosity at 52.5 s^{-1} with time (in mPa/min), for mixtures with different admixture combinations.

	V SLOPE	V @ 15 MIN	V @ 30 MIN	V @ 60 MIN	V @ 90 MIN
REFS	3.04 mPas/min	0.194 Pas	0.263 Pas	0.350 Pas	0.427 Pas
REF + VMA 1	6.90 mPas/min	0.220 Pas	0.294 Pas	0.414 Pas	0.514 Pas
SP 2	7.25 mPas/min	0.287 Pas	0.478 Pas	0.735 Pas	0.835 Pas
SP 2 + VMA 2	3.49 mPas/min	0.331 Pas	0.395 Pas	0.500 Pas	0.594 Pas

4.1.1.4 Effect of SCMs

Silica fume is known to be more colloidal, causing quicker flocculation, and to accelerate the hydration reaction due to a quicker precipitation of hydration products. Furthermore, as silica fume particles sit in between cement particles, the average distance to be bridged to bond two particles together is reduced, which should lead to a quicker increase in rheological properties. Comparing the OPC to the OPC + SiF, and the OPC+FA to the reference mixtures clearly shows a much quicker increase in yield stress in presence of silica fume (Table 9). For viscosity though, in presence of fly ash, the viscosity increase seems to be accelerated with the use of silica fume, but this is no longer observed in absence of fly ash (Table 10). Fly ash, at this early age, is minimally reactive, and acts rather as a mineral filler, or as inert particles. Table 9 and Table 10 show, when comparing OPC to OPC + FA, and OPC + SiF to reference, that fly ash slows down the increase in yield stress and viscosity, with the only exception being the OPC + SiF vs. reference for viscosity. Also striking, for the selected materials and replacement rates, the effects of silica fume and fly ash cancel each other out in terms of workability loss. In general terms, it is expected that increasing the quantity of fly ash will cause a further decrease in workability loss, while for silica fume, the opposite is expected. However, this cannot be extrapolated too much, as the dosages of dispersing admixture need to change as well, which on their term could influence the behavior.

Figure 15 and Figure 16 summarize the results so far, showing that increasing temperature, adjusting dispersant type and omitting the fly ash are the most efficient ways to increase the yield stress faster with time, while increasing temperature and adjusting dispersant type are the main ways to increase viscosity faster with time. As a result, any study being performed on rheology and the increase in rheological properties with time will need to consider the strong temperature sensitivity, and that all results can be easily changed when changing admixtures.

Table 9. Change in yield stress with time (in mPa/min), for mixtures with different SCMs.

	YS SLOPE	**YS @ 15 MIN**	**YS @ 30 MIN**	**YS @ 60 MIN**	**YS @ 90 MIN**
REFS	69.6 mPa/min	2.06 Pa	3.42 Pa	5.53 Pa	7.33 Pa
OPC + FA	27.9 mPa/min	1.05 Pa	1.72 Pa	2.66 Pa	3.17 Pa
OPC + SIF	132 mPa/min	3.44 Pa	6.02 Pa	10.34 Pa	13.35 Pa
OPC	69.2 mPa/min	1.12 Pa	2.26 Pa	3.71 Pa	6.50 Pa

Table 10. Change in differential viscosity at 52.5 s^{-1} with time (in mPa/min), for mixtures with different SCMs.

	V SLOPE	**V @ 15 MIN**	**V @ 30 MIN**	**V @ 60 MIN**	**V @ 90 MIN**
REFS	3.04 mPas/min	0.194 Pas	0.263 Pas	0.350 Pas	0.427 Pas
OPC + FA	1.55 mPas/min	0.231 Pas	0.258 Pas	0.308 Pas	0.347 Pas
OPC + SIF	2.9595mPas/min	0.307 Pas	0.347 Pas	0.404 Pas	0.536 Pas
OPC	3.16 mPas/min	0.312 Pas	0.383 Pas	0.519 Pas	0.542 Pas

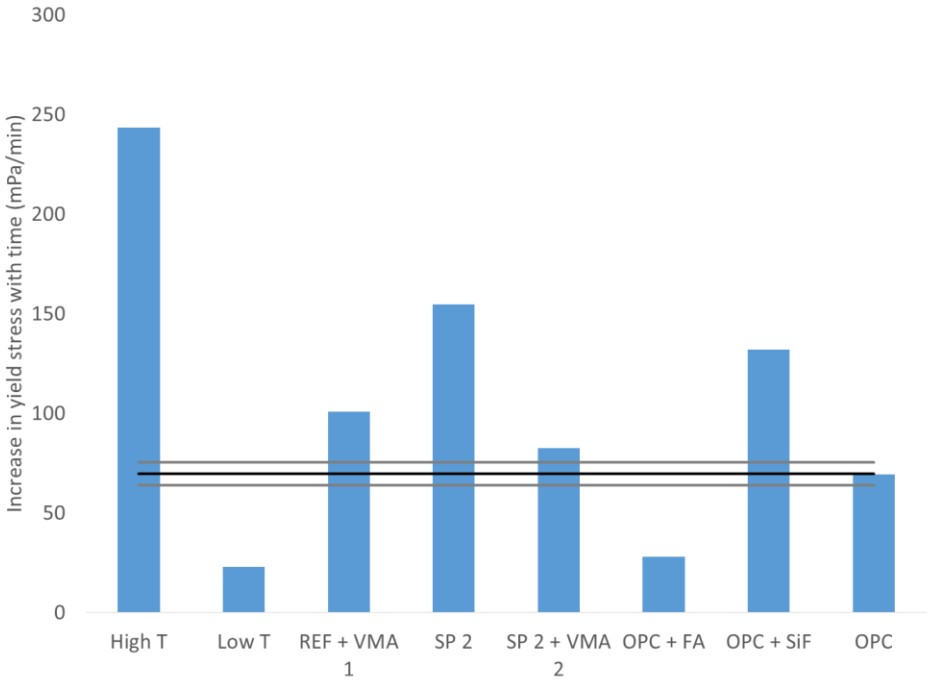

Figure 15. Summary for the increase in yield stress with time. The black line indicates the average of the four reference mixtures, while the gray lines represent the 95% confidence interval.

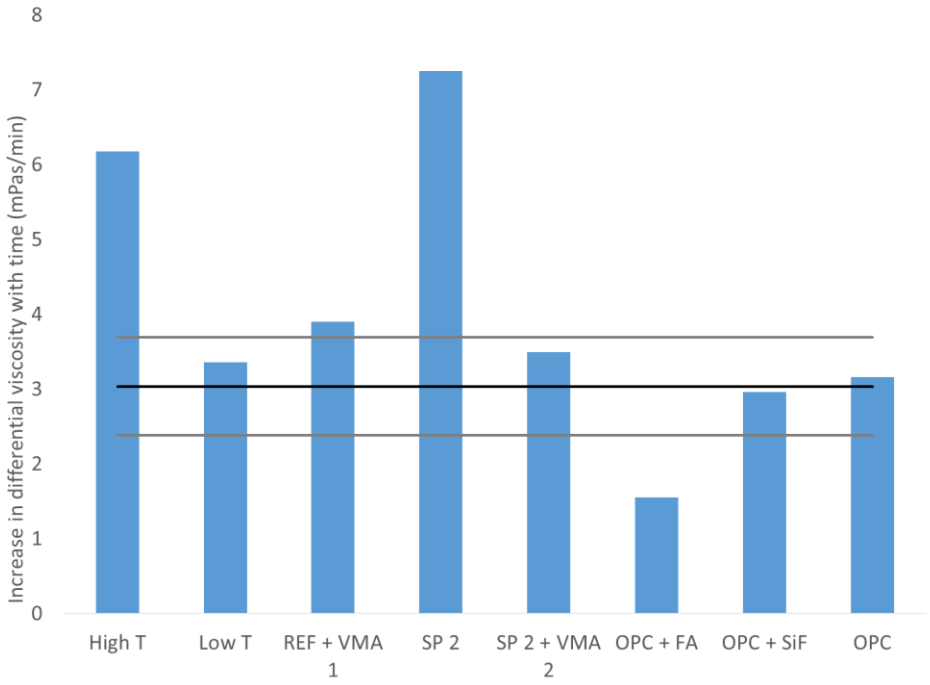

Figure 16. Summary for the increase in differential viscosity with time. The black line indicates the average of the four reference mixtures, while the gray lines represent the 95% confidence interval.

4.1.1.5 Water content

The influence of water content has been studied by means of mixtures with pure OPC, while keeping the mini-slump flow constant. The results are compared to the OPC mixture from section 4.1.1.4. Table 12 shows the effect of the water content on the change of viscosity with time, following perfectly the expectations: the lower the water content, the closer the cement particles, the easier to form connections between the particles, the quicker the viscosity increases. For the yield stress though (Table 11), the trend is similar, apart from the OPC mixture itself. Compared to the other results, the change in water content (5 or 10 l/m^3 in the equivalent concrete) does not cause substantially large changes, although larger variations are expected with more significant changes in water content.

Table 11. Change in yield stress with time (in mPa/min), for mixtures with different water contents.

	YS SLOPE	**YS @ 15 MIN**	**YS @ 30 MIN**	**YS @ 60 MIN**	**YS @ 90 MIN**
OPC	69.2 mPa/min	1.12 Pa	2.26 Pa	3.71 Pa	6.50 Pa
WATER -5	146 mPa/min	1.63 Pa	2.91 Pa	7.19 Pa	12.46 Pa
WATER +5	102 mPa/min	3.00 Pa	4.88 Pa	7.59 Pa	10.83 Pa
WATER +10	57 mPa/min	3.28 Pa	4.53 Pa	6.16 Pa	7.67Pa

Table 12. Change in differential viscosity at 52.5 s^{-1} with time (in mPa/min), for mixtures with different water contents.

	V SLOPE	**V @ 15 MIN**	**V @ 30 MIN**	**V @ 60 MIN**	**V @ 90 MIN**
OPC	3.16 mPas/min	0.312 Pas	0.383 Pas	0.519 Pas	0.542 Pas
WATER -5	3.66 mPas/min	0.590 Pas	0.580 Pas	0.695 Pas	0.851 Pas
WATER +5	2.42 mPas/min	0.204 Pas	0.232 Pas	0.301 Pas	0.385 Pas
WATER +10	2.17 mPas/min	0.140 Pas	0.177 Pas	0.241 Pas	0.304 Pas

4.1.1.6 Effect of SP dosage or mini slump flow

The effect of the SP dosage, reflected by the change in mini slump flow is investigated by four separate series. Two series only have OPC, but they have an increased water content of +14 and +28 ml/l, respectively. The two additional series contain either fly ash or silica fume, with increased water contents of +14 and +28 ml/l, as well. The water content selection was based on the availability to get results on a paste without SP.

Table 13 to Table 20 show the change in yield stress and viscosity increase for each series. Figure 17 and Figure 18 give an overview of the obtained values, and allow to sketch a trend in the results. For the yield stress, with decreasing SP dosage, generally, the yield stress increases slower with time (Figure 17). This makes sense, as less repulsive (electrostatic or steric) forces are in the system which can be decreased with an increased growth of hydration products. The change is in the same order as incorporating or omitting the SCMs, and can influence the results from the previous sections. For the viscosity, the opposite trend is observed: more SP causes a faster increase in viscosity, although these changes are minor compared to the change in temperature.

Table 13. Change in yield stress with time (in mPa/min), for mixtures with different SP contents for mixtures with pure OPC and +5 water content.

	YS SLOPE	YS @ 15 MIN	YS @ 30 MIN	YS @ 60 MIN	YS @ 90 MIN
SF 330	102 mPa/min	3.00 Pa	4.88 Pa	7.59 Pa	10.83 Pa
SF 300	82.2 mPa/min	3.71 Pa	5.57 Pa	8.26 Pa	9.92 Pa
SF 270	87.0 mPa/min	7.85 Pa	9.62 Pa	11.86 Pa	
SF 220	78.2 mPa/min	11.66 Pa	13.11 Pa	15.26 Pa	17.63 Pa
NO SP	83.0 mPa/min	14.61 Pa	17.38 Pa	20.12 Pa	21.05 Pa

Table 14. Change in differential viscosity at 52.5 s^{-1} with time (in mPa/min), for mixtures with different SP contents for mixtures with pure OPC and +5 water content.

	V SLOPE	V @ 15 MIN	V @ 30 MIN	V @ 60 MIN	V @ 90 MIN
SF 330	2.42 mPas/min	0.204 Pas	0.232 Pas	0.301 Pas	0.385 Pas
SF 300	2.11 mPas/min	0.236 Pas	0.295 Pas	0.409 Pas	0.385 Pas
SF 270	3.34 mPas/min	0.299 Pas	0.365 Pas	0.452 Pas	
SF 220	4.62 mPas/min	0.402 Pas	0.466 Pas	0.580 Pas	0.755 Pas
NO SP	3.79 mPas/min	0.660 Pas	0.763 Pas	0.903 Pas	0.945 Pas

Table 15. Change in yield stress with time (in mPa/min), for mixtures with different SP contents for mixtures with pure OPC and +10 water content.

	YS SLOPE	YS @ 15 MIN	YS @ 30 MIN	YS @ 60 MIN	YS @ 90 MIN
SF 330	57.2 mPa/min	3.28 Pa	4.53 Pa	3.16 Pa	7.67 Pa
SF 300	58.7 mPa/min	5.85 Pa	7.56 Pa	8.93 Pa	10.50 Pa
SF 270	43.0 mPa/min	8.51 Pa	9.77 Pa	10.76 Pa	11.93 Pa
NO SP	33.3 mPa/min	12.30 Pa	12.32 Pa	13.28 Pa	14.73 Pa

Table 16. Change in differential viscosity at 52.5 s^{-1} with time (in mPa/min), for mixtures with different SP contents for mixtures with pure OPC and +10 water content.

	V SLOPE	V @ 15 MIN	V @ 30 MIN	V @ 60 MIN	V @ 90 MIN
SF 330	2.17 mPas/min	0.140 Pas	0.177 Pas	0.241 Pas	0.304 Pas
SF 300	3.06 mPas/min	0.176 Pas	0.247 Pas	0.316 Pas	0.416 Pas
SF 270	2.81 mPas/min	0.208 Pas	0.273 Pas	0.345 Pas	0.426 Pas
SF 220	3.24 mPas/min	0.361 Pas	0.436 Pas	0.518 Pas	0.612 Pas

Table 17. Change in yield stress with time (in mPa/min), for mixtures with different SP contents for mixtures with OPC + FA and +5 water content.

	YS SLOPE	YS @ 15 MIN	YS @ 30 MIN	YS @ 60 MIN	YS @ 90 MIN
SF 330	59.7 mPa/min	6.20 Pa	7.98 Pa	9.21 Pa	11.00 Pa
SF 270	54.7 mPa/min	8.54 Pa	9.75 Pa	11.26 Pa	12.74 Pa
NO SP	49.5 mPa/min	10.90 Pa	11.44 Pa	12.73 Pa	14.63 Pa

Table 18. Change in differential viscosity at 52.5 s^{-1} with time (in mPa/min), for mixtures with different SP contents for mixtures with OPC + FA and +5 water content.

	V SLOPE	V @ 15 MIN	V @ 30 MIN	V @ 60 MIN	V @ 90 MIN
SF 330	2.68 mPas/min	0.200 Pas	0.264 Pas	0.322 Pas	0.411 Pas
SF 270	3.50 mPas/min	0.199 Pas	0.261 Pas	0.361 Pas	0.465 Pas
SF 220	4.47 mPas/min	0.319 Pas	0.418 Pas	0.537 Pas	0.664 Pas

Table 19. Change in yield stress with time (in mPa/min), for mixtures with different SP contents for mixtures with OPC + SiF and +10 water content.

	YS SLOPE	YS @ 15 MIN	YS @ 30 MIN	YS @ 60 MIN	YS @ 90 MIN
SF 330	54.6 mPa/min	2.43 Pa	3.29 Pa	4.91 Pa	6.54 Pa
SF 270	75.8 mPa/min	12.82 Pa	14.94 Pa	16.90 Pa	18.77 Pa
NO SP	33.5 mPa/min	17.12 Pa	17.59 Pa	18.21 Pa	19.73 Pa

Table 20. Change in differential viscosity at 52.5 s^{-1} with time (in mPa/min), for mixtures with different SP contents for mixtures with OPC + SiF and +10 water content.

	V SLOPE	V @ 15 MIN	V @ 30 MIN	V @ 60 MIN	V @ 90 MIN
SF 330	2.68 mPas/min	0.115 Pas	0.156 Pas	0.240 Pas	0.312 Pas
SF 270	3.50 mPas/min	0.167 Pas	0.228 Pas	0.320 Pas	0.415 Pas
SF 220	4.47 mPas/min	0.279 Pas	0.361 Pas	0.439 Pas	0.527 Pas

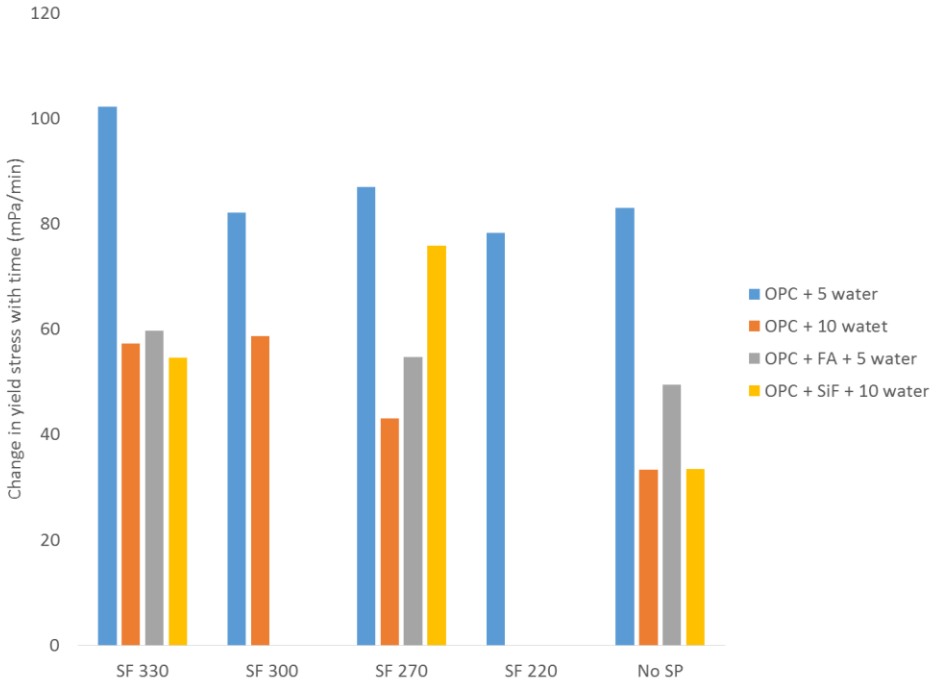

Figure 17. Overview of influence of initial mini slump flow on the change in yield stress with time.

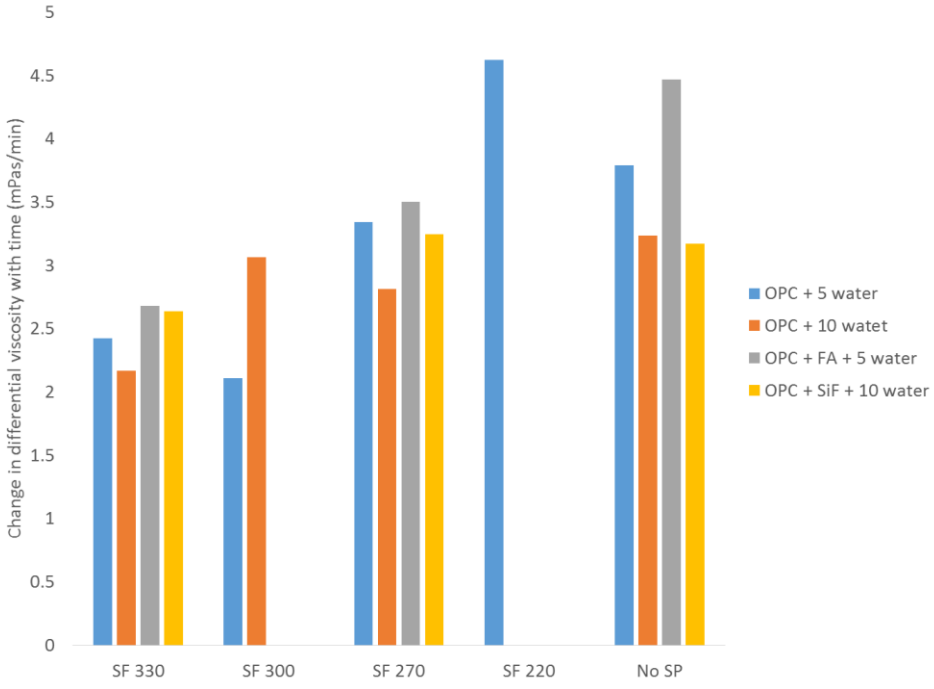

Figure 18. Overview of change in differential viscosity with change in initial mini slump flow.

4.1.1.7 Summary

The influence of the mix design on the workability loss of a set of flowable cement pastes has been investigated by means of the increase in yield stress and differential viscosity with time, up to 90 min. Of the parameters investigated and in the range of each parameter investigated, temperature appears to have the largest effect. Significantly higher increases in yield stress and viscosity were observed when increasing the

temperature from 23 to 37°C. Although the high temperature is relatively high compared to standard concrete operations, the effect of temperature is important. At least for the workability loss, temperature needs to be well-monitored and developed solutions for concrete workability might not work at a substantially different temperature.

Decreasing the dispersing admixture dosage is a parameter which generally reduces the increase in yield stress and increases the increase in viscosity with time, but its significance compared to temperature and admixture combinations is not as large. However, it should also be kept in mind that the yield stress values of a dispersed mixture do not exceed the yield stress values of a less dispersed mixture at the same time. So, although the difference between the values decreases with time, within the 90 min evaluated, the effectiveness of the SP is not canceled by the workability loss.

The workability loss is also influenced by the admixtures employed, due to differences in molecular structures and working mechanisms. Silica fume enhances the hydration process and those accelerates the workability loss, while fly ash acts rather as an inert system (this early in the process), and seems to slow down the workability loss. Increasing the water content slows down the workability loss.

4.1.2 Breakdown of structure

As discussed in section 3.3.2.4, A_{thix} values could not be adequately calculated, based on static yield stress data. Instead, a new strategy was proposed to evaluate the reversible build-up of structure: the pre-shear curve at 60 min of age and at 12.5 s^{-1} is used to determine the difference in shear stress at the beginning and at the end. Most of the breakdown happens in the first shearing interval, so it could be an adequate measure of the reversible build-up of structure. Following the exponential equation (eq. 9), the difference in shear stress is the new parameter for structural build-up.

Figure 19 shows the breakdown for shear stress for a series of mixtures. The black line represents the average of the four repeatability tests, with a breakdown of nearly 8 Pa at a shear rate of 12.5 s^{-1}. This is approximately 40% of the initial (peak) value. The gray lines represent the 95% confidence interval, showing that the measurement is quite repeatable.

The graph also shows the influence of temperature, as an increase in temperature results in approximately double the breakdown. A decrease in temperature appears to have no effect, but this is due to more breakdown happening at higher shear rates for the higher temperatures. Adding a VMA substantially increases the breakdown (and thus the rebuild at rest) for SP 1. SP 2 generates a larger breakdown as well, while adding VMA 2 does not substantially increase or decrease the breakdown value. However, it should be kept in mind that the amount of SP 2 was substantially increased when adding the VMA.

Omitting silica fume from the mixture substantially decreases the amount of breakdown and the amount of build-up, so silica fume is helpful in increasing thixotropy. One striking result though is that omitting the fly ash from the reference mixture causes a significant decrease in breakdown value, while for the mixture without silica fume, the omission of the fly ash does not have an effect.

Figure 20 shows the effect of small changes in water content on the breakdown value. It appears that changing the water content does not have an influence on the thixotropy. However, theoretically, increasing the water content should increase thixotropy. It could however be that the effect of a decrease in water content is compensated by the increase in SP. For the evaluated mixtures, both seem to cancel each other but it is uncertain whether this is generally true for larger changes in water content.

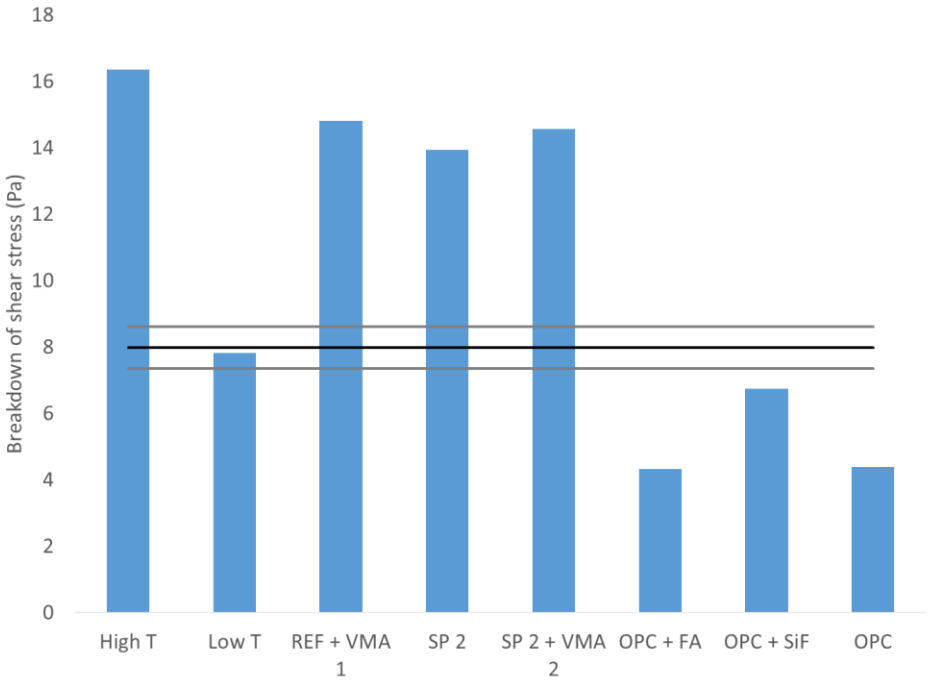

Figure 19. Breakdown of structure for reference mixtures (black line is the average of four, the gray lines are the 95% confidence intervals), and other parameters, such as temperature, admixture combination and SCMs.

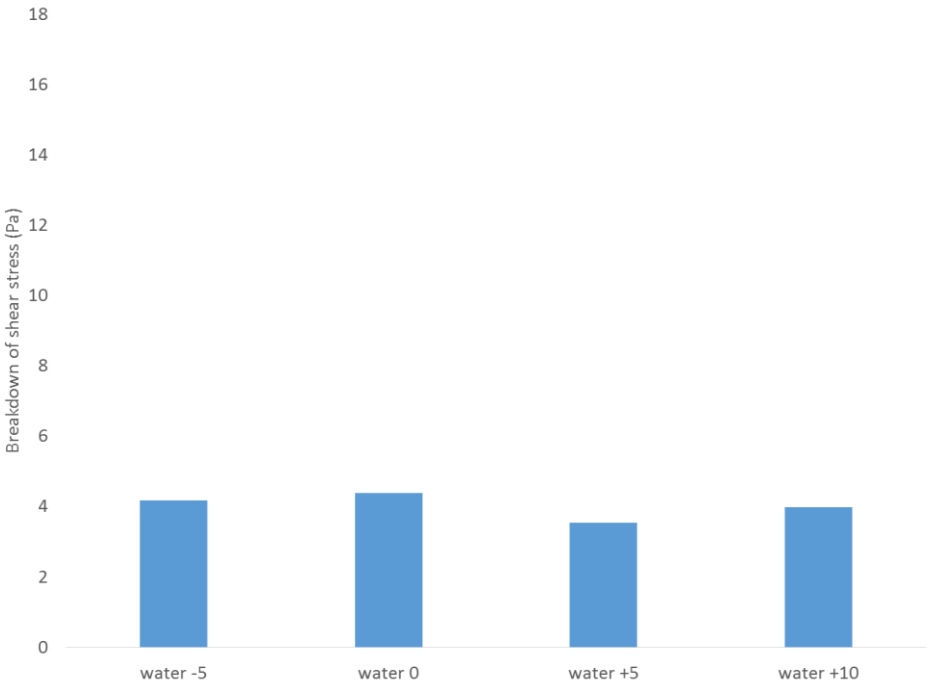

Figure 20. Breakdown of structure for mixtures with pure OPC and changes in water content.

Figure 21 shows the breakdown of structure with changing initial mini slump flow (and thus SP content), for the same mixture series as discussed in section 4.1.1.6. The general trend, which appears to be relatively

strong in comparison to other parameters, is that the breakdown substantially decreases with an increase in SP quantity. This confirms why the results in Figure 20 go against common knowledge.

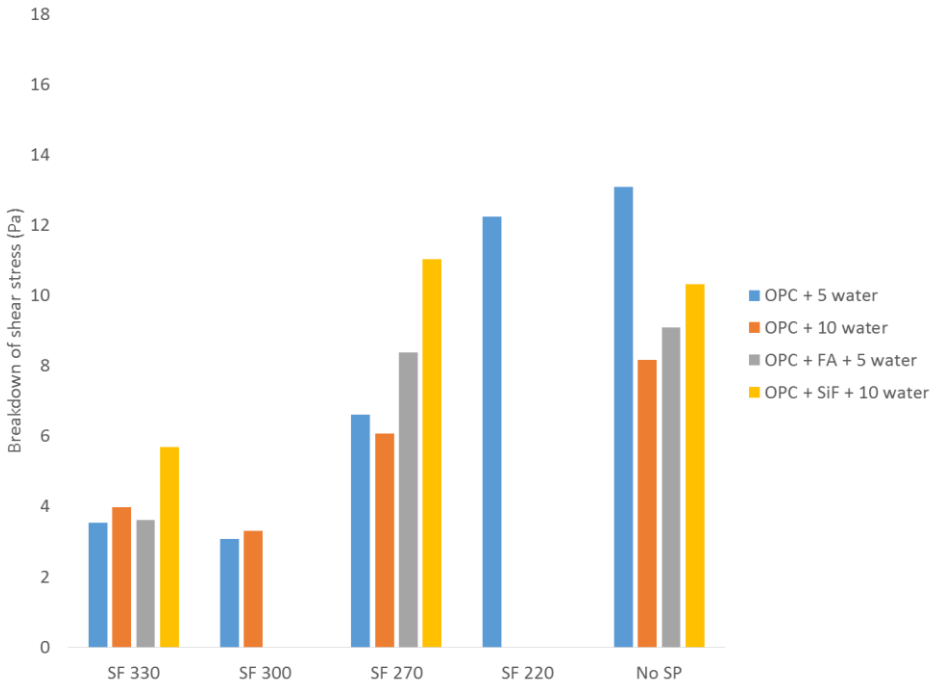

Figure 21. Breakdown of structure decreases with an increase SP dosage.

In summary, an alternative method was proposed to evaluate structural build-up and breakdown. Although not perfect, the proposed methodology gives a good indication of the parameters influencing build-up and breakdown. Temperature is still critical, similar as to workability loss, and a concrete mix design requiring certain time-dependent properties will need to be evaluated and if necessary adjusted to temperature.

The used PCE-based dispersing admixture is a thixotropy killer, while its effect on workability loss is not as significant. Hence, when developing a mixture which needs to be fluid and thixotropic at the same time, special attention will be required to the dispersing admixture. If some materials are used to enhance thixotropy which require a significant amount of dispersing admixture, results opposite to expectations may be obtained.

The influence of water was not visible in the results, but it is suspected that its effect is countered by the change in SP dosage. As different SPs deliver different thixotropy values, reconsideration of the admixture producer may require a reformulation of the mixture if certain properties are required. VMAs are helpful in increasing thixotropy, but the increase in SP dosage may counter this, as demonstrated for SP-VMA 2.

The use of silica fume appears very beneficial in the current study, but the same concern about higher dosages and increased dispersing admixture amounts are to be made. At which point does an increase in silica fume and SP dosage no longer contribute to the thixotropic build-up?

4.2 Shear-dependent properties

This section of the report discusses the influence of applied shear on the rheological properties of cement pastes. It follows the protocol discussed in sections 3.3.1.3 and 3.3.2.3. The results at 60 min are discussed due to a longer resting time allowing for more rebuild, and to ensure the C_3A reaction is no longer influencing the properties. At each shear rate, four parameters are discussed:

- $\Delta\eta$, which is the difference in shear stress at 1 s and at the end of each pre-shear period, divided by the applied shear rate. On each pre-shear profile at each shear rate, a curve in the form of Eq. 9 is fitted. This procedure has been used on the 12.5 s^{-1} pre-shear curves for thixotropy (except dividing by the applied shear rate), and is now applied on all shear rates. It shows, at each shear rate, how much structure is destroyed due to the (additional) application of shear.
- $\Delta\mu_{ave}$, which is the difference in average differential viscosity at the applied shear rate, compared to the value at 100 s^{-1}. The average differential viscosity is calculated based on the applied 6th order polynomial, between 8 and 12.5 s^{-1}. Each value shows the difference between the viscosity at the applied shear rate and the value at 100 s^{-1}.
- $\Delta\mu_{diff}$ follows a similar style as $\Delta\mu_{ave}$, but the value is based on the differential viscosity based on the modified Bingham model at 10 s^{-1}.
- $\Delta\tau_5$ accounts for the change in the value of shear stress at 5 s^{-1} at each applied shear rate, compared to the value at 100 s^{-1}. It is based on the 6th order polynomial and is the parameter closest to yield stress which is reliable.

4.2.1 General profiles and influence of temperature

Figure 22 shows the change in apparent viscosity in each pre-shear period ($\Delta\eta$). The black line represents the average for the four reference mixtures, the gray lines indicate the 95% confidence interval. As can be seen, a substantial amount of structure is broken at the first application of shear (12.5 s^{-1}). However, at each subsequent increase in shear rate, additional structure is broken. Care has been taken for the measurements that equilibrium is achieved at the end of each pre-shear period, so the breakdown at higher shear rates is effectively structure which could not be broken at the lower shear rate. As such, one can introduce the concept of "strength of connections" between particles, not only the number of connections. Figure 23 shows an example of the fitted pre-shear curves for one of the reference mixtures, clearly showing the larger breakdown at 12.5 s^{-1}, and the achievement of equilibrium at each step.

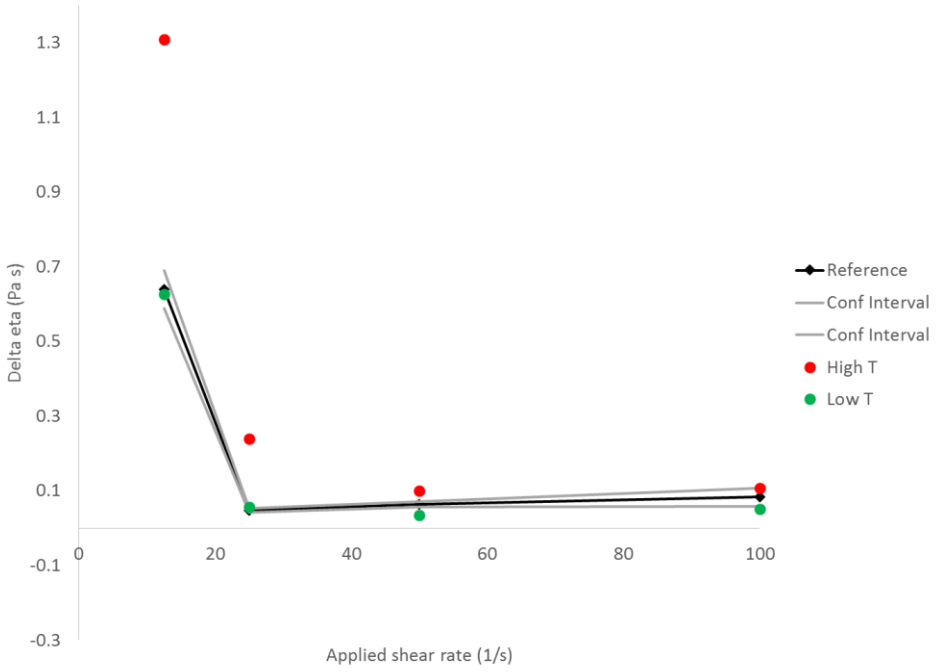

Figure 22. Δη for the reference mixtures (average in black, confidence interval in gray), and the reference mixtures at higher and lower temperature.

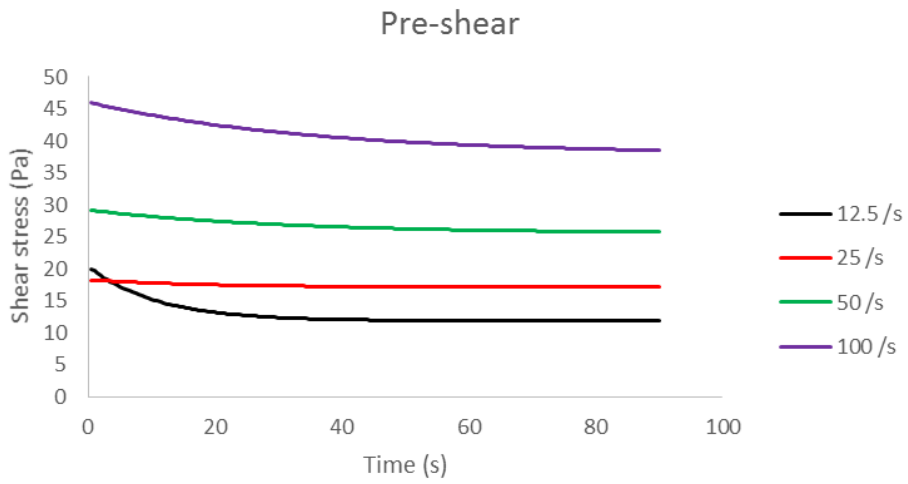

Figure 23. Fitted pre-shear curves for each of the applied shear rates, for one of the reference mixtures.

What also can be seen in Figure 22 is the influence of temperature. Higher temperature, which leads to accelerated hydration, causes larger breakdown values, especially at 12.5 s^{-1}. However, the difference of breakdown between the high temperature and the reference mixture at 25 s^{-1} is also remarkable, indicating that at higher temperature and probably extended resting time, not only more connections are created, but they are also stronger. The difference in structural breakdown between the reference mixture and the low temperature is insignificant at 12.5 and 25 s^{-1}, but less structure is broken at the higher shear rates when lower temperatures are imposed.

It should also be mentioned that the observed values for the change in apparent viscosity are not negligible. The average apparent viscosity at the end of the pre-shear period at 100 s^{-1} for the reference mixtures is approximately 0.4 Pa s. This means that the observed $\Delta\eta$ at 100 s^{-1} is approximately 15% of the final value.

One of the consequences of different connections breaking at different shear rates is that the rheological properties of the cement pastes at different shear rates should be different. Figure 24, Figure 25 and Figure 26 show the change in average viscosity, differential viscosity and shear stress at 5 s^{-1} respectively. Regardless of the flow curve parameter considered, a systematic decrease in rheological properties is observed with each additional increase in shear rate. And again, the change is not negligible. At 100 s^{-1}, μ_{ave} = 0.39 Pa s for the reference mixture. A $\Delta\mu_{ave}$ of 0.06, 0.11 or 0.16 Pa s, for the test at 50, 25 and 12.5 s^{-1}, respectively, is a substantially large change in viscosity.

Similarly to the results in Figure 22, an increase in temperature leads to larger differences in μ_{ave}, μ_{diff} and τ_5, which are substantially different from the values at reference temperature. Recalling the discussions on workability loss and thixotropy from sections 4.1.1.2 and 4.1.2, increasing temperature was the most significant factor. Similarly, the increase in temperature caused the largest changes in rheological properties due to applied shear, as more structure is built, it gets stronger, and more can be broken. Contrary to Figure 22 though, the lower temperature shows for each of the selected parameters a systematically lower change in rheological properties in Figure 24 to Figure 26.

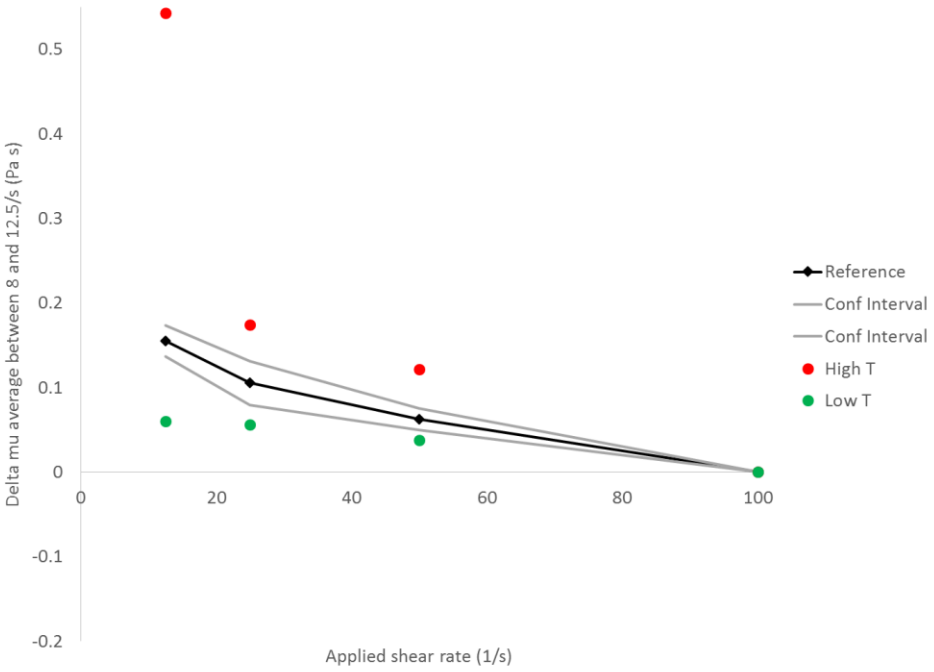

Figure 24. $\Delta\mu_{ave}$ for the reference mixtures and the mixtures at different temperatures.

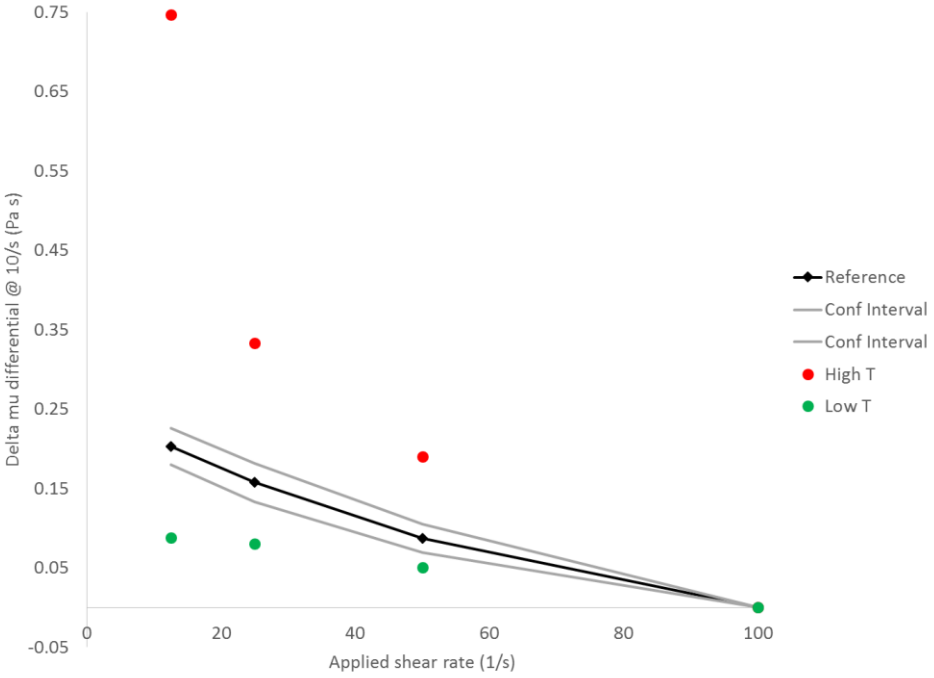

Figure 25. $\Delta\mu_{diff}$ for the reference mixtures and the mixtures at different temperatures.

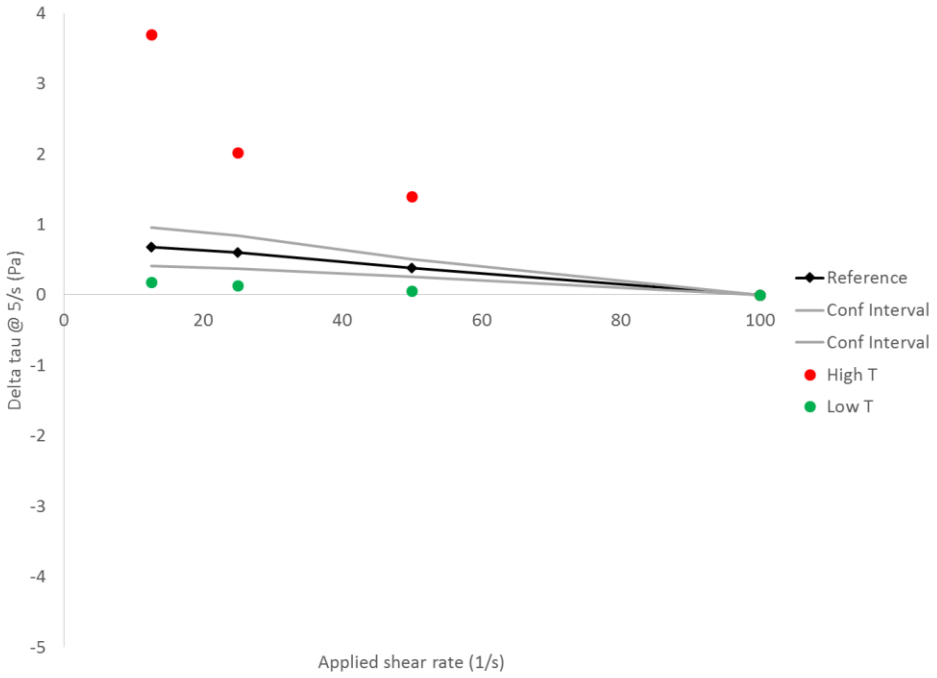

Figure 26. $\Delta\tau_5$ for the reference mixtures and the mixtures at different temperatures.

4.2.2 Influence of admixture combinations

As has been discussed in previous sections on workability loss and thixotropy, adding a VMA, or changing the dispersing admixture affects the time-dependency of the rheological properties due to changes in molecular architecture and working principles. Unfortunately, these latter properties are remaining a secret for these commercially available products. Hence, one can only compare if changing the admixtures has a significant influence, and to which extent it is significant. Figure 27 shows the change in $\Delta\eta$ when employing SP 1 with VMA 1, and SP 2 with and without VMA 2. Similarly to the discussions on workability loss and thixotropy, SP 2 enhances the sensitivity to time and to shear. The addition of VMA 1 also seems to increase the amount of breakdown at each shear rate, indicating more and stronger connections, while for VMA 2, based on Figure 27, the mixture shows more breakdown at each shear rate, except at 25 s^{-1}.

Figure 28 to Figure 30 show the changes in μ_{ave}, μ_{diff} and τ_5 for the mixtures with different admixture combinations. Similarly as in Figure 27, each of the VMAs caused larger changes in rheological properties due to the applied shear. The behavior of SP 2 is a bit more complicated. Figure 28 shows a larger change in viscosity compared to SP 1 for 25 and 50 s^{-1}, but a lower change at 12.5 s^{-1}. Furthermore, $\Delta\mu_{ave}$ is larger at 25 s^{-1} than at 12.5 s^{-1} for SP 2, which means that the viscosity has increased with increasing the shear rate. However, Figure 30 shows a much higher $\Delta\tau_5$ at 12.5 s^{-1}, potentially indicating that the yield stress has decreased considerably between 12.5 and 25 s^{-1}. Figure 31 shows the raw data for the flow curves for mixture SP 2, in which clearly the same trend can be observed as in Figure 14 for the reference mixtures. The flow curve at 12.5 s^{-1} is higher than the one at 25 s^{-1}.

Figure 29 shows also some deviations in values, compared to Figure 28, again for the mixture with SP-2. If there is a substantial difference in behavior between $\Delta\mu_{ave}$ and $\Delta\mu_{diff}$, the authors have the tendency to follow $\Delta\mu_{ave}$ preferentially. Again, $\Delta\mu_{diff}$ is determined by evaluating the differential viscosity at 10 s^{-1} based on the modified Bingham model applied to the entire data set. Figure 31 shows that the flow curve at 100 s^{-1} shows some severe shear-thinning, potentially leading to an inaccurate estimate of μ_{diff} at 10 s^{-1}.

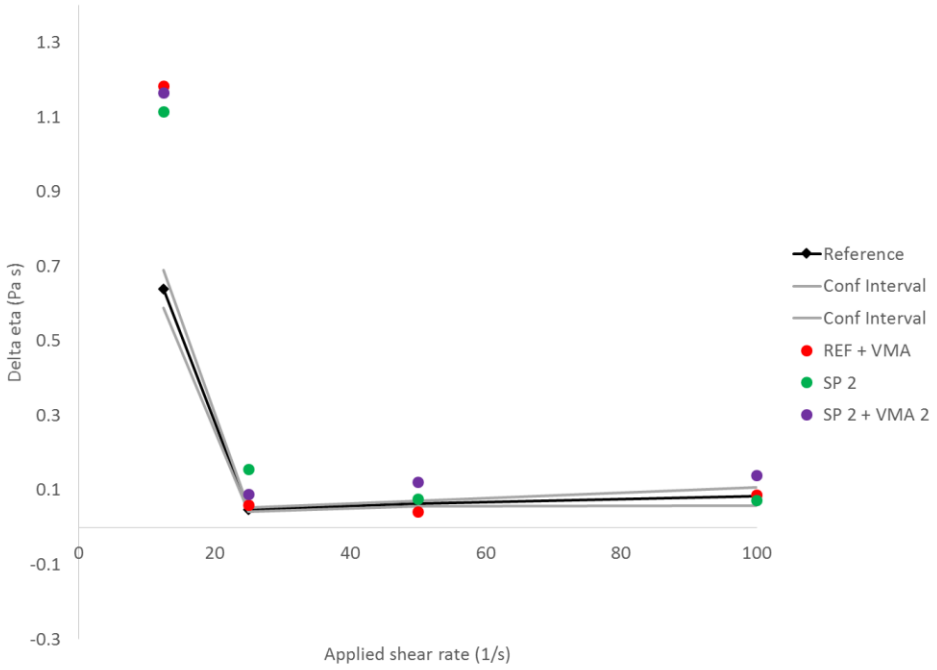

Figure 27. Δη for the reference mixtures (average in black, confidence interval in gray), and the mixtures with different admixture combinations.

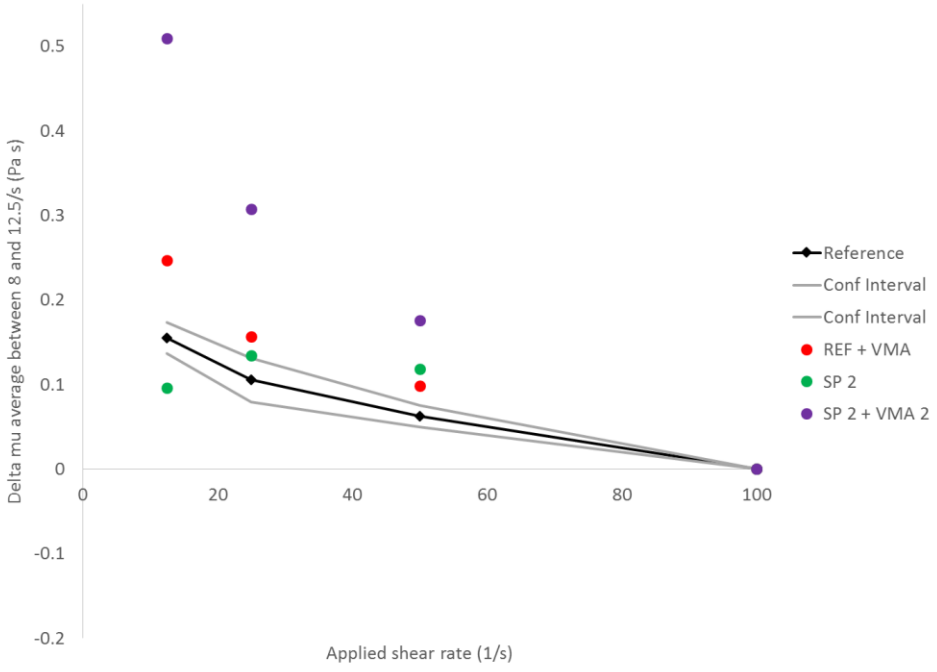

Figure 28. $\Delta\mu_{ave}$ for the reference mixtures and the mixtures with different admixture combinations.

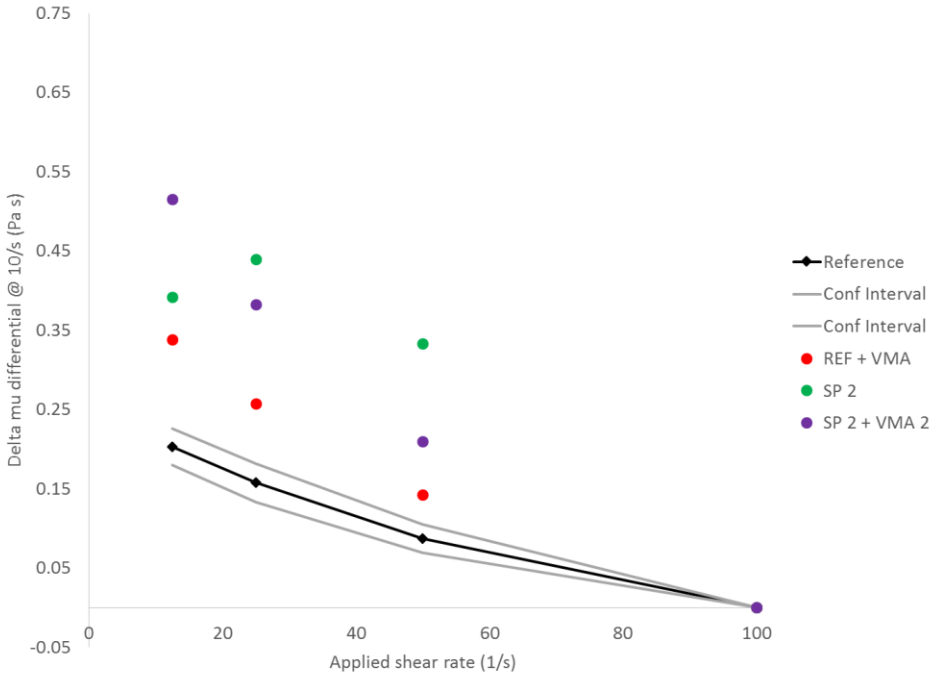

Figure 29. $\Delta\mu_{diff}$ for the reference mixtures and the mixtures with different admixture combinations.

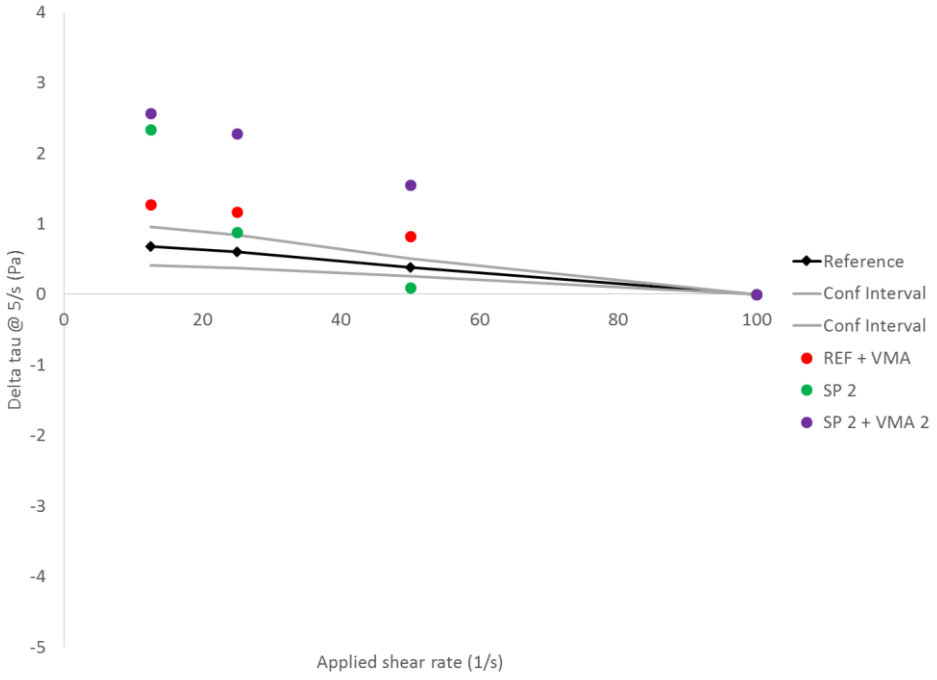

Figure 30. $\Delta\tau_5$ for the reference mixtures and the mixtures with different admixture combinations.

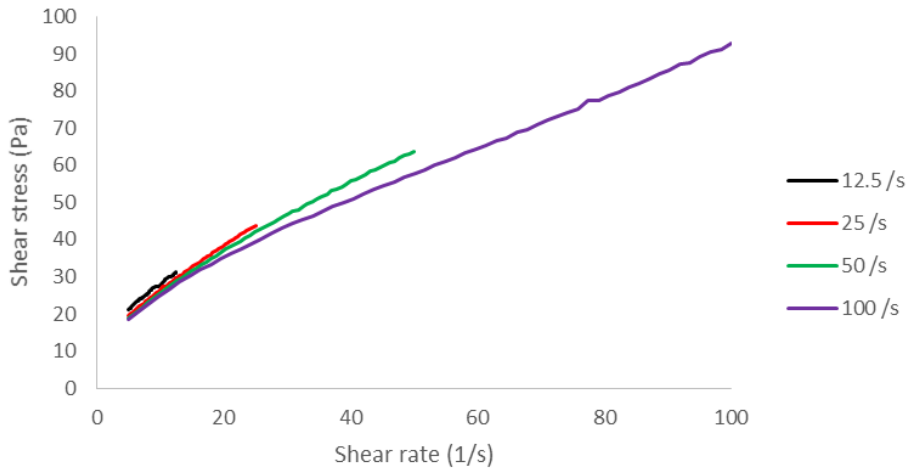

Figure 31. Flow curves at different shear rates for mixture SP 2.

4.2.3 Influence of supplementary cementitious materials

When changing the SCMs, the main conclusions were that omitting the silica fume caused a decrease in workability loss and a decrease in thixotropy. Omitting the fly ash had, generally, the opposite effect. Figure 32 to Figure 35 show a similar image for $\Delta\eta$, $\Delta\mu_{ave}$, $\Delta\mu_{diff}$ and $\Delta\tau_5$, respectively. Omitting the silica fume decreases $\Delta\eta$ (compare black and red, and green and purple), although for the mixtures without fly ash, the effect is only visible at 12.5 s^{-1} for $\Delta\eta$. The pure OPC mixture shows the smallest $\Delta\mu_{ave}$ but largest $\Delta\tau_5$ changes, and, quite remarkable, the $\Delta\tau_5$ is negative for the OPC + FA mixture, meaning that the yield stress increases with applied shear. This phenomenon will return in upcoming sections.

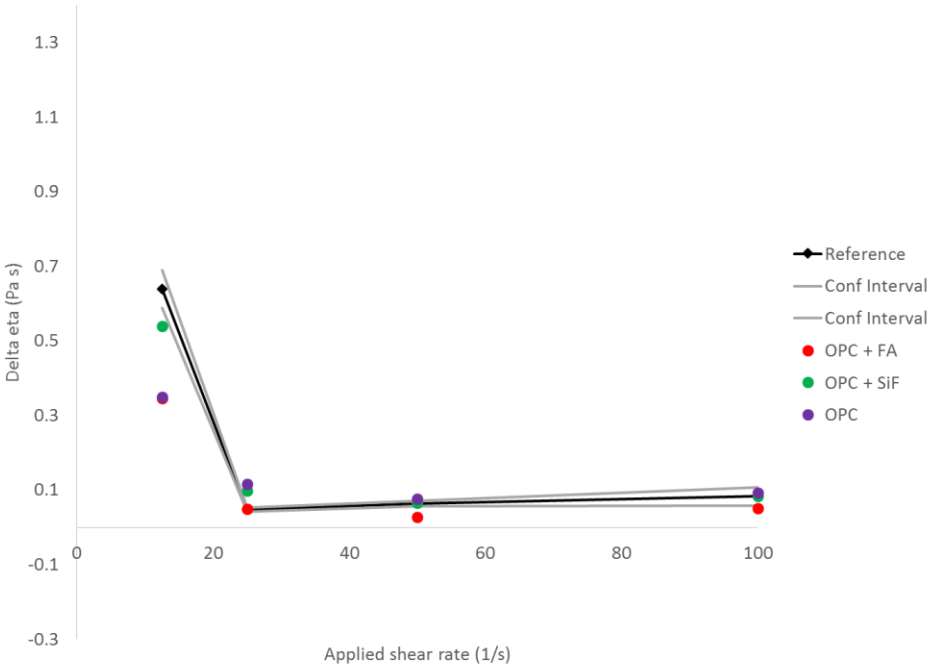

Figure 32. $\Delta\eta$ for the reference mixtures (average in black, confidence interval in gray), and the mixtures with different SCMs.

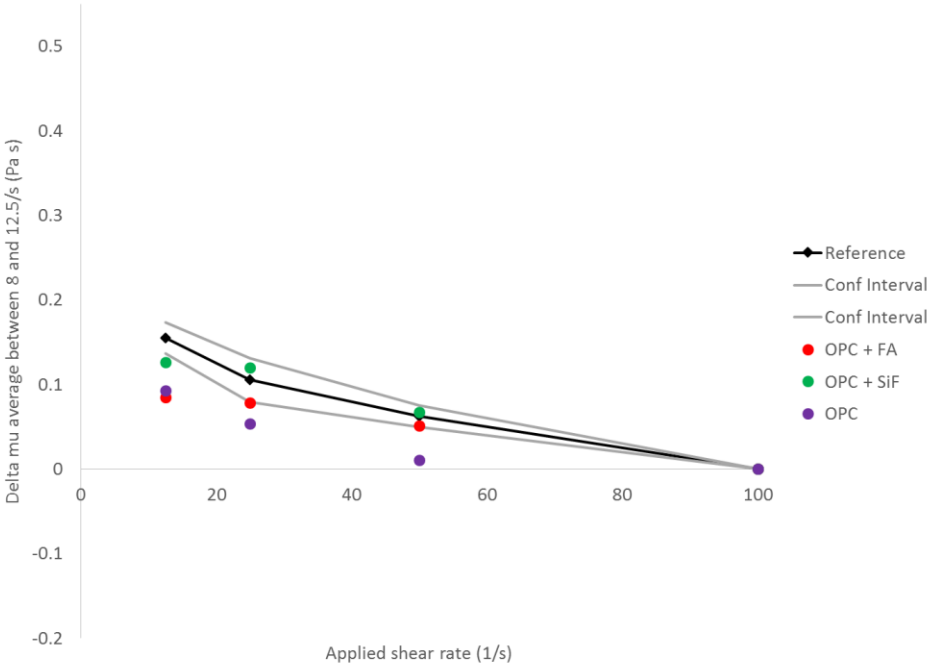

Figure 33. $\Delta\mu_{ave}$ for the reference mixtures and the mixtures with different SCMs.

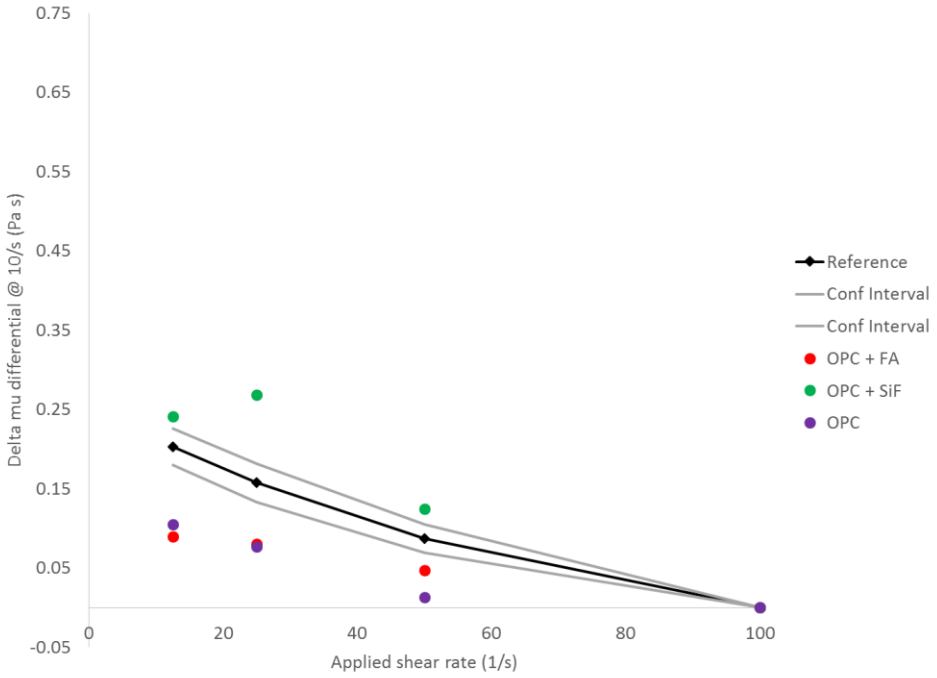

Figure 34. $\Delta\mu_{diff}$ for the reference mixtures and the mixtures with different SCMs.

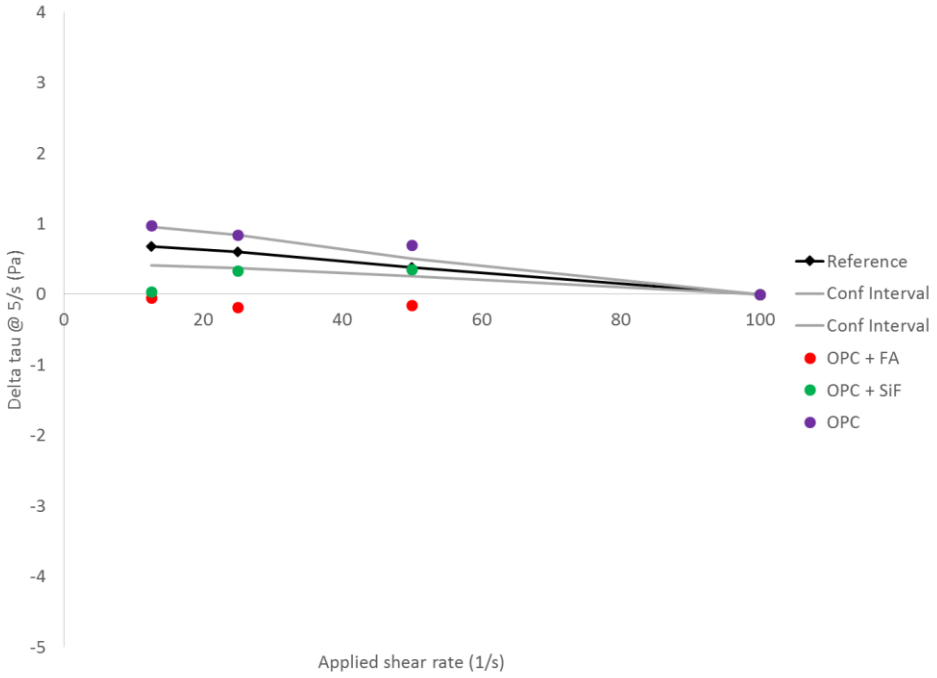

Figure 35. $\Delta\tau_5$ for the reference mixtures and the mixtures with different SCMs.

4.2.4 Effect of small changes in water content

For mixtures with different water contents, the discussion becomes a bit more complicated. For the mixture with a decrease of 14 ml of water (water -5), $\Delta\eta$ is slightly larger (Figure 36), $\Delta\mu$ is considerably larger (Figure 37, Figure 38), and $\Delta\tau_5$ is smaller compared to the reference mixture (Figure 39). Decreasing water should increase breakdown of structure, which is what is observed here, except for the $\Delta\tau_5$. However, increasing the water leads to some unexpected results. $\Delta\eta$ is negative for both mixtures at 25 s^{-1}. Figure 40 shows the fitted pre-shear curves for the "water + 10" mixture, clearly showing a build-up phase at the 25 s^{-1} preshear period. This is on first sight astonishing, as the value of 25 s^{-1} is well above what is expected for shear-induced build-up in cement pastes [38]. At this point, the research team is unsure whether this is a measurement artefact, as potentially sedimentation could become a problem, or whether this is a physical feature of the paste. However, it is observed here for mixtures with an increased water content, and as will be shown in the next section, this is also observed for mixtures with lower SP contents. Also striking from Figure 37 is the strong change in μ_{ave} from 50 to 100 s^{-1}, compared to previous results. Figure 39 shows a systematic increase in τ_5 at any shear rate for the mixtures with a more elevated water content. The yield stress increases with increasing applied shear rate. Again, it is unclear whether this is a physical effect or a measurement artefact.

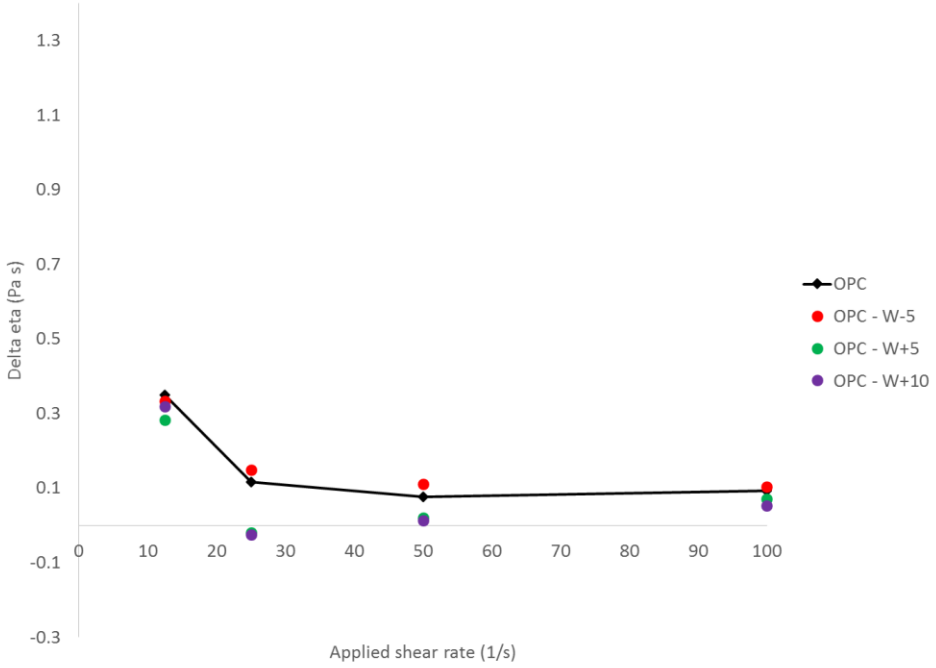

Figure 36. Δη for mixtures with different water contents.

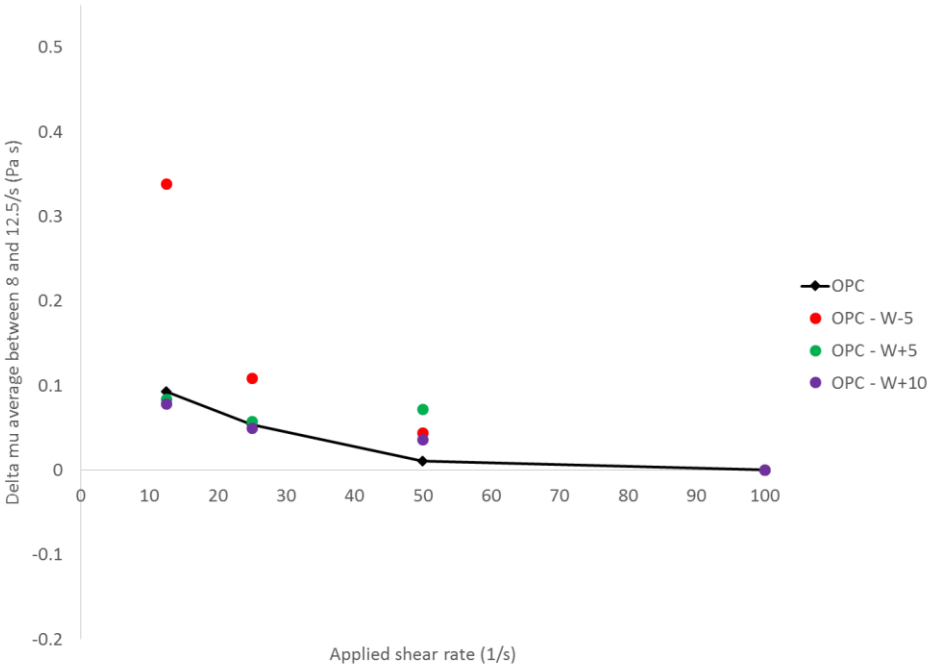

Figure 37. $\Delta\mu_{ave}$ for mixtures with different water contents.

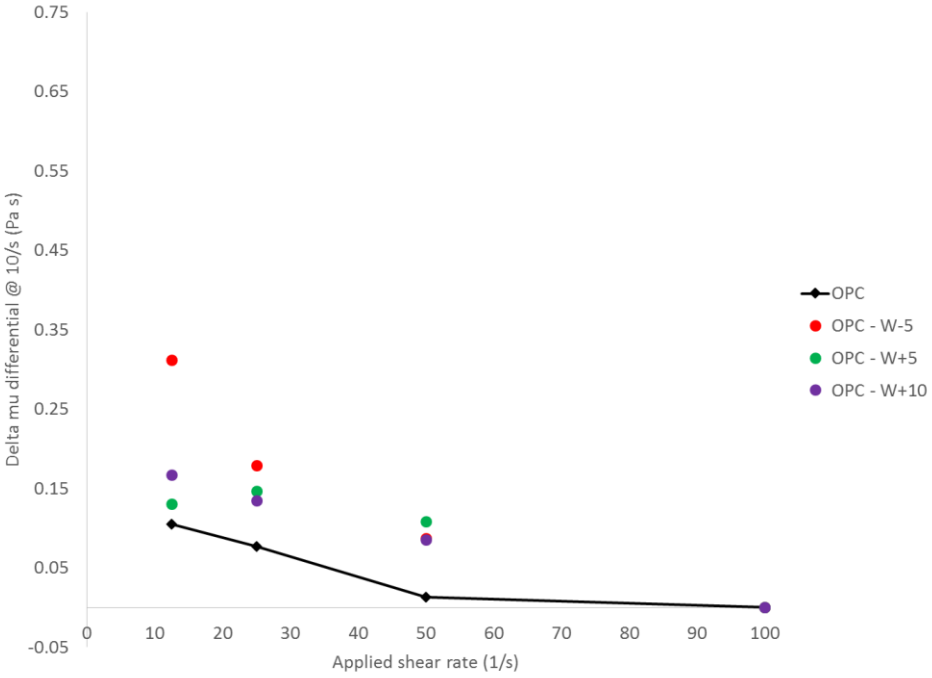

Figure 38. $\Delta\mu_{diff}$ for mixtures with different water contents.

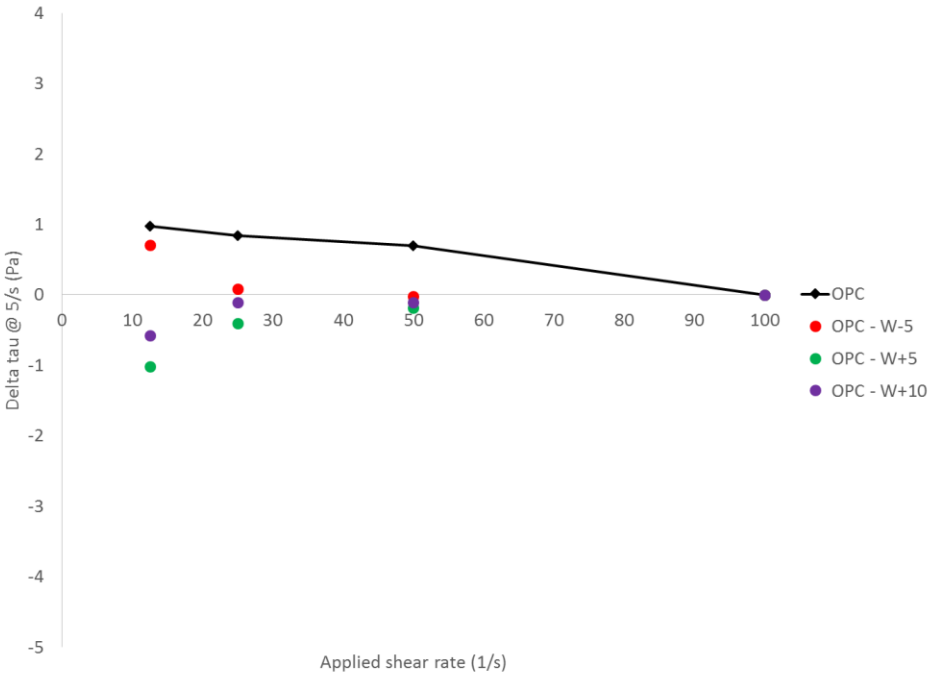

Figure 39. $\Delta\tau_5$ for mixtures with different water contents.

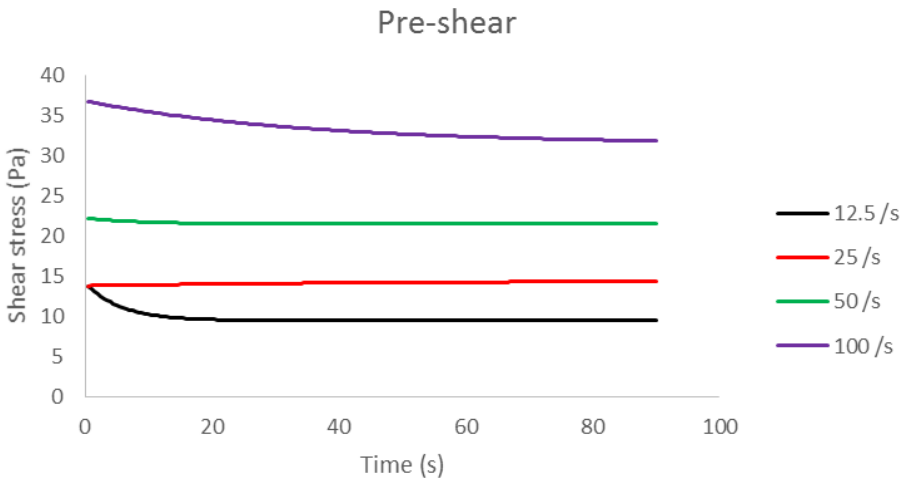

Figure 40. Pre-shear curves for the mixture Water +10. Note that the curve at 25 s^{-1} has an increasing trend!

4.2.5 Influence of SP-dosage or initial mini-slump flow

From the discussions on workability loss and thixotropy, it is shown that the SP dosage has a minor, but complicated effect on the workability loss: yield stress increases faster, viscosity increases slower with increased SP dosage. It has an important effect on thixotropy, as more SP decreases the thixotropic capacity of the mixtures. All previous results were obtained by comparing four series of mixtures with different slump flows. The same mixtures are evaluated here in Figure 41 to Figure 52. The $\Delta\mu_{diff}$ curves have been omitted because of inaccurate fitting of the modified Bingham model to get a representative viscosity at 10 s^{-1}, especially at 100 s^{-1} applied shear.

Similar as an increase in water content, a decrease in initial slump flow, and thus a decrease in SP content, causes some $\Delta\eta$ to be negative, not only at 25 s^{-1}, but also at 50 s^{-1}, and even at 100 s^{-1} for the mixture with OPC, silica fume water + 10. This means that the restructuring under shear, or the measurement artefact, becomes more important when the sample has lower workability to start with. Figure 53 shows the fitted pre-shear curves for the mixture OPC + 10 Water, No SP, clearly showing that the observed rebuild is not negligible. Concerning the $\Delta\mu_{ave}$ curves, the interpretation is not straightforward, although there is a tendency towards smaller decreases and even increases in viscosity with applied shear with decreased SP dosage. The influence on $\Delta\tau_5$ sheds no doubt though: the yield stress increases with increasing applied shear for every of the investigated mixtures in this section. Figure 54 shows the flow curves for mixture OPC + 10 water, No SP. The curves are in opposite order compared to Figure 14 and Figure 31. The mixture's rheological properties increase when increasing the shear rate from 12.5 to 50 s^{-1}. At 100 s^{-1}, the curve more or less overlaps with the 50 s^{-1} curve.

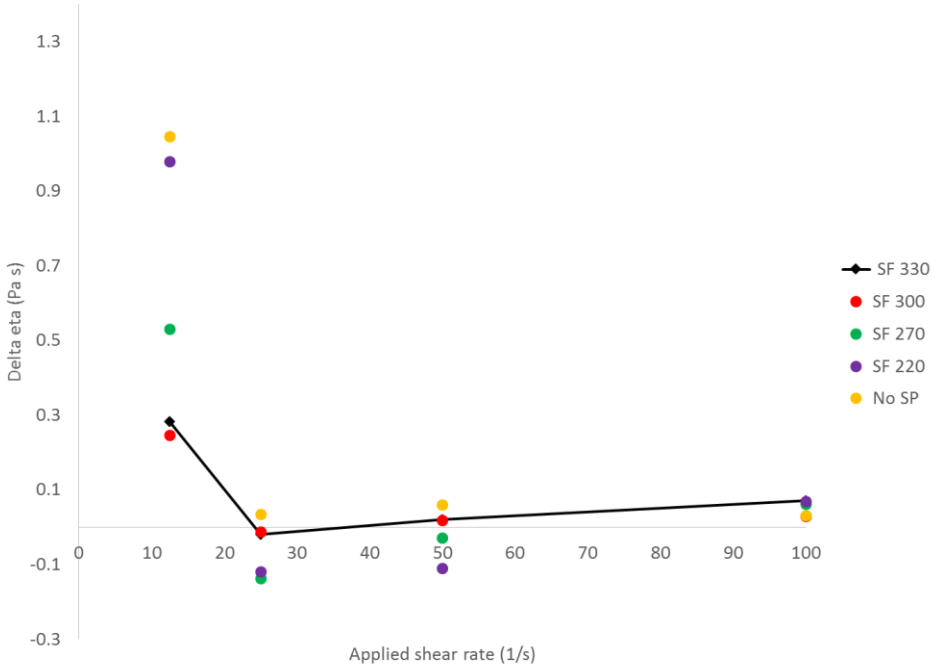

Figure 41. Δη for mixtures with different initial slump flow (OPC + 5 water).

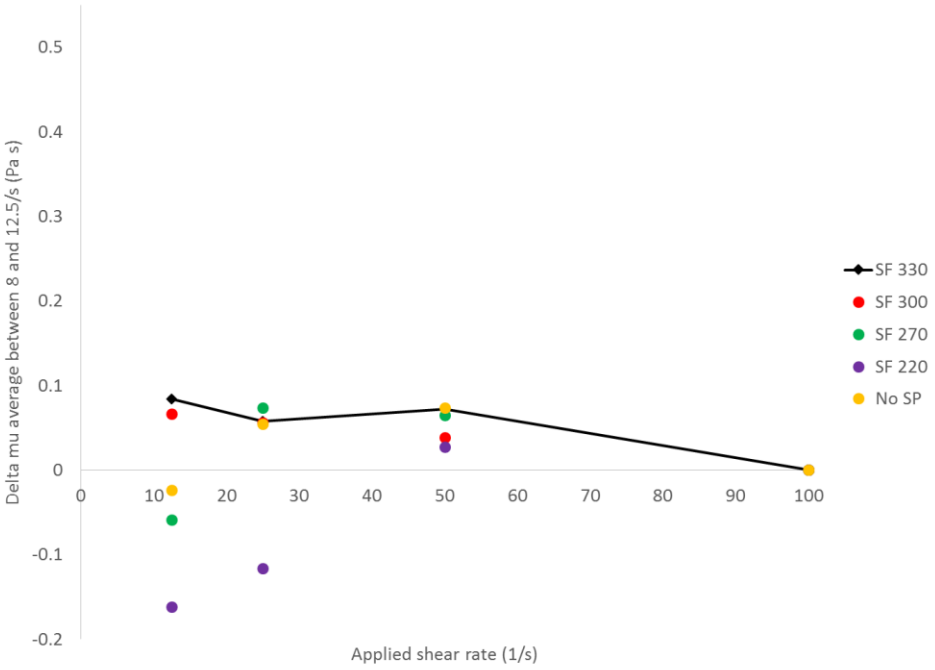

Figure 42. $\Delta\mu_{ave}$ for mixtures with different initial slump flow (OPC + 5 water).

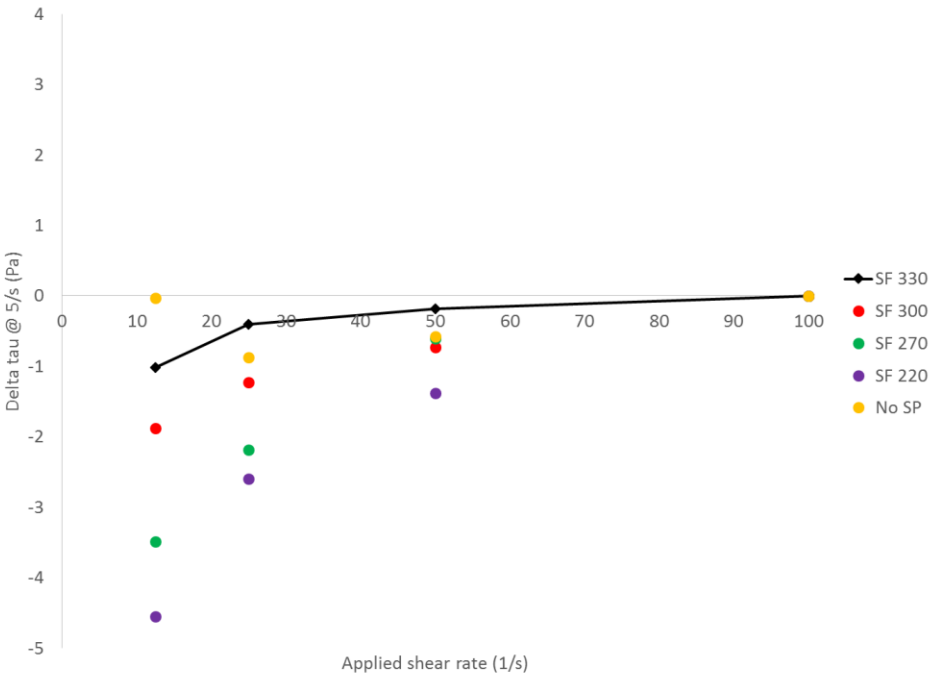

Figure 43. $\Delta\tau_5$ for mixtures with different initial slump flow (OPC + 5 water).

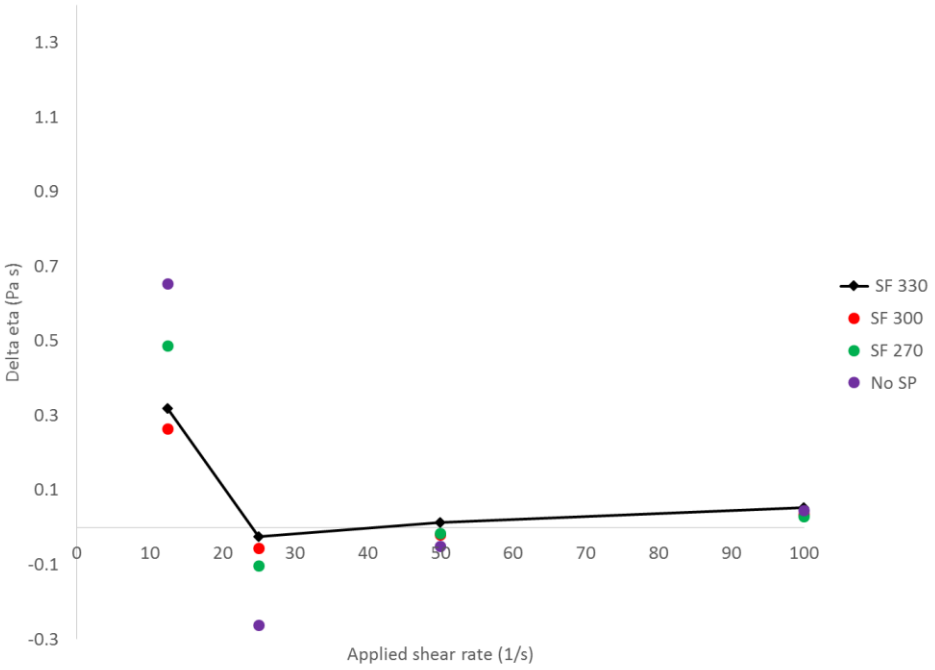

Figure 44. Δη for mixtures with different initial slump flow (OPC + 10 water).

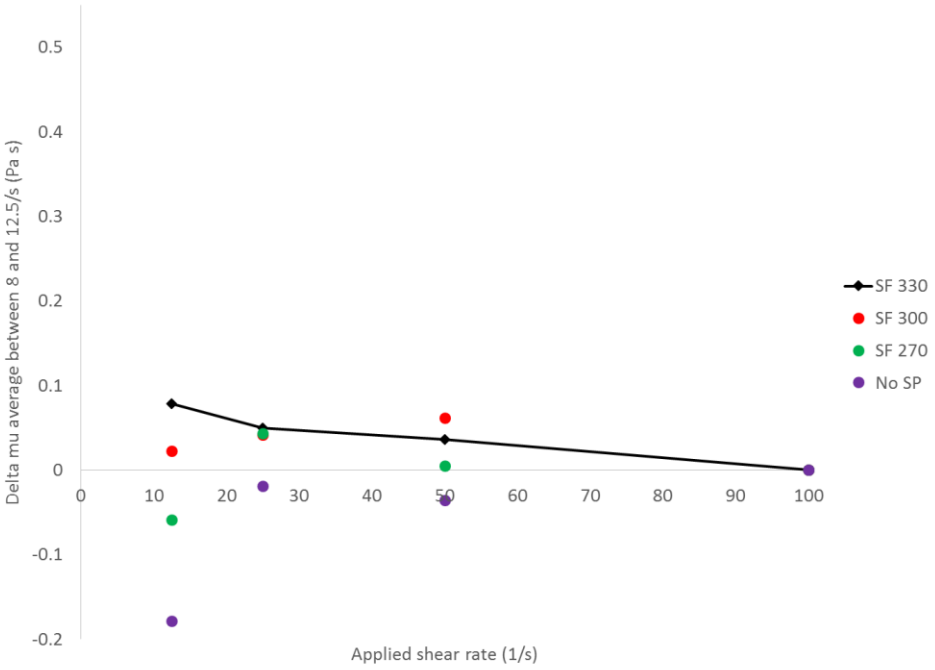

Figure 45. $\Delta\mu_{ave}$ for mixtures with different initial slump flow (OPC + 10 water).

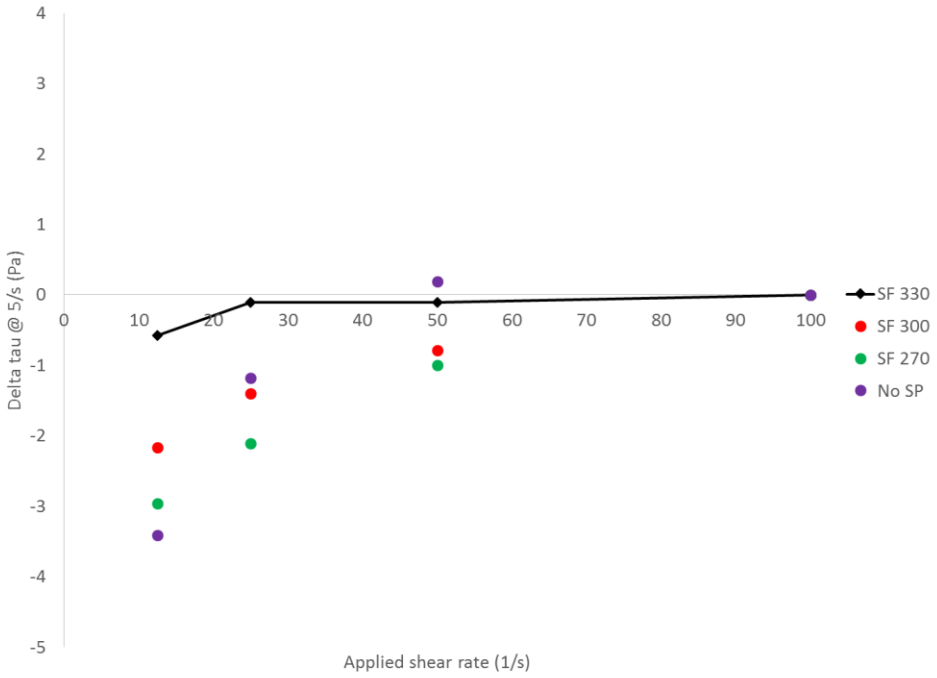

Figure 46. $\Delta\tau_5$ for mixtures with different initial slump flow (OPC + 10 water).

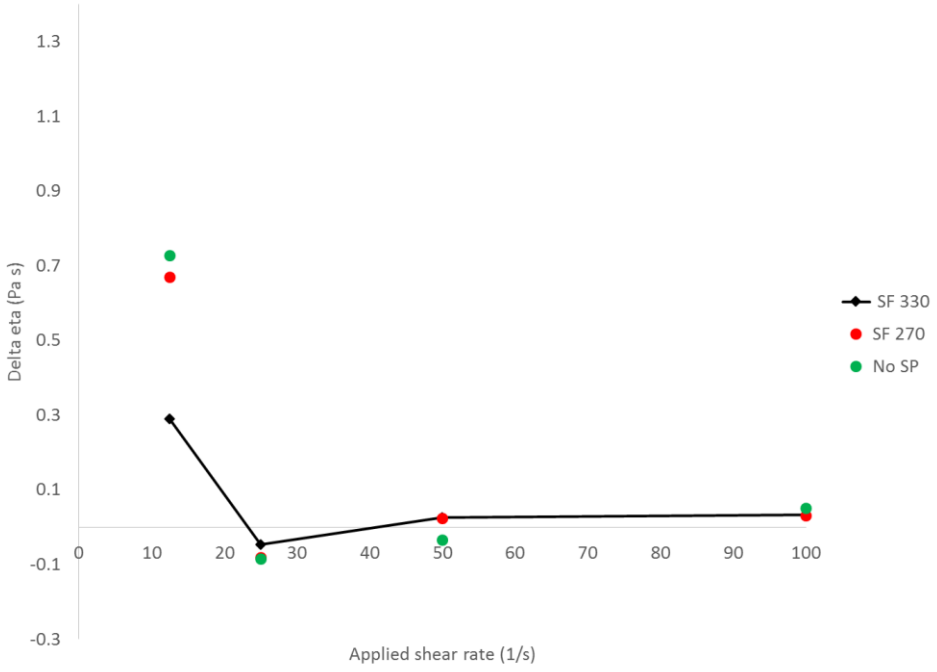

Figure 47. $\Delta\eta$ for mixtures with different initial slump flow (OPC + FA + 5 water).

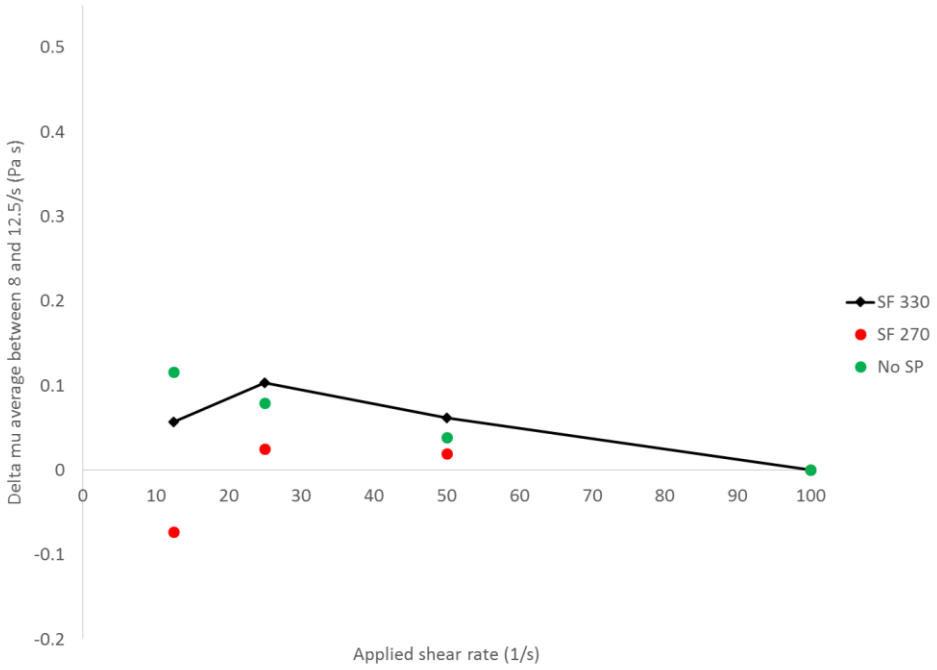

Figure 48. $\Delta\mu_{ave}$ for mixtures with different initial slump flow (OPC + FA + 5 water).

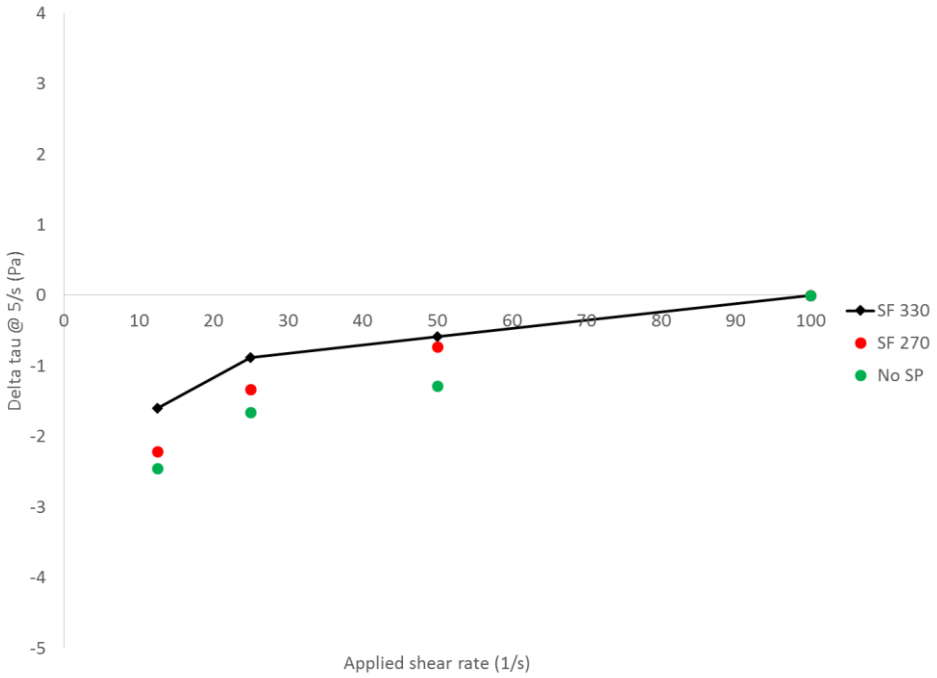

Figure 49. $\Delta\tau_5$ for mixtures with different initial slump flow (OPC + FA + 5 water).

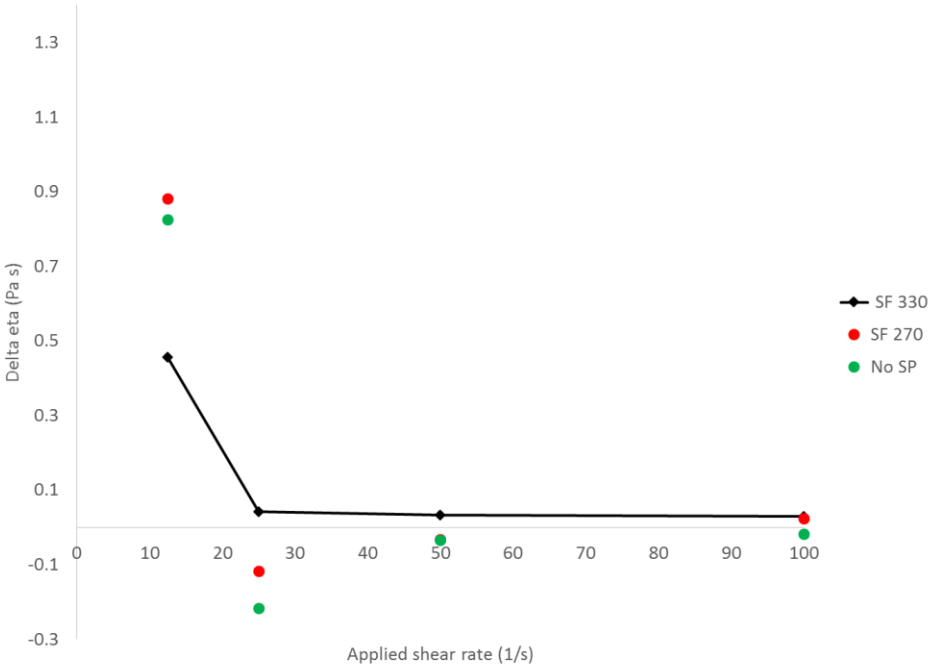

Figure 50. Δη for mixtures with different initial slump flow (OPC + SiF + 10 water).

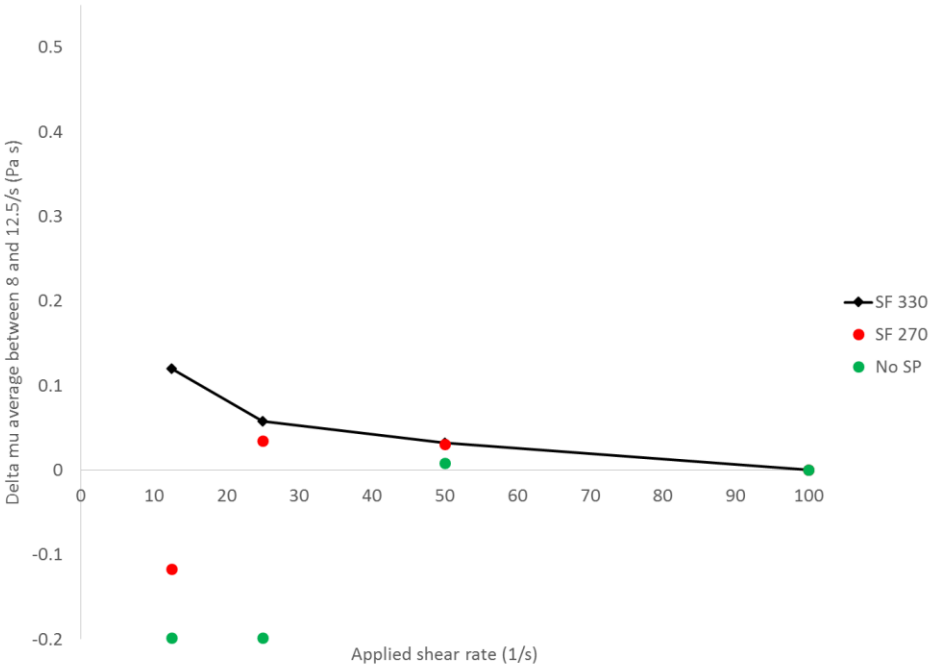

Figure 51. $\Delta\mu_{ave}$ for mixtures with different initial slump flow (OPC + SiF + 10 water).

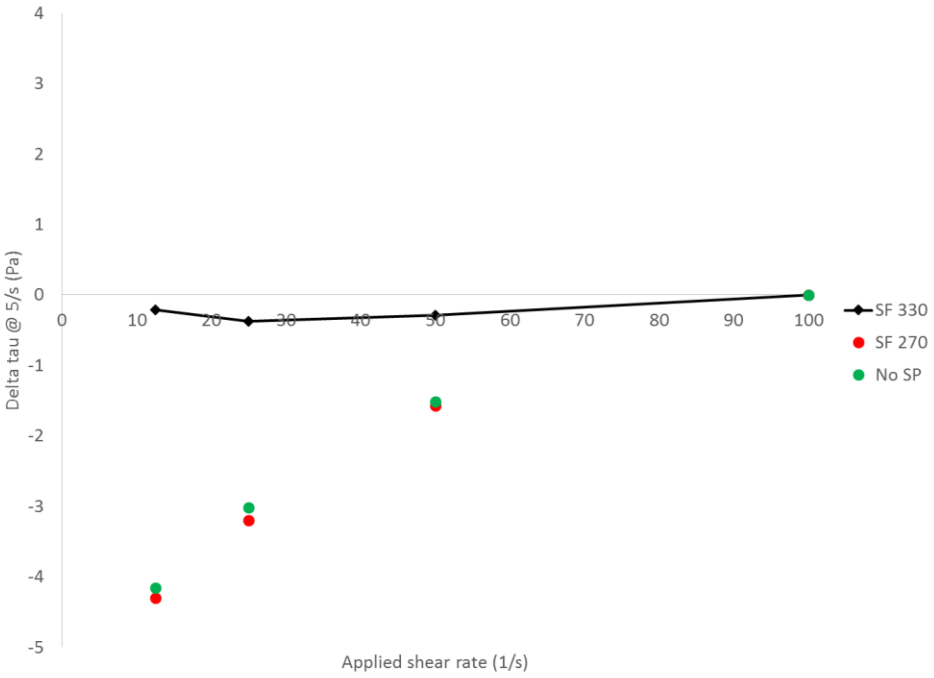

Figure 52. $\Delta\tau_5$ for mixtures with different initial slump flow (OPC + SiF + 10 water).

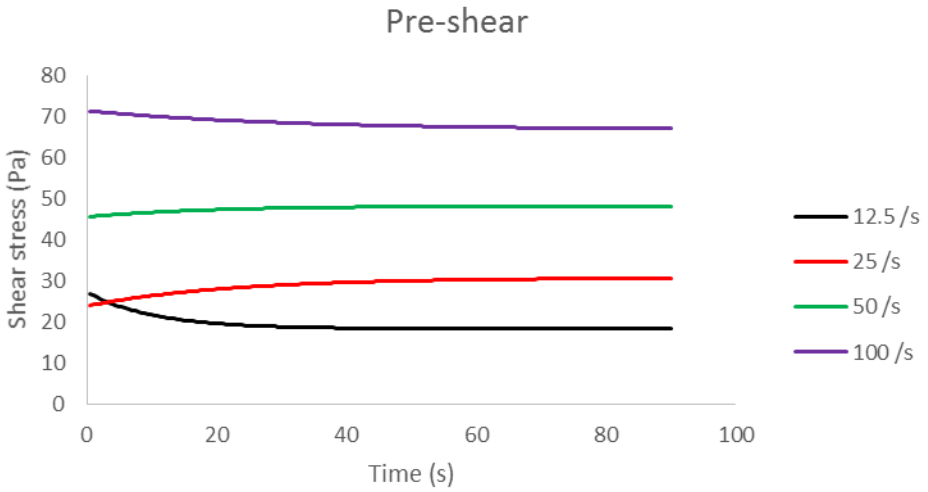

Figure 53. Fitted pre-shear curves for OPC + 10 Water, No SP, showing clearly breakdown at 12.5 and 100 s^{-1}, and build-up at 25 and 50 s^{-1}.

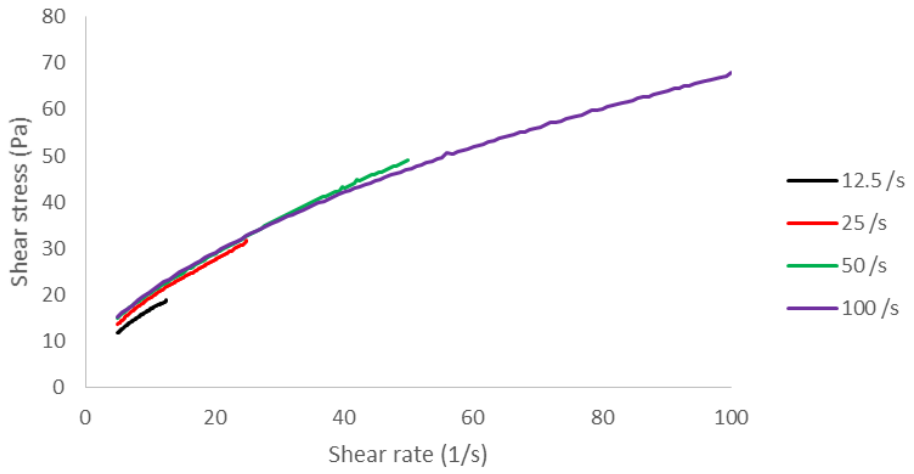

Figure 54. Flow curves for OPC + 10 Water, No SP.

4.2.6 Summary

For well-dispersed mixtures with a sufficiently low water content, increasing the applied shear rate causes more breakdown, and thus a decrease in rheological properties. It should be noted that the majority of the breakdown happens at 12.5 s^{-1}, but non-negligible breakdown values are also observed at higher shear rate. This means that certain connections between cement particles can only by broken at more elevated shear rates or shear stresses. Changing the temperature substantially affects the behavior. An increase in temperature causes more connections to form (hence the increase in thixotropy), but also stronger connections to form (resulting in a faster increase in workability loss). A clear increase in the number of stronger connections (broken at higher shear rates), has been observed at higher temperature.

Changing the dispersing agent type and incorporating a VMA lead to qualitatively the same behavior, but with different quantities. The addition of a VMA appeared to enhance the sensitivity of the rheological properties to shear, even for the SP 2 – VMA 2 combination.

Adding silica fume as an SCM increases the sensitivity of the rheological properties to shear. This seems logical, as silica fume enhances the creating of connections, which is visible through the increase in thixotropy. Adding fly ash generally reduces the sensitivity, although a first remarkable effect is observed: the yield stress sometimes increased with increasing shear rate.

For mixtures with higher water contents, or not-so-well-dispersed mixtures, the picture becomes more complicated. Build-up is observed during the pre-shear period at some of the applied shear rates. In first instance, at 25 s^{-1}, some mixtures also at 50 s^{-1}, and for one mixture even at 100 s^{-1}. The result on viscosity is not straightforward, but the change in yield stress is clear: it increases with increasing applied shear rate.

The cause of this effect is currently unknown, and it cannot be excluded that this is a measuring artefact. However, the results are in line with the results reported by Feys et al., when discussing the changes in rheology due to pumping [4]. During pumping, viscosity decreases systematically with each increase in flow rate, which is observed here as well for well-dispersed systems. However, pumping has a dual effect on yield stress: it can increase or decrease. At that point, Feys et al. explained this by considering if there is any non-adsorbed SP remaining in the water, which can be absorbed after a stronger shearing process [4]. This theory might still be applicable, as the not-so-well-dispersed mixtures are the ones showing the increase in yield stress, the well-dispersed systems show a decrease. But again, measuring the rheological properties of mixtures with low workability is a challenge, and more research is needed to ensure no measuring artefact affects the quality of the results.

5 Conclusions and Future Work

5.1 Conclusions of this project

This research project investigated the change of rheological properties of cement pastes with time and applied shear. It focused on the workability loss (the permanent changes in rheology), the build-up of structure, and the breakdown of structure at different applied shear rates. All properties were investigated by one extensive measuring procedure in the Anton Paar MCR 302.

The workability loss was assessed by calculating the slope of the yield stress and the differential viscosity at the median shear rate with time. These parameters were obtained by fitting the modified Bingham model to each flow curve which was obtained at 100 s^{-1} applied shear rate: i.e. at 15, 30, 60 and 90 min after contact between cement and water.

The thixotropy was initially intended to be measured by means of A_{thix}, the slope of static yield stress with time, but some issues were encountered in assessing reliable static yield stress values. Instead, the change in shear stress during the first pre-shear curve, at 12.5 s^{-1} shear rate and at 60 min of age was used to determine the reversible rheological properties. However, this method is not fully accurate to determine the full reversibility, as some additional structure gets broken at more elevated shear rates.

The breakdown under shear was determined by the change in apparent viscosity, which is the change in shear stress divided by the applied shear, during the pre-shear period. This parameter quantifies how much structure is broken at a certain shear rate. Careful investigation of the pre-shear periods indicated that equilibrium was reached for each reported measurement. To determine the parameters of the flow curves: i.e. yield stress and viscosity, a 6^{th} order polynomial was applied. This polynomial was evaluated at 5 s^{-1} shear rate to get a sufficiently reliable parameter related to the yield stress. Extrapolation provided serious difficulties in determining yield stress values which corresponded to the observations in the flow curves. Furthermore, this 6^{th} order polynomial was derived to the shear rate, and evaluated and averaged at each measured point between 8 and 12.5 s^{-1}, to obtain what is called the average viscosity. It is a differential viscosity per definition. Also the differential viscosity at 10 s^{-1} based on the modified Bingham model was included for the analysis, but this did not always yield consistent results. The authors are aware that this procedure is not according to the best practices for analysis of rheological properties, but it was the only one suitable to deliver reliable data.

Based on a set of four mixtures containing 25% fly ash, 2.5% silica fume, a w/cm of 0.38 and an initial mini slump flow of 330 mm, data show adequate repeatability for the workability loss, the thixotropic build-up, and each parameter obtained for the breakdown analysis. Two additional measurements were performed on this reference mixture, one at 37°C, one at 7°C, compared to the standard 23°C. Temperature had a strong influence on all parameters, including workability loss, thixotropic build-up and the sensitivity of the rheology to the applied shear rate. The results with the different flow curves also show that at higher temperature, not only more connections are formed between the particles, the connections are also stronger. Hence, for any analysis, strength of connections must also be considered.

The influence of the dosage of the dispersing admixture (a PCE-based commercially available superplasticizer), evaluated through the initial slump flow delivered interesting results. Increasing the dosage increased the rate of change of dynamic yield stress with time, but decreased how quickly viscosity increased. However, the changes are less significant than the changes resulting from the temperature. Increasing initial mini slump flow had a detrimental effect on the thixotropic properties. PCE-based dispersants are thixotropy-killers, which is logical since their main function is to prevent flocculation of particles. On the sensitivity of the rheological properties with applied shear rate, the results need to be split between well-dispersed systems (with an initial mini SF of 330 mm), and not-so-well dispersed systems (with lower initial mini slump flow

values). For the former group, the results behave as discussed for the reference mixtures: the more shear applied, the lower the viscosity, the lower the yield stress. Breakdown occurs at each applied pre-shear step. For the latter group, breakdown always occurs at 12.5 s^{-1}, but a majority of mixtures show rebuild at 25 s^{-1}, a large group shows rebuild at 50 s^{-1}, and while almost all show a breakdown at 100 s^{-1}, one mixture actually showed rebuild at that shear rate as well. Concerning the rheological properties, the change in viscosity due to applied shear is inconclusive, but the yield stress seems to increase with each increment in applied shear. A speculation can be made following the hypothesis of Feys et al. when they discussed the influence of pumping on rheology [4]. However, a clear explanation for this phenomenon is not yet found, and it needs to be investigated whether this is due to a measurement artefact or not.

The type of SP, evaluated here by comparing two PCE-based dispersants, delivers qualitatively similar results, but the order of magnitude of the changes can be substantially different, even up to the magnitudes observed for the changes in temperature. Concerning the VMA, the combination of VMA 1 with SP 1 delivered a faster increase in dynamic yield stress and viscosity (workability loss), a more pronounced structural build-up and a more pronounced sensitivity to applied shear. However, the combination of VMA 2 with SP 2, when comparing to the mixture with SP 2 without VMA, slowed down the workability loss and thixotropic rebuild. The sensitivity to shear was more or less unaffected. The discrepancy between both results can not only be explained by the (unknown) working mechanisms of the VMA, but also by the substantially increased dosage of SP 2 to incorporate VMA 2, while the SP 1 dosage was almost unaltered to incorporate VMA 1. Regardless, the results show that the changes in rheology are strongly dependent on the employed admixtures.

For the SCMs, the use of silica fume enhanced workability loss, thixotropic build-up and made the mixtures more sensitive to the applied shear. Fly ash appeared to be, generally, inert, reducing workability loss, thixotropy and the sensitivity to the applied shear. Silica fume is known to accelerate hydration, fly ash is known to retard it, so the results make sense.

The water content has been changed, but only slightly. The changes correspond to ± 5 and + 10 l/m^3 of concrete. For the workability loss, the general trend is that yield stress and viscosity increase faster with a lower water content. This is logical seen the reduced distance between particles, so it is easier to form connections. The thixotropy appeared unaffected, which is contradictory to literature. However, the change in water content was small, and the SP dosage was adjusted to maintain a constant mini slump flow. Higher water content meant lower SP content, and both effects are canceling each other. At lower water content, the sensitivity to shear increased, but at higher water contents, similar results as for not-so-well-dispersed systems were observed. Breakdown at each pre-shear step, except at 25 s^{-1}, and an increase in yield stress with applied shear.

5.2 Consequences for research and future work

The main striking result is the thixotropy-killing capacity of the used PCE-dispersant. If new thixotropy-enhancing admixtures are to be used, care will need to be taken to see how much the increase in the PCE-dispersant is required to maintain workability, as it may have a strong contraproductive effect. Even increasing the amount of silica fume to enhance thixotropy may even trigger the same effect. Furthermore, when changing admixture producers or products, it will need to be reinvestigated to which magnitude each parameter has an effect.

The main future research suggestion of this work is to continue the investigation on the shear-dependency of the rheological properties. Not only would a more extensive parametric study be beneficial to understand, describe and even model the shear-dependency, the underlying mechanisms for the re-build under shear for some mixtures, and the increase in yield stress need to be discovered. Sedimentation might need to be monitored for the mixtures with higher water content, and potential plug flow could be another cause of an artefact influencing all data. If the observed shear-induced build-up is not a measurement artefact, it will need

to be investigated what the cause is of this phenomenon. The entire investigation shows a non-negligible dependency of the rheological properties to the applied shear rate, not only whether a shear rate is applied or not. Upscaling this to concrete scale, it means that the internally applied shear rate inside the paste in concrete will be dependent on paste volume.

5.3 Consequences for practice

First, the shear-dependency of the rheological properties will cause the rheological properties to be dependent on mixing energy, mixing time, resting time, shear rate during placement, especially during pumping. For mixtures which require a certain range of rheological properties for their application, this may be a major challenge. Mock-up tests with exactly the same equipment and exactly the same procedure may be necessary. It still needs to be researched what the consequences on concrete scale are, but based on the research from Feys et al. [4], considering some extreme conditions, the effects might be significant.

The temperature dependency seemed very strong in this research project, although an extreme range of temperatures has been employed. But even if the temperature range would be halved, meaning working between 15 and 30 °C, significant changes in workability loss, thixotropy and shear-rate dependency may be observed at different temperatures. The temperature-dependency, which is hard to control, might be a major constraint in implementing sensitive rheologically-specific mixtures. Adjustments in mix design dependent on the season might be necessary.

As shown in this project, a change in admixture type or producer may substantially affect the time- and shear-dependency of the rheological properties. Simply switching admixture producer might have serious consequences as the more sensitive mixtures might need to be fully re-designed.

A compatibility issue may exist in creating a super-thixotropic and self-consolidating concrete at the same time, especially when PCE-dispersants are envisioned. If thixotropy is needed, the PCE dosage will need to be strictly controlled, as the effect of the PCE quantity seemed very strong on thixotropy. Similarly as explained above, the implementation of strong thixotropy-enhancing admixtures will need to take into consideration how much the PCE-dosage needs to be increased. It is imaginable that the beneficial effect of the thixotropy-enhancer is nullified by the required increase in PCE-dosage to maintain workability.

Acknowledgements

The authors would like to acknowledge the US Department of Transportation, through the RE-CAST Tier 1 UTC for the financial support of the project, as well as the Center for Infrastructure Engineering Studies (CIES) at Missouri S&T for making the rheometer available to the research team.

References

[1] K. Wang, S. Shah, D. White, J. Gray, T. Voigt, L. Gang, J. Hu, C. Halverson and B. Pekmezci, "Self-Consolidating Concrete--Applications for Slip-Form Paving: Phase I (Feasibility Study) - Federal Highway Administration Transportation Pooled Fund Study TPF-5(098)," Center for Portland Cement Concrete Pavement Technology, Iowa State University, Ames, IA, 2005.

[2] K. Wang, S. Shah, J. Grove, P. Taylor, P. Wiegand, B. Steffes, G. Lomboy, Z. Quanji, L. Gang and N. Tregger, "Self-consolidating concrete, applications for slip-form paving: phase II," National Concrete Pavement Technology Center, Institute for Transportation, Iowa State University, Ames, IA, 2011.

[3] J. Wallevik, Rheology of Particle Suspensions - Fresh Concrete, Mortar and Cement Paste with Various Types of Lignosulfonates. Ph-D dissertation, Trondheim: The Norwegian University of Science and Technology, 2003.

[4] D. Feys, G. De Schutter, K. Khayat and R. Verhoeven, "Changes in rheology of self-consolidating concrete induced by pumping," *Materials and Structures*, vol. 49, no. 11, pp. 4657-4677, 2016.

[5] D. Feys, Interactions between rheological properties and pumping of self-compacting concrete, PhD disseration, Ghent: Ghent University, 2009.

[6] C. Macosko, Rheology Principles, Measurements and Applications, New York: Wiley-VCH, 1994.

[7] J. Mewis and N. Wagner, Colloidal suspension rheology, Cambridge University Press, 2012.

[8] R. Hunter, "Zeta potential in colloid science: principles and applications (Vol. 2)," *Academic Press*, 2013.

[9] J. Perrin, "Atoms," *translated by Hammick DL*, 1916.

[10] P. Hiemenz, 1986. Principles of colloid and surface chemistry (Vol. 188), New York: Marcel Dekker, 1986.

[11] R. Rajagopalan and P. Hiemenz, Principles of colloid and surface chemistry, New York: Marcel Dekker, 1997.

[12] B. Derjaguin and L. Landau, "Theory of the stability of strongly charged lyophobic sols and of the adhesion of strongly charged particles in solution of electrolytes.," *Acta Physicochim: USSR*, vol. 14, pp. 633-662, 1941.

[13] E. Verwey, J. Overbeek and K. Van Nes, "Theory of the stability of lyophobic colloids: the interaction of sol particles having an electric double layer.," *Elsevier Publishing Company,* 1948.

[14] B. Maranzano and N. Wagner, "The effects of particle size on reversible shear thickening of concentrated colloidal dispersions," *The Journal of chemical physics,* vol. 114, no. 23, pp. 10514-10527, 2001.

[15] A. Einstein, "A new determination of molecular dimensions," *Ann. Phys,* pp. 289-306, 1906.

[16] A. Einstein, "Correction to my paper: "A new determination of molecular dimensions," *Ann. Phys.,* vol. 34, pp. 591-592, 1911.

[17] J. Brady and G. Bossis, "Stokesian dynamics," *Annual review of fluid mechanics,* vol. 20, no. 1, pp. 111-157, 1988.

[18] A. Sierou and J. Brady, "Accelerated Stokesian dynamics simulations," *Journal of fluid mechanics,* vol. 448, pp. 115-146, 2001.

[19] A. Ladd, "Numerical simulations of particulate suspensions via a discretized Boltzmann equation. Part 2. Numerical results," *Journal of fluid mechanics,* vol. 271, pp. 311-339, 1994.

[20] S. Chen and G. Doolen, "Lattice Boltzmann method for fluid flows," *Annual review of fluid mechanics,* vol. 30, no. 1, pp. 329-364, 1998.

[21] N. Martys, "Study of a dissipative particle dynamics based approach for modeling suspensions," *Journal of Rheology,* vol. 49, no. 2, pp. 401-424, 2005.

[22] S. Kim and S. Karrila, Microhydrodynamics: Principles and Selected Applications, 1991.

[23] J. Brady and J. Morris, "Microstructure of strongly sheared suspensions and its impact on rheology and diffusion.," *Journal of Fluid Mechanics,* vol. 1997, pp. 103-139, 1997.

[24] R. Ball and J. Melrose, "Lubrication breakdown in hydrodynamic simulations of concentrated colloids," *Advances in colloid and interface science,* vol. 59, pp. 19-30, 1995.

[25] D. Dratler and W. Schowalter, "Dynamic simulation of suspensions of non-Brownian hard spheres," *Journal of Fluid Mechanics,* vol. 325, pp. 53-77, 1996.

[26] A. Sierou and J. Brady, " Rheology and microstructure in concentrated noncolloidal suspensions," *Journal of Rheology,* vol. 46, no. 5, pp. 1031-1056, 2002.

[27] J. Chong, E. Christiansen and A. Baer, "Rheology of concentrated suspensions," *Journal of applied polymer science,* vol. 15, no. 8, pp. 2007-2021, 1971.

[28] A. Shapiro and R. Probstein, "Random packings of spheres and fluidity limits of monodisperse and bidisperse suspensions," *Physical review letters,* vol. 68, no. 9, p. 1422, 1992.

[29] C. de Kruif, E. Van Iersel, A. Vrij and W. Russel, "Hard sphere colloidal dispersions: Viscosity as a function of shear rate and volume fraction," *The Journal of chemical physics,* vol. 83, no. 9, pp. 4717-4725, 1985.

[30] G. Scott and D. Kilgour, "The density of random close packing of spheres," *Journal of Physics D: Applied Physics,* vol. 2, no. 6, p. 863, 1969.

[31] S. Torquato, T. Truskett and P. Debenedetti, "Is random close packing of spheres well defined?," *Physical review letters,* vol. 84, no. 10, p. 2064, 2000.

[32] I. Krieger and T. Dougherty, "A mechanism for non-Newtonian flow in suspensions of rigid spheres," *Transactions of the Society of Rheology,* vol. 3, no. 1, pp. 137-152, 1959.

[33] J. Chong, E. Christiansen and A. Baer, "Rheology of concentrated suspensions," *Journal of applied polymer science,* vol. 15, no. 8, pp. 2007-2021, 1971.

[34] R. Bagnold, "Experiments on a gravity-free dispersion of large solid spheres in a Newtonian fluid under shear.," *Proceedings of the Royal Society of London. Series A. Mathematical and Physical Sciences,* vol. 225, no. 1160, pp. 49-63, 1954.

[35] H. Laun, "Rheological properties of aqueous polymer dispersions," *Die Angewandte Makromolekulare Chemie,* vol. 123, no. 1, pp. 335-359, 1984.

[36] H. Barnes, "Thixotropy—a review," *Journal of Non-Newtonian Fluid Mechanics,* vol. 70, no. 1-2, pp. 1-33, 1997.

[37] N. Roussel, "A thixotropy model for fresh fluid concretes: theory, validation and applications," *Cement and Concrete Research,* vol. 36, no. 10, pp. 1797-1806, 2006.

[38] S. Jarny, N. Roussel, S. Rodts, F. Bertrand, R. Le Roy and P. Coussot, "Rheological behavior of cement pastes from MRI velocimetry," *Cement and Concrete Research,* vol. 35, no. 10, pp. 1873-1881, 2005.

[39] D. Cheng, "Hysteresis loop experiments and the determination of thixotropic properties," *Nature,* vol. 216, no. 5120, pp. 1099-1100, 1967.

[40] O. Wallevik, D. Feys, J. Wallevik and K. Khayat, "Avoiding inaccurate interpretations of rheological measurements for cement-based materials," *Cement and Concrete Research,* vol. 78, pp. 100-109, 2015.

[41] D. Feys, R. Cepuritis, S. Jacobsen, K. Lesage, E. Secrieru and A. Yahia, "Measuring rheological properties of cement pastes: most common techniques, procedures and challenges," *Rilem Technical Letters,* vol. 2, pp. 129-135, 2018.

[42] J. Yammine, M. Chaouche, M. Guerinet, M. Moranville and N. Roussel, "From ordinary rhelogy concrete to self compacting concrete: A transition between frictional and hydrodynamic interactions.," *Cement and Concrete Research,* vol. 38, no. 7, pp. 890-896, 2008.

[43] X. Chateau, G. Ovarlez and K. Trung, "Homogenization approach to the behavior of suspensions of noncolloidal particles in yield stress fluids," *Journal of Rheology,* vol. 52, no. 2, pp. 489-506, 2008.

[44] F. Mahaut, X. Chateau, P. Coussot and G. Ovarlez, "Yield stress and elastic modulus of suspensions of noncolloidal particles in yield stress fluids," *Journal of Rheology,* vol. 52, no. 1, pp. 287-313, 2008.

[45] G. H. Tattersall and P. F. Banfill, The rheology of fresh concrete, London: Pitman, 1983.

[46] D. Feys, R. Verhoeven and G. De Schutter, "Why is fresh self-compacting concrete shear thickening?," *Cement and Concrete Research,* vol. 39, no. 6, pp. 510-523, 2009.

[47] A. Yahia and K. Khayat, "Analytical models for estimating yield stress of high-performance pseudoplastic grout," *Cement and Concrete Research,* vol. 31, no. 5, pp. 731-738, 2001.

[48] D. Feys, J. Wallevik, A. Yahia, K. Khayat and O. Wallevik, "Extension of the Reiner–Riwlin equation to determine modified Bingham parameters measured in coaxial cylinders rheometers," *Materials and Structures,* vol. 46, no. 1-2, pp. 289-311, 2013.

[49] J. Wallevik, "Rheological properties of cement paste: thixotropic behavior and structural breakdown," *Cement and Concrete Reseach,* vol. 39, pp. 14-29, 2009.

[50] P. Billberg, Billberg, P., 2006. Form pressure generated by self-compacting concrete: influence of thixotropy and structural behaviour at rest, PhD dissertation, Stockholm: Royal Institute of Technology, 2006.

[51] K. Khayat and J. Assaad, "Effect of w/cm and high-range water-reducing admixture on formwork pressure and thixotropy of self-consolidating concrete," *ACI Materials Journal,* vol. 103, no. 3, pp. 186-193, 2006.

[52] N. Roussel, "Steady and transient flow behaviour of fresh cement pastes," *Cement and Concrete Research,* vol. 35, no. 9, pp. 1656-1664, 2005.

[53] G. Tattersall, "Structural breakdown of cement pastes at constant rate of shear," *Nature,* vol. 175, no. 4447, p. 166, 1955.

[54] N. Roussel, G. Ovarlez, S. Garrault and C. Brumaud, "The origins of thixotropy of fresh cement pastes," *Cement and Concrete Research,* vol. 42, no. 1, pp. 148-157, 2012.

[55] I. Topccedil and T. Uygunoğlu, "Influence of mineral additive type on slump-flow and yield stress of self-consolidating mortar," *Scientific Research and Essays,* vol. 5, no. 12, pp. 1492-1500, 2010.

[56] M. Rahman, M. Baluch and M. Malik, "Thixotropic behavior of self compacting concrete with different mineral admixtures," *Construction and Building Materials,* vol. 50, pp. 710-717, 2014.

[57] H. Roby, "Pressureof Concrete on Forms," *Civil Engineering,* vol. 5, 1935.

[58] J. Assaad and K. Khayat, "Variations of lateral and pore water pressure of self-consolidating concrete at early age," *ACI Materials Journal,* vol. 101, no. 4, pp. 310-317, 2004.

[59] S. Nunes, P. Oliveira, J. Coutinho and J. Figueiras, "Rheological characterization of SCC mortars and pastes with changes induced by cement delivery," *Cement and Concrete Composites,* vol. 33, no. 1, pp. 103-115, 2011.

[60] K. Juvas, A. Kappi, K. Salo and E. Nordenswan, "The effects of cement variations on concrete workability," *Nordic Concrete Research,* vol. 26, pp. 39-46, 2001.

[61] Z. Quanji, Thixotropic behavior of cement-based materials: effect of clay and cement types. MSc dissertation, Ames, IA: Iowa State University, 2010.

[62] N. Yıldız, M. Erol, B. Baran, Y. Sarıkaya and A. Çalımlı, "Modification of rheology and permeability of Turkish ceramic clays using sodium silicate," *Applied Clay Science,* vol. 13, no. 1, pp. 65-77, 1998.

[63] Z. Quanji, G. Lomboy and K. Wang, "Influence of nano-sized highly purified magnesium alumino silicate clay on thixotropic behavior of fresh cement pastes," *Construction and Building Materials,* vol. 69, pp. 295-300, 2014.

[64] R. Ferron, A. Gregori, Z. Sun and S. Shah, "Rheological method to evaluate structural buildup in self-consolidating concrete cement pastes," *ACI Materials Journal,* vol. 104, no. 3, pp. 242-250, 2007.

[65] S. Kawashima, J. Kim, D. Corr and S. Shah, "Study of the mechanisms underlying the fresh-state response of cementitious materials modified with nanoclays," *Construction and Building Materials,* vol. 36, pp. 749-757, 2012.

[66] J. Assaad and K. Khayat, "Assessment of thixotropy of self-consolidating concrete and concrete-equivalent-mortar—effect of binder composition and content," *ACI Materials Journal,* vol. 101, no. 5, pp. 400-408, 2004.

[67] E. Ore and J. Straughan, "Effect of cement hydration on concrete form pressure," *ACI Journal,* vol. 65, no. 2, pp. 111-120, 1968.

[68] N. Roussel and F. Cussigh, "Distinct-layer casting of SCC: the mechanical consequences of thixotropy," *Cement and Concrete Research,* vol. 38, no. 5, pp. 624-632, 2008.

[69] K. Khayat, "Viscosity-enhancing admixtures for cement-based materials—an overview," *Cement and Concrete Composites,* vol. 20, no. 2-3, pp. 171-188, 1998.

[70] A. Ghezal, K. Khayat and D. Beaupré, "Effect of High-Range Water-Reducer—Viscosity-Modifying Admixture Combination on Rheological Properties of Concrete Equivalent Mortar," in *Proceedings of the First North American Conference on the Design and Use of Self-Consolidating Concrete (pp. 159-165),* Stockholm, 2002.

[71] J. Assaad and K. Khayat, "Effect of viscosity-enhancing admixtures on formwork pressure and thixotropy of self-consolidating concrete," *ACI Materials Journal,* vol. 103, no. 4, pp. 280-287, 2006.

[72] X. Kong, Y. Zhang and S. Hou, "Study on the rheological properties of Portland cement pastes with polycarboxylate superplasticizers," *Rheologica Acta,* vol. 52, no. 7, pp. 707-718, 2013.

[73] M. Heikal, M. Morsy and I. Aiad, "Effect of treatment temperature on the early hydration characteristics of superplasticized silica fume blended cement pastes," *Cement and Concrete Research,* vol. 35, no. 4, pp. 680-687, 2005.

[74] C. Jolicoeur and M. Simard, "Chemical admixture-cement interactions: phenomenology and physico-chemical concepts," *Cement and Concrete composites,* vol. 20, no. 2-3, pp. 87-101, 1998.

[75] F. Kreppelt, M. Weibel, D. Zampini and M. Romer, "Influence of solution chemistry on the hydration of polished clinker surfaces—a study of different types of polycarboxylic acid-based admixtures," *Cement and Concrete Research,* vol. 32, no. 2, pp. 187-198, 2002.

[76] Y. Zhang, X. Kong, Z. Lu, Z. Lu and S. Hou, "Effects of the charge characteristics of polycarboxylate superplasticizers on the adsorption and the retardation in cement pastes," *Cement and Concrete Research,* vol. 67, pp. 184-196, 2015.

[77] R. Flatt and P. Bowen, "Yodel: a yield stress model for suspensions," *Journal of the American Ceramic Society,* vol. 89, no. 4, pp. 1244-1256, 2006.

[78] R. Flatt and P. Bowen, "Yield stress of multimodal powder suspensions: an extension of the YODEL (Yield Stress mODEL)," *Journal of the American Ceramic Society,* vol. 90, no. 4, pp. 1038-1044, 2007.

[79] J. Gołaszewski and J. Szwabowski, " Influence of superplasticizers on rheological behaviour of fresh cement mortars," *Cement and concrete research,* vol. 34, no. 2, pp. 235-248, 2004.

[80] L. Struble and G. Sun, "Viscosity of Portland cement paste as a function of concentration," *Advanced Cement Based Materials,* vol. 2, no. 2, pp. 62-69, 1995.

[81] J. Petit, E. Wirquin and B. Duthoit, "Influence of temperature on yield value of highly flowable micromortars made with sulfonate-based superplasticizers," *Cement and concrete research,* vol. 35, no. 2, pp. 256-266, 2005.

[82] J.-Y. Petit, K. Khayat and E. Wirquin, "Coupled effect of time and temperature on variations of yield value of highly flowable mortar," *Cement and Concrete Research,* vol. 36, pp. 832-841, 2006.

[83] J. Petit, K. Khayat and E. Wirquin, "Coupled effect of time and temperature on variations of plastic viscosity of highly flowable mortar," *Cement and Concrete Research,* vol. 39, no. 3, pp. 165-170, 2009.

[84] W. Kurdowski, Cement and concrete chemistry, Springer Science & Business, 2014.

[85] E. Gartner, J. Young, D. Damidot and I. Jawed, "Hydration of Portland Cement," in *Structure and Performance of Cements, 2nd Ed. by Bensted, J. and Barnes, P.*, New York, Taylor and Francis, 2002.

[86] J. De Jong, H. Stein and J. Stevels, "Hydration of tricalcium silicate," *Journal of Applied Chemistry,* vol. 17, no. 9, pp. 246-250, 1967.

[87] K. Fujii and W. Kondo, "Kinetics of the hydration of tricalcium silicate," *Journal of the American Ceramic Society,* vol. 57, no. 11, pp. 492-497, 1974.

[88] D. Ménétrier, I. Jawed, T. Sun and J. Skalny, "ESCA and SEM studies on early C3S hydration," *Cement and concrete research,* vol. 9, no. 4, pp. 473-482, 1979.

[89] V. Ramachandran, "Action of triethanolamine on the hydration of tricalcium aluminate," *Cement and Concrete Research,* vol. 3, no. 1, pp. 41-54, 1973.

[90] K. Takemoto and H. Uchicawa, "Hydration of pozzolanic cement," in *7 th ICCC*, Paris, 1980.

[91] K. Mohan and H. Taylor, "Paste of Iricalcium silicate with fly ash analytical electron microscopy, trimethylsilitation and other studies, Effect of fly ash incorporation in cement and concrete.," in *Proceedings of Annual Meeting of the Materials Research Society*, Boston, MA, 1981.

[92] J. Skalny and J. Young, "Mechanisms of Portland cement hydration," in *Proceedings, 7th International Symposium Chemical of Cement*, Paris, 1980.

[93] C. Plowman and J. Cabrera, "Mechanism and kinetics of hydration of C3A and C4AF extracted from cement," *Cement and Concrete Research,* vol. 14, no. 2, pp. 238-248, 1984.

[94] H. Stein and J. Stevels, " Influence of silica on the hydration of 3CaO, SiO2," *Journal of Applied Chemistry,* vol. 14, no. 8, pp. 338-346, 1964.

[95] S. Beedle, G. Groves and S. Rodger, "The effect of fine pozzolanic and other particles on the hydration of C3S," *Advances in Cement Research,* vol. 2, no. 5, pp. 3-8, 1989.